Εθνικό Μετσόβιο Πολυτεχνείο
Σχολή Αγρονόμων & Τοπογράφων Μηχανικών
Τομέας Τοπογραφίας
Εργαστήριο Φωτογραμμετρίας
&
NATIONAL INSTITUTE OF APPLIED SCIENSES OF STRASBOURG

Ανάπτυξη Αλγορίθμου για τη Συνένωση Συζυγών Θραυσμάτων

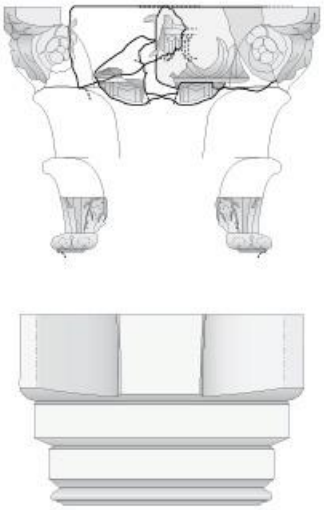

Διπλωματική Εργασία

Ταούκη Ρόζα

Αθήνα, Ιούλιος 2018

NATIONAL TECHNICAL UNIVERSITY OF ATHENS
&
NATIONAL INSTITUTE OF APPLIED SCIENSES OF STRASBOURG

Development of an Algorithm for Uniting Conjugate Fragments

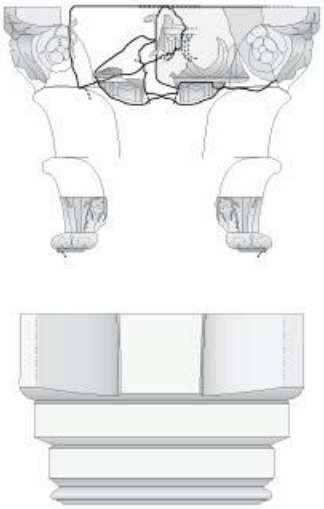

Diploma Thesis
of
Roza Taouki

Athens, July 2018

Η εκπόνηση της παρούσας διπλωματική εργασίας πραγματοποιήθηκε ως συνεργασία του εργαστηρίου Φωτογραμμετρίας της Σχολής Αγρονόμων και Τοπογράφων Μηχανικών ΕΜΠ με το εργαστήριο Φωτογραμμετρίας του πανεπιστημίου INSA Strasbourg στα πλαίσια του Erasmus. Οι επιβλέποντες καθηγητές της εργασίας είναι ο Γεωργόπουλος Ανδρέας, καθηγητής της Σ.Α.Τ.Μ και ο Grussenmeyer Pierre, καθηγητής της σχολής INSA Strasbourg. Για τον λόγο αυτό, η συγγραφή της εργασίας έγινε στην αγγλική γλώσσα.

This Diploma Thesis was carried out with collaboration of the Laboratory of Photogrammetry of the National Technical University of Athens with the National Institute of Applied Sciences of Strasbourg within the Erasmus framework. The supervisors of the present Diploma Thesis are Georgopoulos Andreas, professor of NTUA and Grussenmeyer Pierre, Professor of INSA Strasbourg. For this reason, this Diploma Thesis is written in English.

Acknowledgements

Having completed the present diploma thesis, I would like to thank all the people that contributed to its development in any possible way. I wish to thank, first and foremost, my Professor Prof. Andreas Georgopoulos, director of the Laboratory of Photogrammetry of the Department of Topography at the School of Rural and Surveying Engineering of National Technical University of Athens (NTUA), for the valuable guidance that he gave me in working upon my thesis. I am grateful for his support and trust as he always encouraged and supported my ideas.

I would also like to express my gratitude to my second supervisor, Professor Pierre Grussenmeyer of National Institute of Applied Science (INSA) of Strasbourg who took on this project with me. I consider it an honor to work in the laboratory of Photogrammetry of INSA with the team of Prof. Grussenmeyer, who was willing to help me and answer my questions whenever I needed.

Acknowledgements are attributed to the Laboratory of Photogrammetry and its members for their help and support, having every intension to answer my questions.

Also, I would like to thank Dimitris Filippas, graduate of the School of Rural and Surveying Engineering of National Technical University of Athens (NTUA), for helping me and supporting me with my questions during my diploma thesis, as this present Thesis was based on his Diploma Thesis.

I would like to thank also Christos Pollalis for the valuable advice in conducting and writing the present thesis as well as Vasilis Gkotsis for his support and his patience during this year.

Most importantly, this thesis would not have been possible without my family's support. I owe my deepest gratitude to my parents, Dimitris and Klairi, my sister Savina and my brother Georges for their love and their support during my studies and especially during writing my diploma thesis.

Περίληψη

Η ταχεία ανάπτυξη της επιστήμης της όρασης των υπολογιστών συνέβαλε στην ανάπτυξη τεχνικών και μεθόδων που αξιοποιούν ακόμα και οι αρχαιολόγοι για την ψηφιοποίηση και ανακατασκευή αρχαίων αντικειμένων. Η παρούσα διπλωματική εργασία προτείνει μια νέα μέθοδο για τη συνένωση συζυγών θραυσμάτων με την εφαρμογή ενός μετασχηματισμού στερεού σώματος. Αρχικά, παρουσιάζονται οι σύγχρονες τεχνικές της καταγραφής της τρισδιάστατης πληροφορίας, εστιάζοντας στην Πολιτιστική Κληρονομιά, καθώς και μια ανασκόπηση της βιβλιογραφίας που πραγματεύεται σχετικές εφαρμογές και την εξέλιξη τους μέχρι σήμερα. Στη συνέχεια, περιγράφεται το αντικείμενο μελέτης που είχε ανατεθεί στο εργαστήριο Φωτογραμμετρίας του πανεπιστημίου INSA Strasbourg, το οποίο ήταν η καταγραφή των ευρημάτων ενός αρχαίου ιερού στην περιοχή Pont-Saint Maxence προκειμένου να καταστεί δυνατή η εικονική ανακατασκευή της εξωτερικής πρόσοψης του ιερού. Η ανακατασκευή του ναού αποτέλεσε κίνητρο για τη δημιουργία ενός προγραμματιστικού εργαλείου, ικανό να ανακατασκευάζει αρχαία αντικείμενα που βρίσκονται σε ανασκαφές. Η παρούσα μέθοδος ως εξέλιξη του αλγορίθμου Fragmatch (προηγούμενη διπλωματική εργασία στο Εργαστήριο Φωτογραμμετρίας της Σχολής Αγρονόμων και Τοπογράφων Μηχανικών), ο οποίος εντοπίζει συζυγή αρχαιολογικά θραύσματα βασιζόμενος κυρίως στη γεωμετρία τους αλλά δεν πραγματοποιεί την ένωσή τους, επιτυγχάνει την συνένωση των συζυγών επιφανειών. Η σημαντικότερη δυσκολία για την πραγματοποίηση ενός προγραμματιστικού εργαλείου συνένωσης επιφανειών ήταν η έλλειψη γνώσης αντιστοιχίας σημείων μεταξύ 2 πιθανών συζυγών θραυσμάτων. Αυτό οφείλεται στην πολυπλοκότητα των επιφανειών που χρησιμοποιήθηκαν ως δεδομένα. Η προτεινόμενη λύση της παρούσας διπλωματικής εργασίας είναι η εφαρμογή ενός μετασχηματισμού στερεού σώματος ο οποίος απαιτεί τέσσερα ομόλογα σημεία στις επιφάνειες των δύο θραυσμάτων. Η αναζήτηση αυτών των σημείων βασίζεται εξ ολοκλήρου στην τριγωνοποίηση Delaunay των δύο νεφών σημείων. Ο αλγόριθμος ψάχνει να αντιστοιχίσει τέσσερα σημεία δύο ίσων και αντίστοιχων τριγώνων, τα οποία θα ικανοποιούν τις συνθήκες ορθογωνικότητας του πίνακα στροφής. Ουσιαστικά, δύο ισότητες τριγώνων που ικανοποιούν τις συνθήκες που τίθενται αρκούν για να εφαρμοστεί ο μετασχηματισμός στερεού σώματος (στροφή και μεταφορά). Μια σειρά από προσομοιώσεις πιστοποιούν την αποτελεσματικότητα του αλγορίθμου σε περιπτώσεις θορύβου και φθοράς. Τέλος, αναφέρονται τα συμπεράσματα αυτής της εργασίας καθώς και τα πλεονεκτήματα και μειονεκτήματα του αλγορίθμου Fragmatch+ μαζί με τις προτάσεις για μελλοντική έρευνα.

Abstract

The rapid development of Computer Vision has contributed to the development of techniques and methods utilized even by archeologists for the digitization and reconstruction of ancient objects. This diploma thesis proposes a new method for the unification of conjugated fragments by applying a rigid body transformation. Initially the modern techniques of the three-dimensional recording of archeological finds are presented and a literature review, dealing with relevant applications and the progress up until now. Then, the project integrated in France is described, which gave incentive to the creation of a computer tool, in order to reconstruct broken objects found on the excavation fields. The underlying concept of the present algorithm is based on an existing algorithm, which detects conjugate archaeological fragments based on their geometry. The main difficulty concerning the numerical realization of the assemblage is that no correspondence among the points of the conjugate surfaces is known in advance. The adopted solution presented in the current thesis considers a Rigid Body Transformation which requires four identical points on the surfaces of the two broken fragments. The quest of those points is based entirely on the Delaunay Triangulation of the two point clouds and the algorithm searches to correspond four points of two identical triangles, which will satisfy the orthogonality conditions of the rotation matrix and thus the transformation will be implemented. The robustness of the algorithm is validated through several test cases. Finally, conclusions of this work are mentioned, followed by an analysis of the advantages and disadvantages of the Fragmatch algorithms along with future work proposals.

Contents

Chapter 1 : Introduction 1
Chapter 2 : Three dimensional recording of archeological fragments 2
2.1 Introduction 2
2.2 Dense Image Matching 3
2.3 Terrestrial Scanning 5
2.4 3D digitizing of cultural heritage 8
2.4.1 Digitation of objects 8
2.4.2 Digitation of monuments 11
2.4.3 Digital Libraries 12
Chapter 3 : State of Art 14
3.1 Introduction 14
3.2 Previous work 14
Chapter 4 : Strasbourg's Project: Description of data 33
4.1 Introduction 33
4.2 Pont-Saint-Maxence Project 34
4.2.1 General Information 34
4.2.2 Sanctuary 34
4.2.3 Hypothesis of Restoration 36
4.2.4 Architectural parts of the sanctuary 38
4.3 3D Digitization of fragments 44
4.3.1 Small blocks of fragments 44
4.3.2 Big blocks of fragments 45
4.4 Point Cloud Registration 45
Chapter 5 : Analysis of Algorithm Fragmatch+ 54
5.1 Introduction 54
5.2 Fragmatch+ : General Information 55
5.3 Part1: Fragmatch 56
5.3.1 Data Input 56
5.3.2 Initialization with ICP algorithm implementation 56
5.3.3 Creating surfaces and vectors 59

5.3.4 Pairwise Matching 63
5.4 Part 2: Fragmatch+ 64
5.4.1 Development of Fragmatch+ 64
5.5 Test Cases 72
5.5.1 Sphere 72
5.5.2 Examples of real fragments 77
Chapter 6 : Conclusions 95
6.1: Conclusions 95
6.2 Future Work 97
Bibliography 98
Table of figures 100

Chapter 1 **: Introduction**

Over the last few years, archaeological science increasingly utilizes the possibilities offered by the use of computers and especially by the innovations implemented in the field of Computer Vision. There is a high demand in documentation of cultural heritage objects such as artifacts, sculptures or buildings. A significant reduction in processing time required for the reconstruction of ancient monuments with the application of automatic or semi-automatic methods and the 3D digitization of fragments has been witnessed. Taking into account, the high demand for the reconstruction of objects, the present algorithm focuses on the development of an algorithm for the unification of conjugate algorithms. The algorithmic method proposed, conducted in the numeric computer environment of Matlab, is based on the geometry of the surfaces using the Delaunay Triangulation method.

The present Thesis contains 6 chapters and is structured as follows: In the Chapter 2, the various methods of the three dimensional recording and 3D digitization of archeological objects and monuments are mentioned as well as the importance of the Cultural Heritage preservation. In Chapter 3, a literature review is presented of different methods developed for the reassembly of three-dimensional broken objects up to present. In Chapter 4, the project integrated in France is extensively described which consisted of the 3D digitization of remnants of an ancient sanctuary of the Pont-Saint Maxence in order to enable the virtual reconstruction of the exterior façade of the sanctuary. The architectural parts of the sanctuary and the recording of those fragments are described while the main focus lies on the data processing and the point cloud registration on Cloud Compare. A pair of fragments with higher probability of matching plane to plane among the others is selected and constituted the practical implementation of the algorithm. In Chapter 5 the development of the present algorithm that unites two surfaces from conjugate fragments is described by applying a Rigid Body Transformation. The steps of the algorithm are analyzed and then the robustness of algorithm is presented through various simulations. In the last chapter (Chapter 6) the conclusions and an overview of the present Thesis are presented as well as recommendations for future work. In the last section, the Bibliography is cited.

Chapter 2 **: Three dimensional recording of archeological fragments**

2.1 Introduction

The rapid evolution of digital cameras and the increasing capabilities of computers together with the evolution of analytical software has dramatically expanded the variety of situations to which photogrammetry may be applied, while simultaneously decreasing the costs of acquisition, processing, and analysis. A variety of resource specialists can greatly benefit from 3D products derived from modern photogrammetric techniques (Matthews, 2008).

Human beings perceive the three-dimensional structure of the world around them with apparent ease and for many decades, what people have taken for granted in human vision systems is what they now struggle to acquire and process with computer vision systems. This leads to the exploration of the 3D vision that can best represent scenes and objects with three dimensions. Nowadays, 3D imaging systems and 3D acquisition and reconstruction algorithms are replacing or updating established 2D techniques. Researchers in computer vision have been developing mathematical techniques for recovering the three-dimensional shape and appearance of objects in imagery. Reliable techniques can now accurately compute a partial 3D model of an environment from thousands of partially overlapping photographs and create accurate dense 3D surface models.

Over the last few years, archaeological science increasingly utilizes the possibilities offered by the use of computers and especially by the innovations implemented in the field of Computer Vision. There is a high demand in documentation of cultural heritage objects such as artifacts, sculptures or buildings. The process of acquiring 3D information from real-life objects is complicated, since it involves resolving the problem of acquiring accurate complex geometry measurements. This is why 3D digitization is a very demanding process in terms of processing power and consumed time. After a rapid advancement in computer and digital technologies, 3D digitization is becoming a more appealing practice both in terms of time and money. A significant reduction in processing time required for the reconstruction of ancient monuments with the application of automatic or semi-automatic methods and the 3D digitization of fragments has been witnessed. New systems have been developed and many hardware choices are available in the market. Still, one of the main problems is that there is not an all-in-one solution, that is, there is not a system to be used in any case of digitization. The characteristics of the digitization object -size, geometry and texture complexity, surface properties and characteristics-, as well as the application to be used, play a very important role in the selection of the system.

2.2 Dense Image Matching

Nowadays 3D modeling of scenes and objects at different scales is generally performed using image or range data. Range or active sensors are a common source of dense point clouds for 3D modeling purposes due to their ability to capture millions of points. More recently, advances in the field of computer vision have allowed for the generation of detailed and reliable point clouds from images (dense image matching) – not only from traditional aerial photographs but also from uncalibrated photos through automated procedures. Thanks to recent significant improvements in hardware (such as better dynamics and radiometry) and algorithms (for example, structure from motion (SfM) or innovative image-matching algorithms), photogrammetry has re-emerged as a competitive technology and resurgence in automated photogrammetric methods is now evident. Image-based surveying and 3D modelling can now deliver, in reasonable time, results of comparable geometric characteristics to those of laser scanning for many terrestrial and aerial applications.

Image matching techniques are applied to find corresponding points, whose spatial intersection gives 3D coordinates in object space. Through automated tie-point search software, hundreds of reliable corresponding points can now be detected and replace labor work on a large scale. The detection of corresponding points is extended to almost every pixel in the image and not only to the well-recognizable points. The resulting set of 3D points constitutes the point cloud, which can be interpolated to derive a dense surface model (DSM). Additionally, known points or ground control points (GCPs) with 3D world coordinates should be added to obtain scale and absolute coordinates. Tie points and GCPs are combined in a bundle block adjustment, resulting in the 3D coordinates of all tie points and, more importantly, the position and orientation of each image.

Photogrammetric methods for dense point clouds generation are increasingly applied in various fields due to their ability to determine 3D information quickly and inexpensive. Nevertheless, a problem arises when it comes to the simplification of corresponding points which require a short baseline as a short baseline between consecutive frames leads to unfavorable geometry of the model. Different methods for dense image matching using a wide baseline have been also proposed resulting in more accurate outcomes but this time finding corresponding points gets more complicated due to depth discontinuity, repeated pattern, occlusions and illumination changes.

The most common classification of image matching algorithms is based on the used primitives - image intensity patterns (windows composed of grey values around a point of interest) or features (e.g. edges and regions) - which are then transformed into 3D information through a mathematical model (e.g. collinearity model or camera projection matrix). According to these primitives, the resulting matching algorithms are generally classified as *area-based matching (ABM*) or *feature-based matching*:

- Area-based matching algorithms have a very high accuracy potential (up to 1/50 pixel) if well textured image patches are used. Disadvantages of ABM are the need for small searching range for successful matching, the large data volume which must

be handled and, normally, the requirement of good initial values for the unknown parameters. Problems occur in areas with occlusions, lack of or repetitive texture and if the surface does not correspond to the assumed model.

- Feature-based matching algorithms are often used as alternative or combined with area-based matching. FBM techniques are more flexible with respect to surface discontinuities, less sensitive to image noise and require less approximate values. Because of the sparse and irregularly distributed nature of the extracted features, the matching results are in general sparse point clouds which are then used as seeds to grow additional matches. However, in order to obtain a dense point cloud, a corresponding point is needed for almost every pixel in the image. The feature-based matching approach is not suitable for this purpose since not every pixel in the image corresponds to a well-recognizable feature. Many pixels will represent a greyish surface of a road or pavement or a green patch of vegetation. These pixels cannot be automatically linked to a feature and will be missed by the feature-based matching (Remondino et al., 2013).

Another possible way to distinguish image matching algorithms is based on the created point clouds, i.e. sparse or dense reconstructions. Sparse correspondences were the initial stages of the matching developments due to computational resource limitations but also for a desire to reconstruct scenes using only few sparse 3D points (e.g. corners). Nowadays all the algorithms focus on dense reconstructions - using stereo or multi-view approaches. (Remondino et al., 2013) There are several types of methods that are used to reconstruct 3D models from a set of images and could be classified into methods that reconstruct the visual hull of the object, approaches that recover the photo-hull of an object and algorithms that minimize the surface integral of a certain cost function over the surface shape.

Over the last few years, algorithms have been developed to create 3D models of objects from images collected on the Internet based on the name of the object. These images from random cameras are categorized, oriented and correspondence points are automatically detected resulting in the desired point cloud.

Manual measurements are also performed in some projects, generally for complex architectural objects or in cultural heritage documentations where highly precise and detailed results are required [Gruen et al., 2004]. Manual measurements are time consuming and provide for less dense 3D point clouds, but have higher reliability compared to automated procedures.

2.3 Terrestrial Scanning

«Photogrammetry is the science of obtaining reliable information about the properties of surfaces and objects without physical contact with the objects, and of measuring and interpreting this information».

Photogrammetry has always been a reliable way of producing linear maps, enlargements, which may be quite useful for preliminary design or planning studies, DEM (Digital Elevation Model) and expansions of objects, such as monuments or other artifacts. However, the recording of the necessary information and the production became much more detailed and faster with the use of the technology of terrestrial laser scanners.

3D laser scanning techniques have been developed since the end of 1990s for 3D digital measurement, documentation and visualization. 3D scanners are very similar to cameras. Like cameras, they have a cone-like field of view, and like cameras, they can only collect information about surfaces that are not obscured. While a camera collects color information about surfaces within its field of view, a 3D scanner collects distance information about surfaces within its field of view. The basic principle of laser scanning is the measuring of the distance between the laser instrument and a point by emitting light and detecting the reflection of the light in order to accurately determine the distance to the reflected object. The "picture" produced by a 3D scanner appears as a dense point cloud (point clouds or DDSM-Dense Digital Surface Model). The main advantage of laser scanners, as active imaging instruments, is their ability to collect three-dimensional coordinates X, Y, Z that determine the position of each point in the system. For most situations, a single scan will not produce a complete model of the subject. Multiple scans from many different directions are usually required to obtain information about all sides of the subject. These scans have to be brought in a common reference system, a process that is usually called alignment or registration, and then merged to create a complete model. Nevertheless, like any kind of measurement, measuring coordinates through a 3D scanner involves various errors that might be caused by the scanner or the target surface. This whole process, going from the single range map to the whole model, is usually known as the *3D scanning pipeline* (Ebrahim, 2013).

There are many different types of laser scanners on the market and they have different specifications for different applications. There are different scanning systems used for capturing internal and external spaces, different sized objects (i.e. from a small object to a large monument), with a wide range of scales (i.e. from few mm up to tens of hundreds of meters) as well as scanning systems for close range applications that reach a few meters and provide accurate results.

The specifications of different scanners are designed with different scanning principles. Terrestrial laser are designed with either pulse-based or phase-based techniques, and the scanning principles can be described simply as the following:

1. **Pulse-based scanner**
   The pulse-based scanner belongs to the time-of-flight (TOF) group of scanners, which is an active scanner that uses laser light to probe the subject. At the heart of this type of scanner is a time-of-flight laser rangefinder. The laser rangefinder finds the distance of a surface by timing the round-trip time of a pulse of light. The accuracy of a time-of-flight 3D laser scanner depends on how precisely we can measure the t time. The typical time-of-flight 3D laser scanners can measure is the distance of 1,000–150,000 points every second.

2. **Phase-based scanner**
   Compared to the pulse based scanner, this type of scanner, also within the ToF group, has a high speed scanning rate and better accuracy, but a short distance in the range of tens of meters. In this case, the transmitted beam is modulated by a harmonic wave and the distance is calculated using the phase difference between the transmitted and received wave. The Phase-based scanner has a higher precision, in the domain of millimeters, and higher measurement rates up to one million points per second, can be obtained applying the phase shift measurement principle.

3. **Triangulation laser scanner**
   The triangulation 3D laser scanners are also active scanners that use laser light to probe the environment. With respect to time-of-flight 3D laser scanner, the triangulation laser shines a laser on the subject and exploits a camera to look for the location of the laser dot. Depending on how far away the laser strikes a surface, the laser dot appears at different places in the camera's field of view. This technique is called triangulation because the laser dot, the camera and the laser emitter form a triangle. The length of one side of the triangle, the distance between the camera and the laser emitter are known. The angle of the laser emitter corner is also known. The angle of the camera corner can be determined by looking at the location of the laser dot in the camera’s field of view. These three pieces of information fully determine the shape and size of the triangle and gives the location of the laser dot corner of the triangle. This scanning method is widely used for complex objects which require high accuracy (of the order of some microns) and high scanning density. However, there is a limitation in their range, which can be up to a few meters only. This measurement technique is mainly used in industrial applications.

As opposed to scanners that measure distances using light properties (speed, wavelength) and were briefly presented above, the scanning techniques presented here use light patterns to "encode" the surface of the object. Commonly, 3D features are obtained via various means including structured-light 3D scanning and optical triangulation. The principles of these 3D imaging techniques are briefly stated as follows:

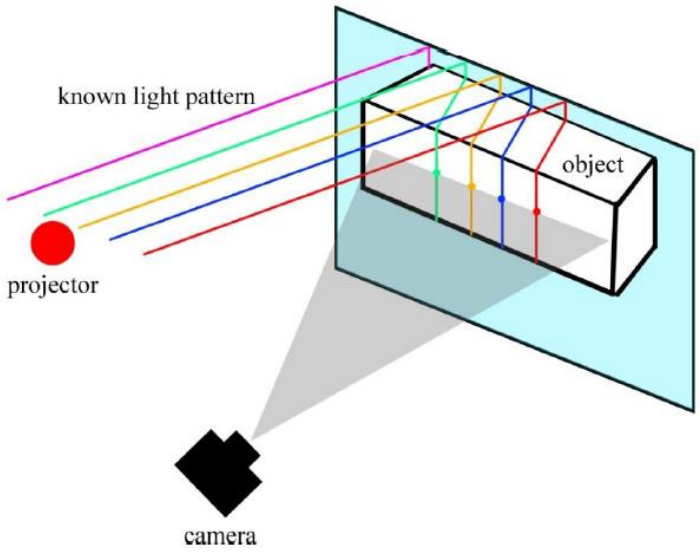

Figure 2-1: The principle behind structured-light 3D scanners, which is based on the distortion of a known light pattern observed from a certain viewpoint.

- **Structured-light 3D scanners**
  Structured-light 3D scanners project a pattern of light on the subject and look at the deformation of the pattern on the subject. The pattern may be one-dimensional or two-dimensional. A sequence of images with different patterns of light projected onto the object surface creates a full 3D point cloud of the stationary object geometry. This method is accompanied by texture acquisition and can lead to very impressive results in terms of accuracy and productivity. The advantage of structured-light 3D scanners is speed. Instead of scanning one point at a time, structured light scanners scan multiple points or the entire field of view at once. This reduces or eliminates the problem of distortion from motion. Some existing systems are capable of scanning moving objects in real-time.

2.4 3D digitizing of cultural heritage

3D digitization of cultural heritage is the first step of the overall process of the complete recording of objects and monuments. It consists of multiple processes and exhibits variations in accordance with specific application requirements. Since size of the digitization subject is one of the most important factors for the selection of the appropriate system and method, 3D digitization of cultural content can be mainly categorized by the size of objects it is applied to. Complete digital recording of Cultural Heritage is a multi-dimensional process. It depends highly on the nature of the subject of recording as well as the purpose of its recording. Due to technical limitations and application requirements, there must be a distinction between the digitization of objects and the digitization of monuments. Digitization of monuments is, in many cases, based on methods that involve traditional topographic techniques (due to the scale in this problem). On the other hand digitization of objects is a field of continuous research and development that can offer with many possibilities, again under the scope of a specific digitization plan. Some methods are briefly described in the following paragraphs.

2.4.1 Digitation of objects

- Laser scanning techniques
  The advantage of using laser sources is that laser light is very bright and highly focused for long distances. As a result the emitted pattern can be always focused on the surface of the objects. One of the most significant advantages of laser scanners is their high accuracy in geometry measurements. On the other hand, it should be noted that in many such systems, geometry can be extracted without any texture information. Additionally, special attention should be paid for surfaces with specific properties, such as reflectance and transparency. One other important aspect is the high cost of such devices, which renders this method useful to specific applications. Finally, the productivity of the method, as well as the portability, depends upon the used system and can vary significantly.

- Shape from structured light
  This method is based on projecting a specific pattern on the surface of the objects and trying to extract geometry information from the deformations of this pattern. The method works by projecting a specific predefined light pattern that covers the whole (or part of the) surface of the objects. This scene is then captured by a typical digital image detector and processed in order to deduce the geometry from the deformations of the pattern in the digital image. These patterns can be simple multiple fringes of different colors or complex patterns with curves, either time or space coded.

Figure 2-2: Shape from structured light

- Shape from silhouette
  This technique is based on multiple photographic capturing of the object from different viewing angles, and deducing the geometry from the object's silhouettes. These silhouettes are extruded and intersected to form the visual hull approximation of the object. Shape from silhouette is an automated process with high productivity and relatively low cost. As of this it is very popular. It can capture both geometry and texture. It is portable and easy to use. The main disadvantage is the medium-to-lower resolution in geometry measurements.

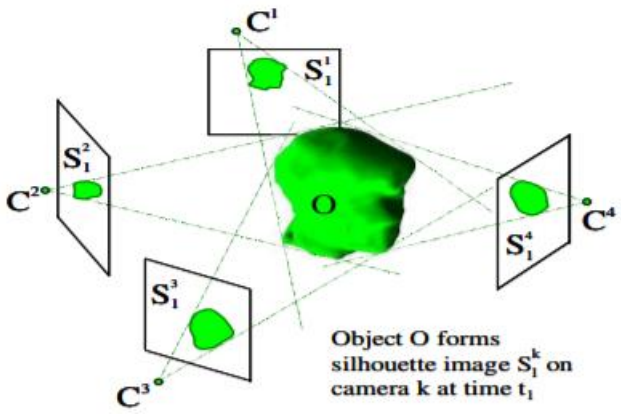

Figure 2-3: Shape from silhouette

- Shape from stereo
  Main goal of this method is the extrapolation of as much geometry information as possible from only a pair of photographs taken from known angles and relative positions, simulating the human visual system. Stereo-photography has a significant application in robotic and computer vision. It is based on taking pairs of photographs

from slightly different angles. When certain parts of the object in the scene are visible to both photographs, specific algorithms from vision can be applied to extract the geometry of the object. The external as well as the internal parameters of the optical system are used for calibration. Calibration is critical in terms of achieving accurate measurements. The method can either be fully automated or man-operated. The final result is a depth map of the object in the scene, reflecting the distance of each recognized point on the surface of the object from the photographic sensor. Advantages of this method are the ability to capture both geometry and texture, the low cost and the portability while a disadvantage of the method is its low resolution.

- Shape from shading
  Shading plays an important role in depth perception. This method requires the capturing of the object from one viewing angle. What should vary is the position of the light source, which would cause the shading to vary on the surface of the object. This way, special algorithms could deduce the geometry of the surface of the object by using multiple photos of different shading conditions. The method is simple and has low cost. It captures both geometry and texture, with a minor disadvantage in capturing texture in shaded areas. It is portable but has the disadvantage of low accuracy.

- Shape from photometry
  Shape from photometry is a variant of shape from shading. Photometric systems usually use a single camera, but take multiple images under varying lighting conditions. Additionally, the usage of reference objects (or, in some cases, reference lighting sources) in the scene is critical, since they are used as calibration objects. Calibrated lights can improve significantly the result of the method but can only be found in special laboratories, so in this case the method is not portable.

- Shape from video
  Shape from video is a variant of shape from stereo. Here the two photo cameras are replaced by a video camera that captures the object in a sequence of images from different views. A key point in the process is the identification of common points between different images and the registration of these points onto a virtual 3D scene. The results are, sometimes, ambiguous due to the fact that there is no prior knowledge about the position of the camera or the objects. Advantages of this method can be considered the low cost, the portability and the ability to capture both texture and geometry. Significant disadvantage is the low resolution in capturing the geometry (Pavlidis et al.,2007).

2.4.2 Digitation of monuments

- Topographic techniques
  The topographic method implements a 3D orthogonal coordinate system by using complicated and high accuracy measuring devices. Mainly, this method using a Geodetic Total Station, a system for measuring angles and distances of characteristic points on the surface of the monument, which are further transformed to coordinates in reference to the initial orthogonal coordinate system. Main advantage of the method is its high accuracy and objectivity of the measurements. It is reliable and it is easy to process its results. A disadvantage is the need of long physical presence near the monument, but it is one of the only methods to be used under difficult conditions, such as complex shape and difficult access. It is referred as ideal for producing high accuracy models of scale 1:50 or smaller.

- Laser scanning techniques
  Laser scanners can actually be considered as advanced geodesic stations and can be used to measure topographic quantities. They can measure the direction of a fictional optical line joining the characteristic points on the surface of the monument to a reference point on the measuring device. Additionally these scanners can estimate their distance from these points. By applying the known triangulation principle they produce Cartesian coordinates automatically. Main advantage is the high accuracy and productivity, as well as the large volume of produced measurement data. It is reliable and objective. On the other hand it is a method of high cost and difficulties in portability and autonomy. It can be applied on almost every monument digitization, but can experience interference from very bright light.

- Photogrammetry
  Common digital photos can be used, under suitable conditions, for measurements that can be of the accuracy obtained by the topographic methods. By applying orientation processes and transformations of digital photogrammetry it is possible to deduce 2D or 3D coordinates from one or two photos. The method is objective and reliable and can be aided by CAD software. It is relatively simple and has low cost. On the other hand it has to be combined with topographical or empirical measurements and the final outcome is a function of the time spent. It can be used for complex objects with high surface detail, but since it is based on photos, there is a need for adequate space. It is also useful when direct access or contact to the monument is prohibited. It can be used to record stages of the monument in time. When combined with accurate measurements it can produce models of high accuracy for scales of 1:100 and even higher (Pavlidis et al.,2007).

2.4.3 Digital Libraries

The recent attention of the scientific community towards 3D digitizing techniques applied to cultural heritage is related to the specific needs of conservation. The effective documentation and display of ancient artifacts and antiquities contribute to the digital preservation of the cultural heritage in order to be conserved for the future generations. The availability of 3D digital replicas, compared to standard 2D photos or video or drawings, generally communicate in more effective way information about scenes or objects that have intrinsic 3D characteristics. Especially for the Cultural Heritage monuments, Digital Libraries have been created, which are available on the Internet. It's a way of "storing history" and "it's about rescuing it collective memory".

Digital libraries or digital repositories are a joint effort of the international community to form platforms which provide free access to primary cultural heritage materials that tell the stories and cultural achievements of all countries. Digital heritage materials must be uniquely identified, and described using appropriate metadata for resource discovery, management and preservation in order to ensure their authenticity. A recent example of such effort in order to create such a Digital Library in Europe is *Europeana*, which is the European Commission's digital platform for cultural heritage. Through this platform, citizens can access European culture for the widest possible variety of purposes. This library gives access to different types of content from different types of heritage and their assembled collections let users explore Europe's cultural and scientific heritage from prehistory to the modern day. Digital libraries of other cultures of the world can be found on the Internet (Athena, Hispana, Hellenic Aggregator etc).

Chapter 3 **: State of Art**

3.1 Introduction

At archaeological sites around the world, archaeologists and anthropologists rarely find intact artifacts. The majority of ancient relics are found shattered into small fragments and much work is spent studying individual fragments and trying to find correlations between the fragments. In these pursuits, they typically examine the geometry of the fragment and match -among other features- the geometry of a given fragment against a set of candidate fragments that are hypothesized to match.

During the past decades, the reconstruction process was manually carried out in the excavation sites by archaeologists who may have spent many hours assembling broken artifacts by hand. Given the fact that the reassembly of fragments was a particularly time-consuming process, especially when fragments were irregularly shaped and uncolored, and required experienced staff, it wasn't always implemented in all archaeological sites. As a result, various excavation materials were left unused and stored for future research.

The 3D digitization of fragments has facilitated the reconstruction process and has replaced most of human labor. 3D digitization of cultural heritage is the first step of the overall process of the complete recording of objects and monuments. Systems have been proposed to first acquire 3D surface scans of the fragments and then use computer algorithms to solve the reconstruction problem. Automated reconstruction systems working from large databases of digitized fragments can now uncover numerous partial or complete reconstructions of artifacts that may have been excavated during different years of the same site, or possibly from different sites altogether. In this way, reconstruction systems not only save researchers time but, given a sufficient database of fragments, also have the capacity to reconstruct artifacts that would have otherwise remained as an incoherent pile of disjoint fragments (Willis & Cooper, 2008).

3.2 Previous work

The problem of reassembly of three-dimensional broken objects has represented a challenge that has been studied for many years and different methods have been developed introducing different solutions. The development of automatic reconstruction systems attempts to solve real-world geometric puzzles and therefore facilitate the work of archeologists. Most of the methods that have been developed are based on the geometry of fragments, since it is the most important restriction to be preserved. These systems should not only be capable of finding matching fragments but also of solving an unknown number of multiple puzzles where all the pieces are unorganized and mixed as well as some parts may also be missing. Providing also an effective representation of geometric data is also an important factor to be taken into account.

A first approach facing the problem of fragmented object reconstruction was the automatic solution of jigsaw puzzles. The familiar two-dimensional jigsaw puzzle's objective is to fit the irregularly shaped pieces together in order to reconstruct the original picture that is given. With some practice, a person can develop techniques

which reduce the time required to assemble a complete puzzle. Standard toy-store jigsaw puzzles obey certain rules that make the problem more tractable that it would otherwise be. Standard rules include: (1) the puzzle has a rectangular outside border; (2) pieces form an overall rectangular grid so that each interior piece has four primary neighbors (left, right, above and below); and (3) pieces interlock with their primary neighbors by tabs, consisting of an “indent” on one piece mating with an “outdent” on its neighbor.
The difficulties are encountered when one attempts to program a digital computer to solve jigsaw puzzles. The difficulties are related to three different aspects of the problem: (1) the description of the pieces (encoding and classifying); (2) the manipulation of the pieces (rotating and matching); (3) the evaluation of the “correct fit”. If the pieces of jigsaw puzzle are turned over so that the picture information is unavailable, the assembly of the puzzle becomes considerably more difficult. In this case, techniques for solution must rely entirely on shape. Puzzle of this type will be referred to as *apictorial* puzzles. The *apictorial* jigsaw problem has two main difficulties. One is combinatorial: there are a very large number of ways that pieces can be assembled. The other is geometric: it is difficult to detect if a pair of complementary pieces really match. When solved by hand, a person can usually feel a snap when making a true match, but scanned piece shapes are not precise enough for such a determination. The contours of the pieces provide a critical factor in determining whether two pieces could be placed next to each other in the constructed image

The problem of solving a jigsaw puzzle with a computer was first proposed by Freeman and Garder in 1964, who declared it as a problem in pattern recognition. However, it is only in recent years that significant advances have been made in automatically solving large puzzles. A new algorithm for automatically solving jigsaw puzzles by shape (Goldberg et al., 2004) was introduced and followed the rules of common puzzles. This algorithm first assembles the border and then fills the interior pieces. Given the fact that the matching of two pieces occurs only in a part of the side and not on the whole, it is essential a partial matching to be made and the boundaries of each side of the pieces to be defined. The technique fits a piece into a pocket not by independent pairwise fitting with top and side, but by fitting it into the embedded partial solution, thus allowing for any number of neighbors around the pocket. The algorithm uses fiducial points (specifically the centers of ellipses fit to the indents and outdents) to find the best translation and rotation of a piece to match a pocket. The distances of these points between the two pieces that match, should be equal points.

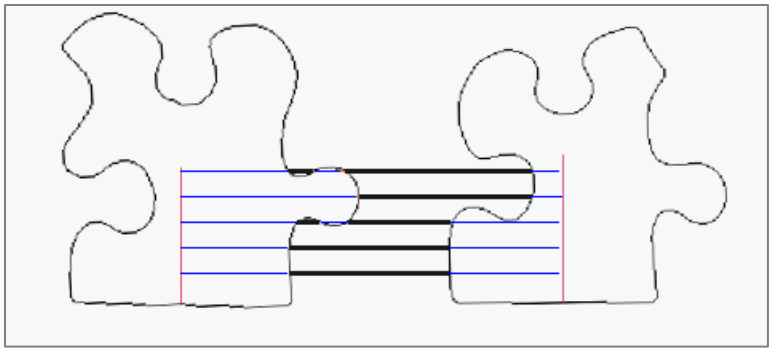

Figure 3-1: For pieces that fit perfectly, the lengths of the bold parts of horizontal lines should be equal

First the order of the border pieces is found which define the outline of the puzzle. Each border piece has a right and left side, unambiguously defined by orienting the piece with its straight side down. Subsequently, it continues by placing each interior piece in an unfilled piece location if it is adjacent to at least two existing pieces.

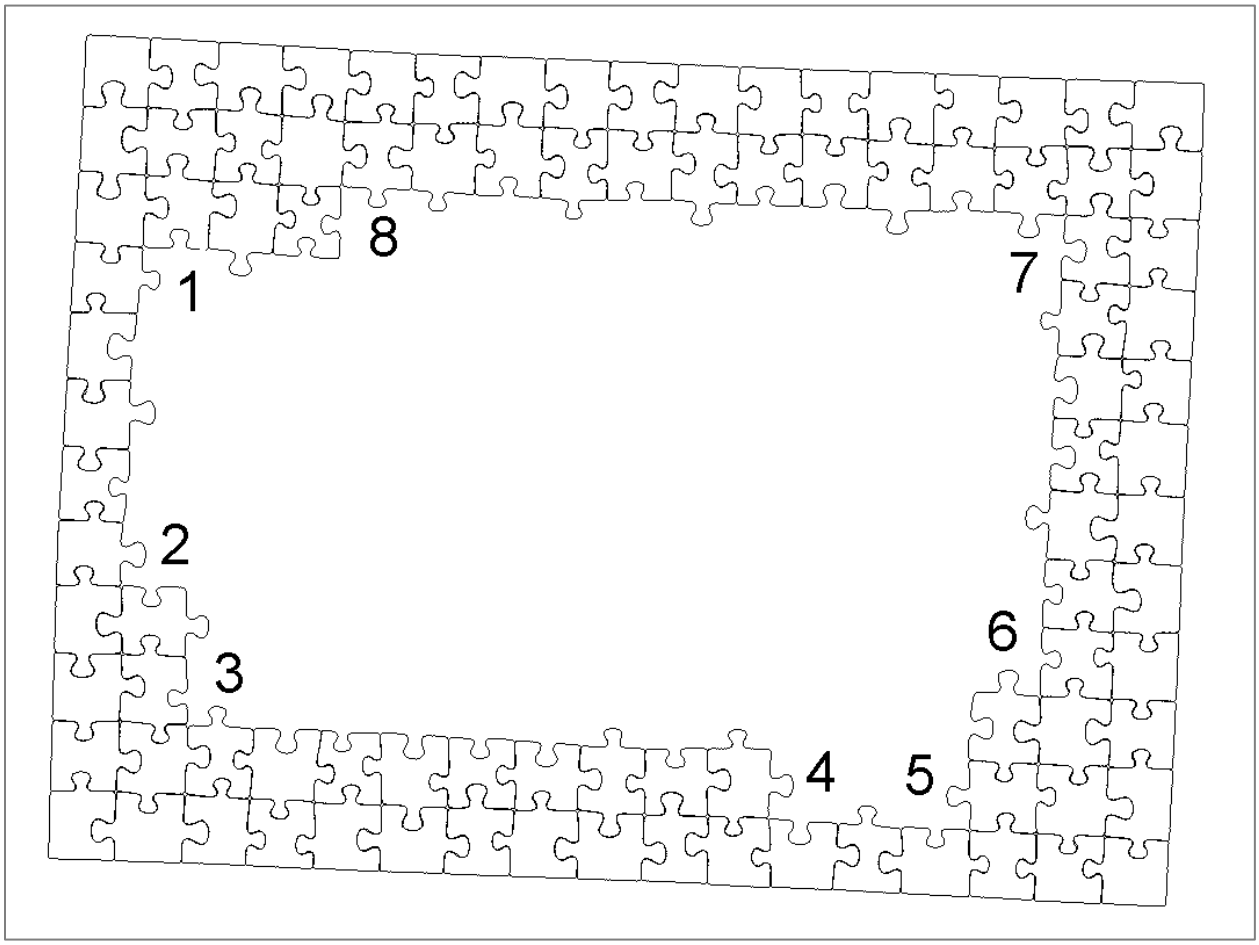

Figure 3-2 : There are 8 eligible pockets at this step.

The problem of reassembling real-world archaeological puzzle pieces is more difficult than assembling commercially produced jigsaw puzzles. Fragments are irregular and

can match along any subset of their complete boundary. Additionally, they introduce a vast variety of possible sources of confusion. Some of these include: (1) physical degradation of the fragments; (2) the number of puzzles being solved may not be known; (3) fragments may be missing as they may have yet to be discovered or may have been destroyed by some physical phenomenon.

An approach for reassembling archeological fragments is through the techniques of matching facing outlines of ceramic pot fragments. Archaeological pottery is assumed to be rotationally symmetric since it was made on a rotating plate. Respecting this property, an algorithm was introduced (Kampel & Sablatnig, 2004) for matching candidate fragments, which consists of a translation along the z-axis with parameter T_z and a rotation around the z-axis with parameter R_z. The basic concept in the method for estimating R_z is that the best fit is likely to occur at the relative pose which minimizes the point-by-point distance between the facing outlines.

The algorithm was applied by the utilization of a synthetic pot that consisted of five parts, one rim and two wall fragments, which lead to the following matching possibilities:

1. Rim fragments: First T_z is computed by aligning the rim along the orifice plane. Next R_z is estimated, so that the positioning transformation with the smallest matching error is considered to be the correct position.
2. Bottom fragments: first T_z is computed by aligning the bottom along the base plane. Next R_z is estimated in the same way as for rim fragments.
3. Wall fragments: Candidate parts are first aligned along their profile sections. Next R_z is estimated in the same way as for rim fragments. Since it is not clear whether a new candidate fragment is in bottom up or bottom down position, we have to compute R_z and T_z for both positions. The positioning transformation with the smallest matching error is considered to be the correct position.

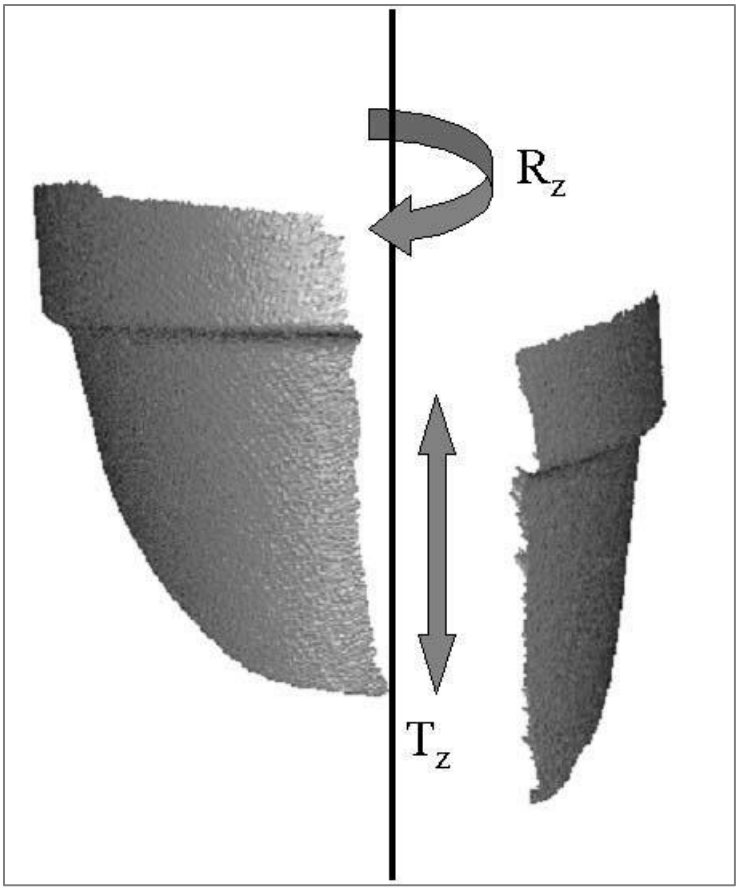

Figure 3-3 : Fragment matching with rotational symmetry.

Matching algorithms of outlines are also applied in more general problems with 3D data, which provide solutions to problems of six degrees of freedom. For two arbitrary objects, assuming a fixed distance between their initial centers, one need to define six degrees of freedom in order for each model to be able to rotate arbitrarily around the three axes of its local orthogonal reference system.

A first approach of automatic 3D reconstruction was based on the underlying assumption that the fractured faces were nearly planar and they matched each other completely (Papaioannou, Karabassi, & Theoharis, 2002). The method focuses on the surface geometry so that the matching and alignment of parts is performed directly through the plane between two arbitrary fragments. Using a projective space as well as GPU depth maps analysis, the original object is reconstructed. The basic concept of this method is that, given two 3D models, the best fit is likely to occur at their relative pose, which minimizes the point-by-point distance between the mutually visible faces of the objects. For this reason, an error measure of the complementary matching is introduced and computed between two object parts at a given relative pose, based on this point-by point distance.

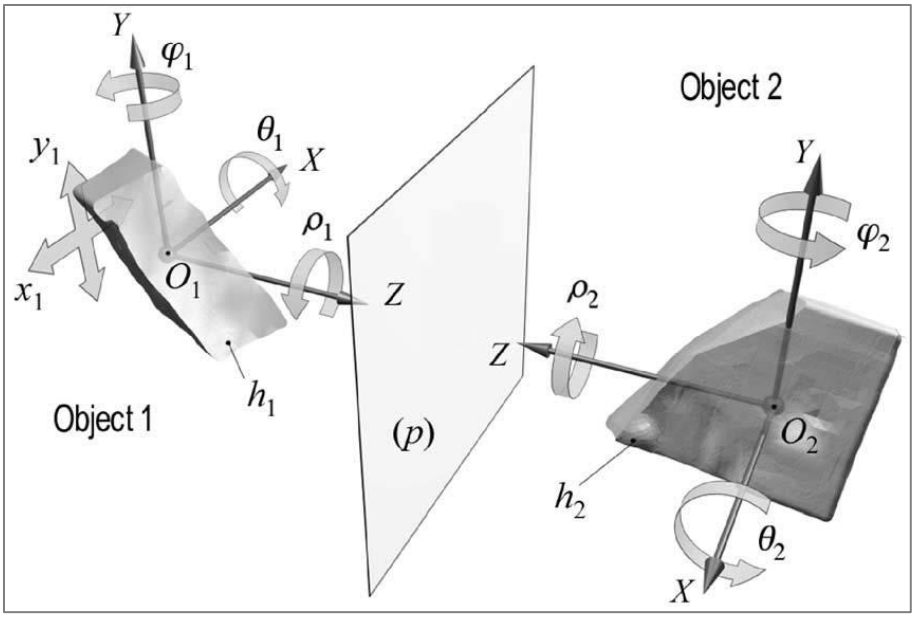

Figure 3-4: Relative pose of the two meshes during the matching process

This matching error is minimized, employing a standard global optimization scheme, to determine the relative positioning of the two fragments that corresponds to their best complementary fit. During the automated assembly, it is assumed that the two object parts can be rigidly attached to one another without having to penetrate each other's surface. For instance, the method cannot be used to connect two links of a chain. The method was tested on the digitized models of real fragments.

For the distance calculations, the reference plane (p) is considered as the view plane and the z-buffer algorithm is exploited. The z-buffer algorithm produces a two-dimensional buffer (the z-buffer or depth-buffer), whose dimensions match those of the view plane. Each value of the z-buffer represents the distance between a pixel on the view plane and the corresponding point on the object, which is closest to the view plane. Assuming that the view plane is parallel to the XY plane, the z-buffer values are the Z coordinates of the object points closest to the view plane. As a result, the two z-buffers, Z_1 and Z_2 are obtained, for each rotation, whose elements correspond to the distances.

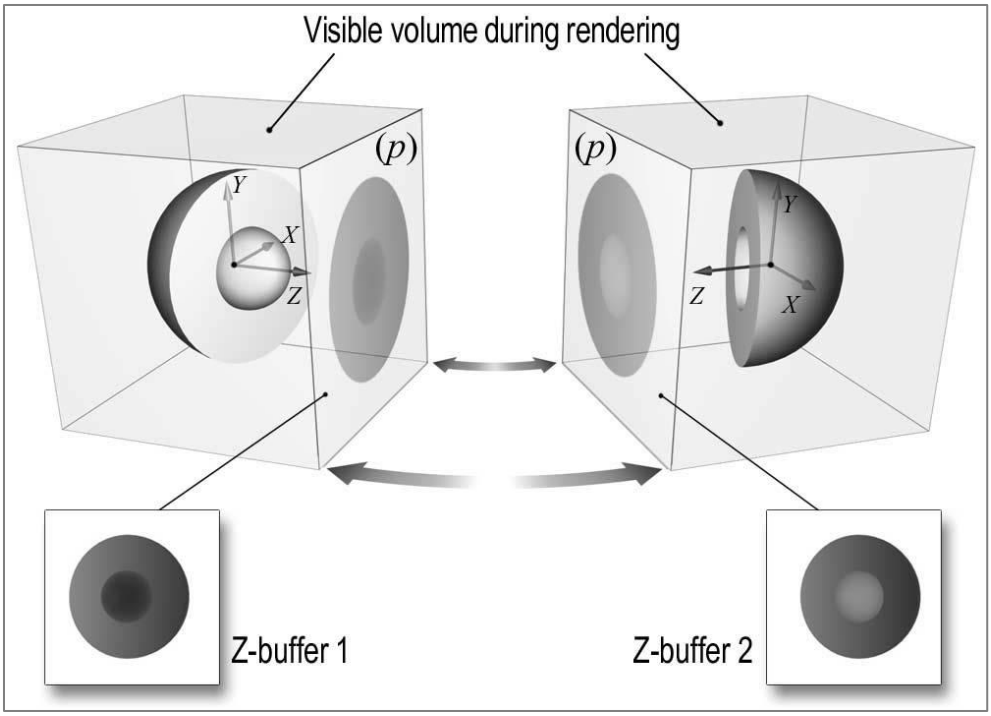

Figure 3-5: The use of z-buffer to calculate the point-to-point distances for the matching. The z-buffers for the two objects are shown at the bottom left and right.

A global registration technique applied to archaeological fragments reconstruction was later proposed (Belenguer & Vidal, 2012) in order to validate further improvements of previous techniques and for performance comparisons based on the Graphics Processing Unit (GPU) Depth Maps technique. The technique takes, as input data, a set of geometric representations of broken flat fragments, and finds the best rigid transformation that maximizes the contact area between them. The fragment characterization is also determined based on a projection that was calculated through the graphics processing unit, and that reduces the complexity of the comparison between fragments. This method does not take for granted that the two broken surfaces perfectly match. The major contributions of the algorithm were: the 3D characterization of fragments based on projective depth maps, entirely calculated on the GPU, a hierarchical characterization of fragments and the ensuring of convergence, without stopping in local minima solutions.

A next method deals with heavily eroded fragments, whose fracture surfaces sometimes did not even touch each other (Koller & Levoy, 2006). In this approach, instead of using the geometry, reconstruction is done by matching incisions on the fragment's top surfaces. The method is divided into the three above stated categories:

I. The *automated boundary incision* matching technique searches for incised topography that corresponds across the boundaries between two candidate adjacent fragments. A preparation of the digital fragment representations for input to this algorithm is required; all of the incised features indicating their positions, directions, and feature type (such as rows of columns, text inscriptions, etc.) are manually annotated. The algorithm searches through all of the annotated fragments, considering each possible pair of fragments, and then considers each reasonable alignment of annotated features between the fragment pairs. Candidate configurations of two fragments are scored based on the alignment of the corresponding feature types, with the highest scores going to those proposed positions which have the highest number of strongly similar features that are best aligned. Fragment pairings with exceptionally high scores are output in a ranked listing for further review by an archaeological expert. This technique is used primarily to find joins between pairs of adjacent fragments.

.

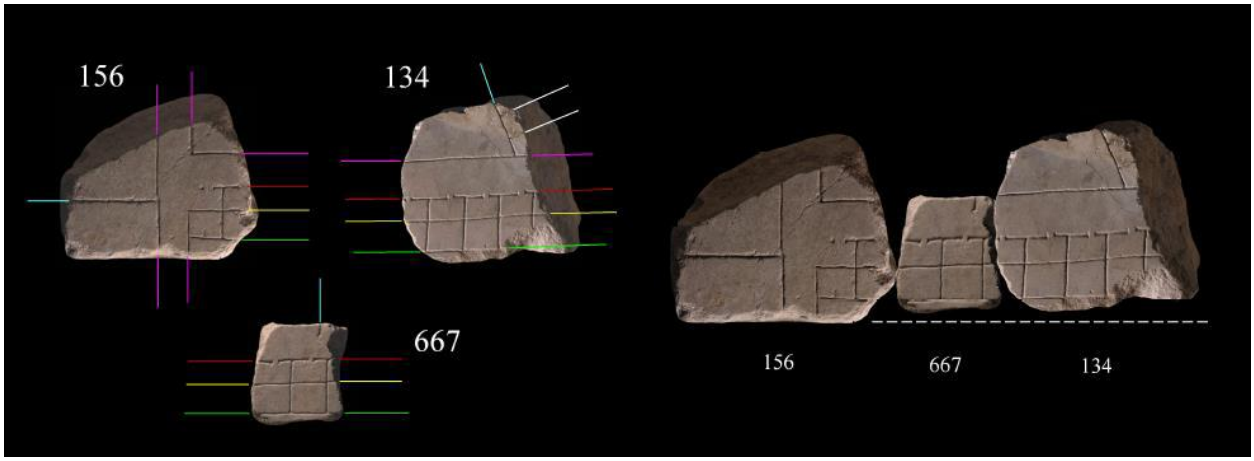

Figure 3-6: Fragments 156, 667 and 134 with their boundary incision annotations indicated

II. The *wall feature matching* is another algorithm that was developed to position fragments in specific locations on the map. The wall feature matching algorithm searches for correspondences between structural features of the fragments (slab edges, etc.) and matching remnants of these features on wall. For each fragment, the algorithm searches all of the possible positions on the wall, assigning a score for each valid position based on the quality of the geometric correspondence between the fragment's clamp hole locations and the pattern of

clamp holes on the wall. Valid fragment positions are further constrained such that slab edges must be in either a vertical or horizontal orientation. The top scoring fragment positions output by the computer algorithm are manually checked to verify their suitability in light of considerations beyond the simple geometric constraints of the wall features.

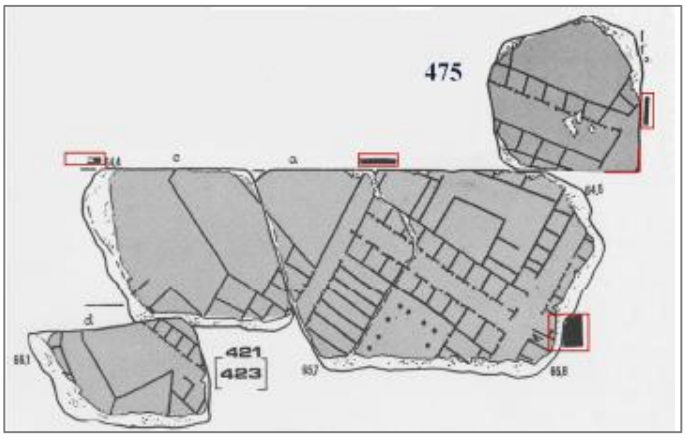

Figure 7: Proposed match between fragments based on geometric constraints

Figure 8: Detail of the interface between fragments 421b (bottom) and 475 (top) in the proposed position.

Another automated fragment matching technique that was developed for aiding reconstruction is *multi-variable clustering*. The goal of the clustering algorithm is to identify new pairings or groupings of fragments which may not have explicitly corresponding incisions, but may share other common characteristics including fragment thickness, marble veining direction, axial direction of the incised architecture, presence and orientation of slab edges, and the back surface condition of the fragments (rough, smooth, or unpreserved). The algorithm searches through the database of digitized and annotated fragments, and assigns high scores to those groups of fragments that have a high degree of correlation based on these fragment properties. The clustering procedure can also be used in a more interactive mode, by searching the database for fragments that meet the constraints posed by a user in a specific query. Such a query might be of the conceptual form, "list all of the fragments that have thicknesses in the range 55 - 60 mm and have a veining direction in the range 30 - 45 degrees relative to a slab edge.". This capability allows researchers to quickly focus on a suitable subset of fragments when experimenting with possible reconstructions.

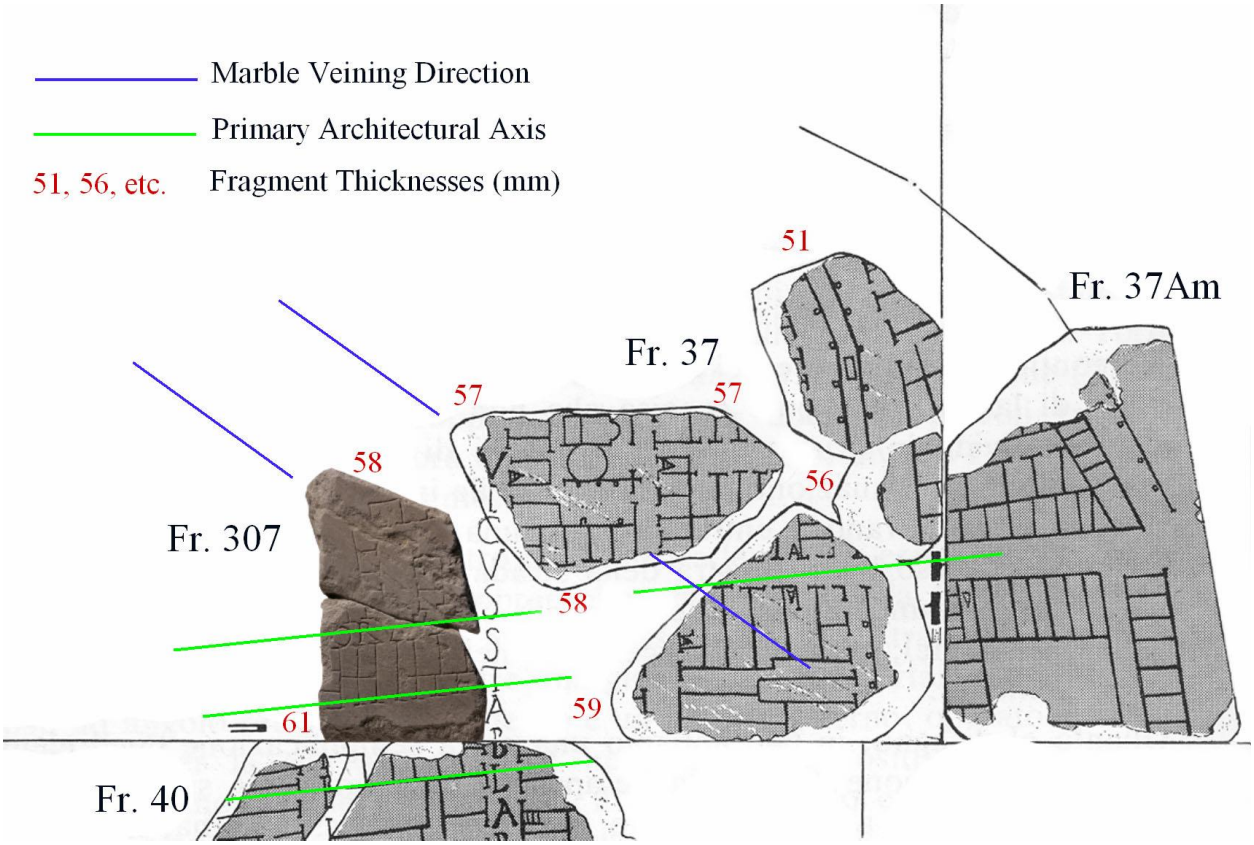

Figure 9: Fragment 307 in a candidate position determined by multi-variable clustering with other fragments

A technique presented afterwards can deal with arbitrarily shaped fracture faces, and with partial matches (Huang et. al.,2006). The algorithm automatically reassembles solid objects by first identifying fractured regions, and then generating clusters of feature patches for alignment-based matching. In the first step the fragments are automatically segmented into a set of faces bounded by sharp curves. By examining the roughness of the face surfaces, the faces are additionally classified into original faces, which come from the boundary surface of the unbroken object, and fractured faces, which were created when the object broke. This segmentation increases the robustness and efficiency of the subsequent matching algorithms in two ways: (1) in the reassembly process of a 3D object only fracture faces can be matched (at least partially) against each other, and each face provides a natural grouping for a set of matching features on the surface of the fragment. Matching pairs of faces instead of considering the entire fragments, therefore, results in a more stable and faster matching algorithm. (2) the robustness of the matching algorithm can be increased by enforcing the consistent alignment of the original faces in the reassembled model.

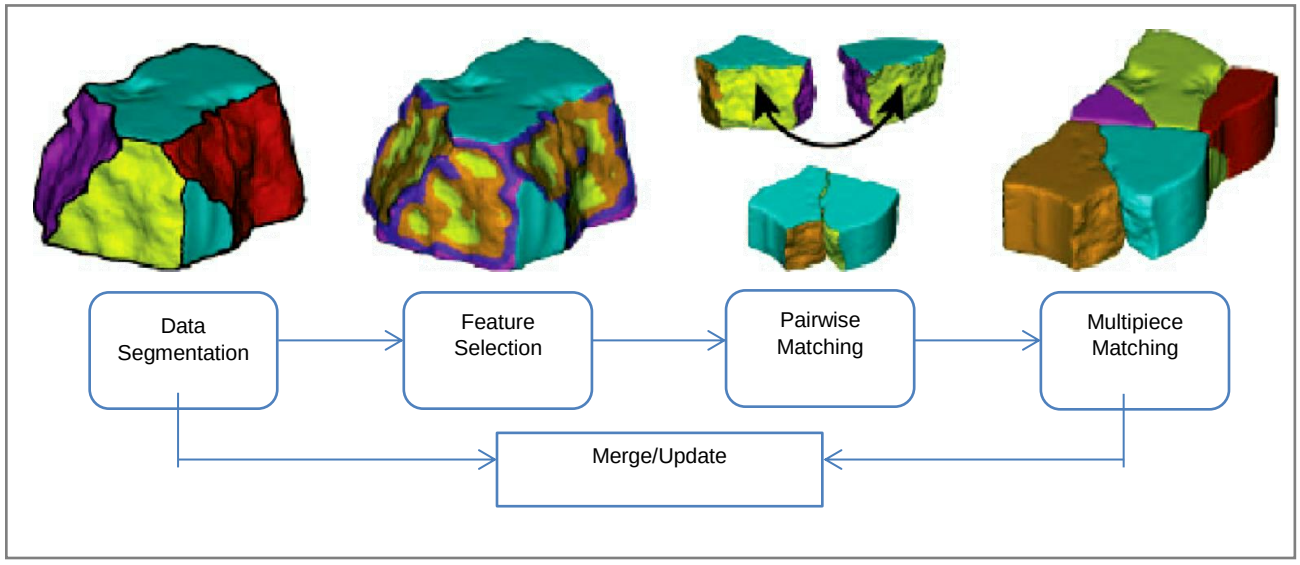

Figure 10: Overview of the algorithm

After the segmentation step, a novel type of patchbased surface features is computed, called “feature clusters” and use these features to match all fracture faces pairwise. There are several differences between this algorithm and prior feature-based matching work: (1) patches are used instead of points as features, (2) the features of patches are allowed to overlap, and (3) the overlap structure verifies potential feature correspondences. It can also find all potential matches between pairs of faces and then verify each match using several consistency checks.

In many cases, pairwise matching is not enough to reassemble the complete 3D object since some of the matches may be incorrect. Additionally, small errors in pairwise matches can accumulate gradually resulting in the fragments not fitting together, where pairwise matching alone is not enough to guarantee that the beginning and end of the chain of fragments will match without penetration. It is necessary therefore that all matching fragments that have been found so far undergo a simultaneous local registration to find a consistent set of matching faces and mutual fragment positions such that they do not penetrate each other. The multi-piece matching is also necessary since some pairwise matches have a better chance to be found and verified after previously found matches were precisely registered onto each other and merged together.

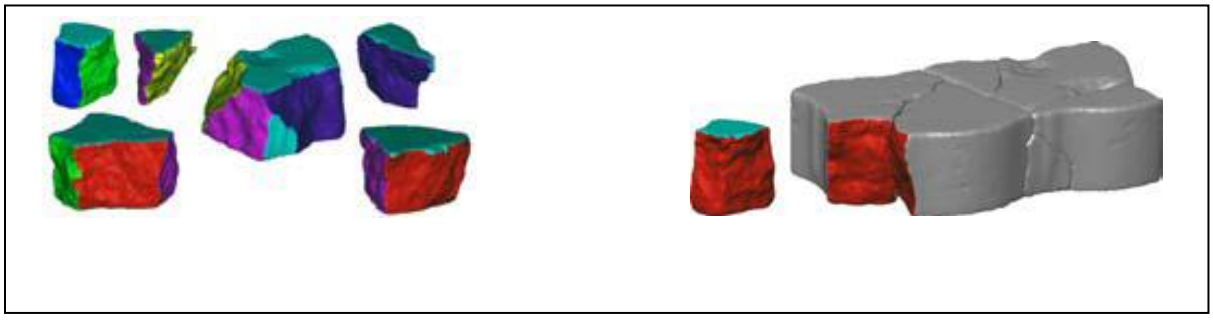

Figure 11: The sixth piece has a better chance to be matched after the first five have been matched and simultaneously registered.

One of the works that exploited the edge of a geometric object to match three dimensional fragments and offered an automatic system for computer-aided documentation and reassembly of wall paintings, exploits the orientation constraints of flat fragments to achieve a simple, fast matcher (Brown et al., 2008). Although the matching is based on 3D edge geometry, the algorithm takes advantage of the fragments' flat front surfaces to limit the search space to planar transformations. A brute-force approach is to select a pair of points on the two fragments, compute an initial alignment based on the points and their normals, run ICP (constrained to a planar transform) to recover a candidate matching alignment and error, and repeat the process for points distributed around each fragment.

With the assumption that each mesh is constituted of only fragment's edges, which is called a "ribbon," and these ribbons have regular sample spacing, each ribbon vertex can be indexed by row and column. Now the correspondences are completely determined by the regular sample structure, and all that remains is to compute the alignment and associated error. The overlap region is then shifted by a single sample, and the process is repeated. The proposed technique analyzes exhaustively every possible alignment of a pair of fragments in a few seconds.

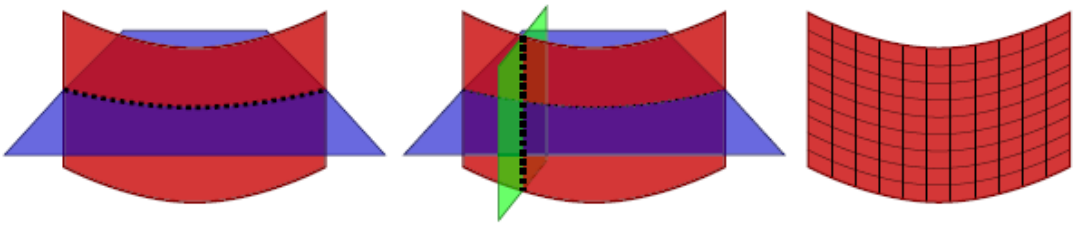

Figure 12: To efficiently compute fragment matches, we regularly resample fragment edges into a "ribbon." A contour is extracted at a fixed offset from the front surface (left), then each sample is extruded vertically in a plane defined by the contour point's smoothed normal (center). Ribbon points are arranged in a grid (right), allowing efficient computation of correspondences.

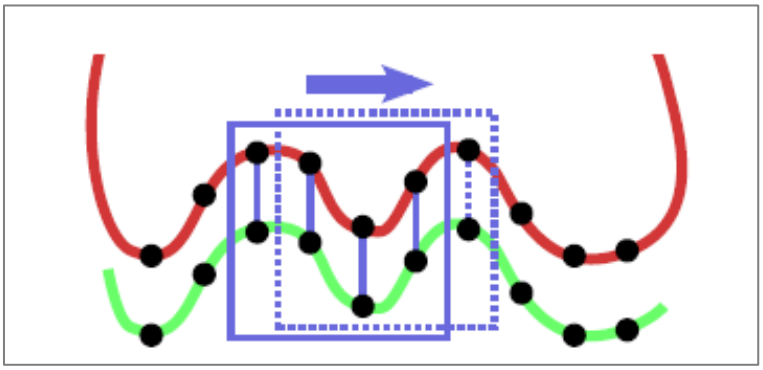

Figure 13: A strip of samples on each ribbon is used to compute a candidate alignment. Then, the overlap region is shifted one sample and a new alignment is computed incrementally in constant time.

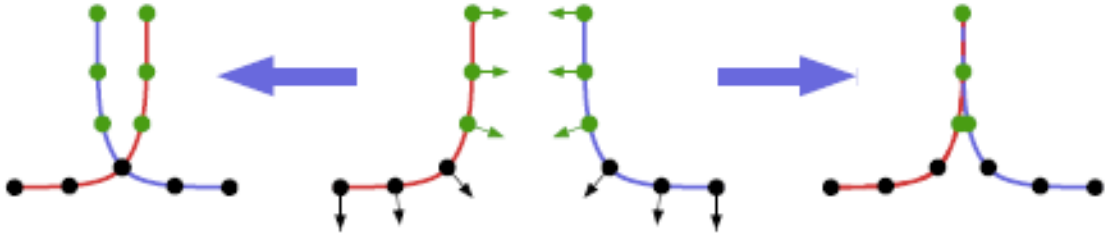

Figure 14: Using all corresponding point pairs on the red and blue curves yields an incorrect alignment (left) because the black points are on eroded portions of the edge. Using only the green points, whose normals' z-components are opposing, yields a correct alignment (right).

An efficient solution for the automatic reconstruction of three-dimensional wall-paintings was later (Papaodysseus et al., 2012) introduced which defined the dataset through the surfaces of the upper, lower, sides, and the central axis of each fragment. In order to get an accurate match, a rotation of the fragment on its central axis was performed at a very small angle around the fixed fragment, which was selected randomly. At the same time, the probability of contact between their surfaces was determined.

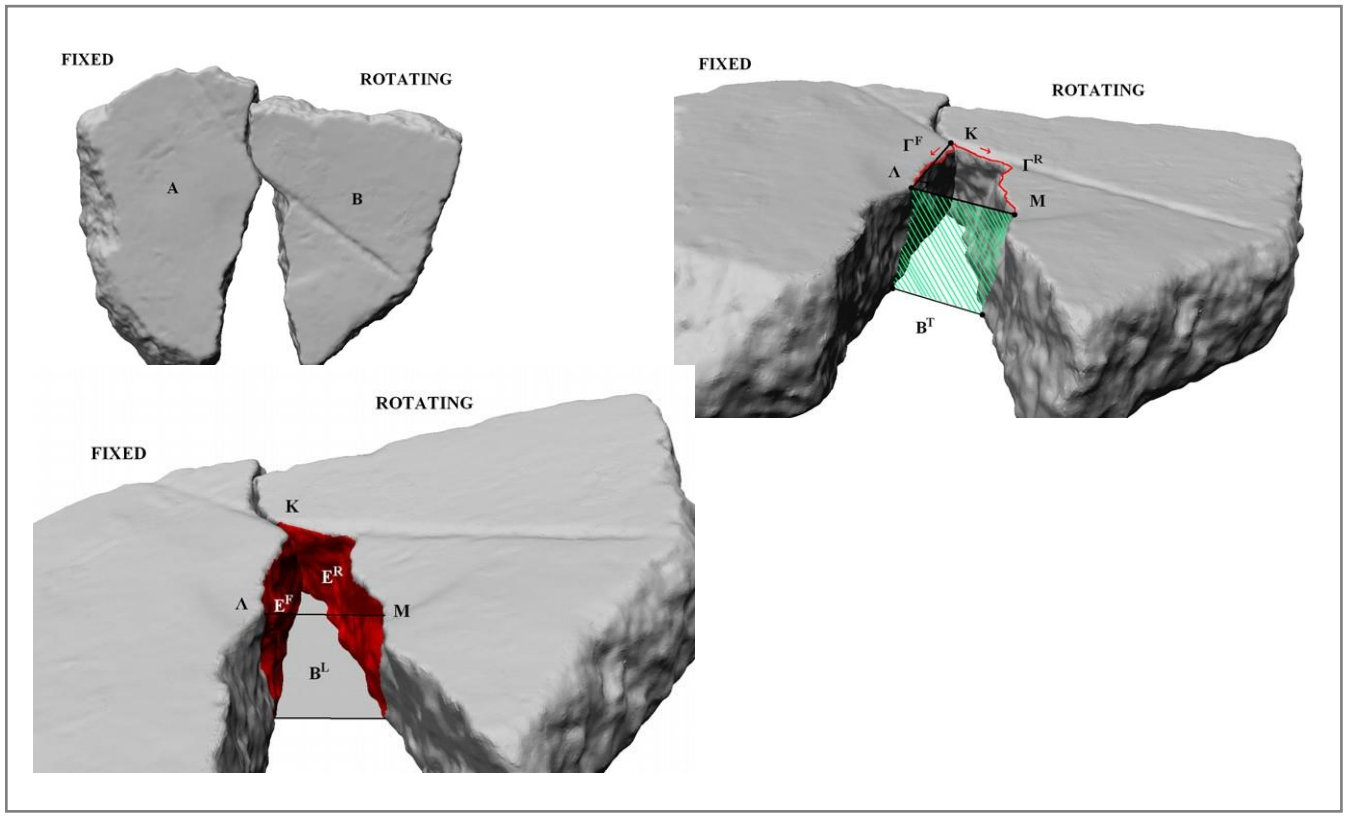

Figure 15: Fixed and rotating fragments' pair relative placement and definition of the contact sub-domain. (a): Proper relative placement of a pair of fragments tested for matching. (b): Fragments pair's terminal barrier plane and the obtained contact curves, Γ^F for the fixed chain and Γ^R for the rotating one. (c): Determination of the fragments pair contact surfaces, E^F on the fixed and E^R on the rotating fragment

There are four criteria applied in each placement to test the matching: (1) the first involves examining the relative lengths of the curves of the upper surfaces to the joint between two fragments that were potential matching for the purpose of reaching a

suitability match, (2) in the second, the overlap is prevented in the connection between the fixed fragment and the fragment that revolved around, through the use of a threshold, (3) the third deals with the geometry of contact surfaces, with the maximum allowed volume of the domain, (4) the last criterion associates the length of the contact curves between the two fragments that had a potential matching, and the matching was achieved when the volumes of the fragments are less than the threshold that has been estimated previously. The proposed method was applied to the 41 fragments and in some cases a success rate reached a percentage of 100%.

Another interesting approach was introduced for the 3D reconstruction of fragments and focused on the assembling of thin shards, which cannot be converted to 2D problem (Zheng, Huang, Li, & Wang, 2014). Instead of the curvatures and torsions, the approach is based on establishing a local Cartesian coordinate at every point of the 3D contour curves. Unlike other current methods, this work doesn't rely on any assumption of known geometry of original objects. For that reason, the initial alignment accumulates many errors and in order to be avoided, a global refinement method is introduced to adjust these errors and improve the reassembling accuracy.

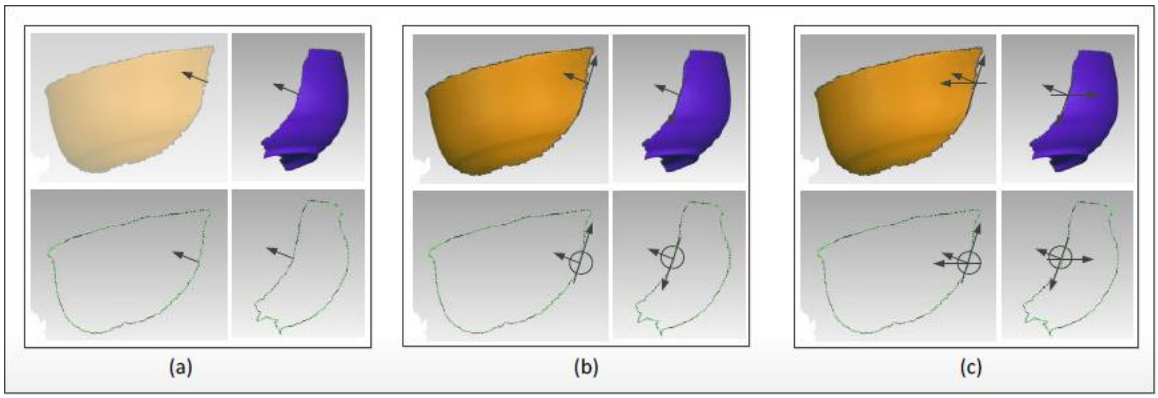

Figure 16: Establishment of the Local Cartesian Coordinates

First of all, the 3D meshes of the fragments are acquired by a structure-light based method, with the corresponding 3D contour curves extracted from the outer boundaries. Then the contour curves are matched and aligned to each other by estimating all the possible 3D rigid transformations of the curve pairs with the defined local Cartesian coordinates, and then the maximum likelihood rigid transformations are selected. In order to adjust the alignment errors effectively, a least square method for globally adjusting the alignment errors is followed which eliminates the nearest point pairs when their distance is larger than a given threshold. The adjusted rigid transformations is checked, if their variations are all small enough in comparison to the last iteration ones

and the procedure is finished. The results of experiments showed that this approach cannot only match and align fragments but also improve the accuracy on a large scale.

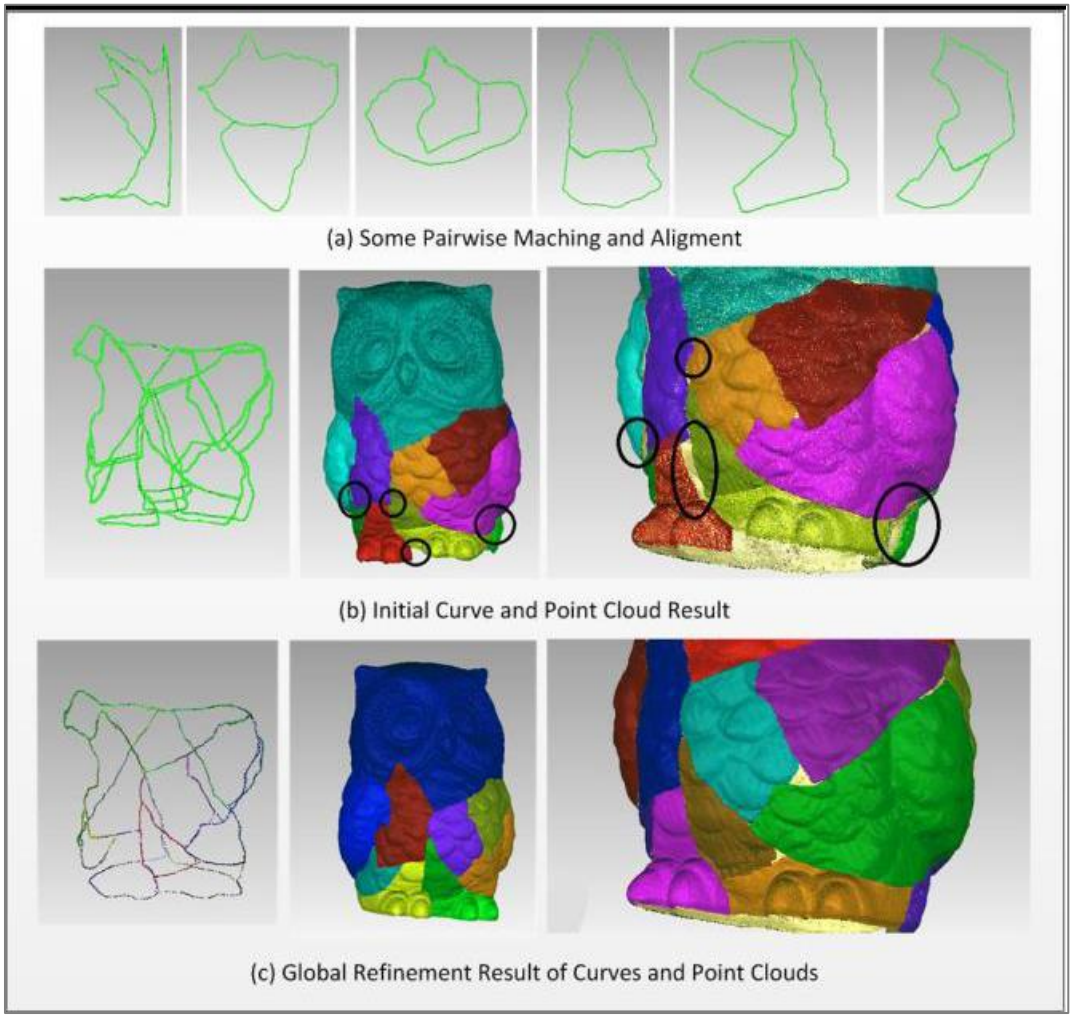

Figure 18: Results of data, where reassembling accuracy reaches 0.47 mm

A more advanced approach for the reassembly of general 3D objects avoids the complexity of previous approaches by using general, robust and well-understood geometric matching methods. An automatic solution of the problem, where an efficient and generic three step minimization scheme, that uses a coarse-to-fine search strategy in order to partially address noise and outliers, is used for the underlying global optimization (Mavridis, Andreadis, & Papaioannou, 2015).

Firstly, a set of potentially fractured facets from each one of the input fragment is extracted and then the matching score is calculated. The matching score is based on the residual distance between two fragments after their rigid registration, which is performed using a three-level coarse-to-fine search strategy. Then the optimal set of pairwise connections is computed, with the additional constraint that the selected

connection should not create geometric penetrations. When a penetration is detected, the corresponding candidate alignment is rejected. In some cases, this procedure might not lead to the desired reassembly. For this reason, the user can also manually include or exclude graph edges from the solution.

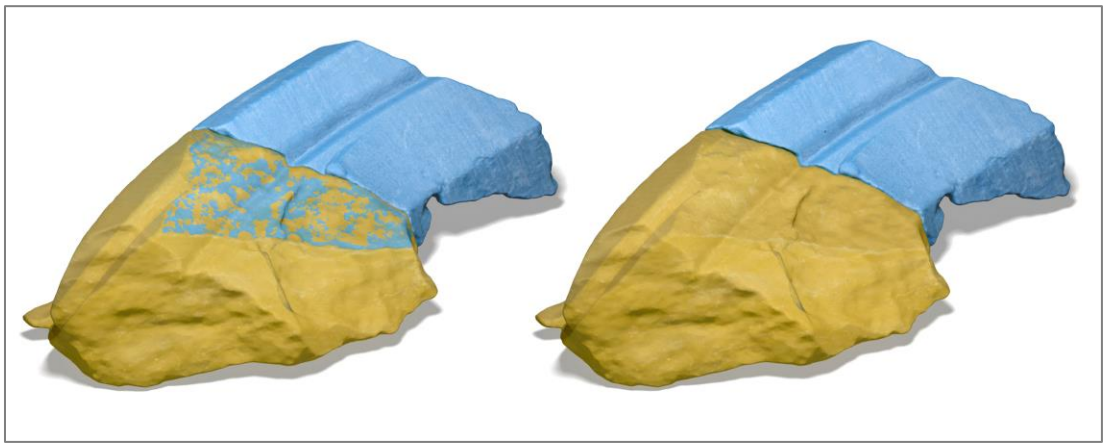

Figure 19: Left: Unconstrained registration yields mutual penetrations of the source and target contact surface, which might be undesirable in object reassembly applications. Right: Inclusion of constraints for non-penetrating registration. To better illustrate the mutual penetrations, the fragment in front is rendered with transparency.

The resulting reassembly pipeline provides highly reliable alignment, as demonstrated through the reassembly of fractured objects from their fragments and the reconstruction of 3D objects from partial scans.

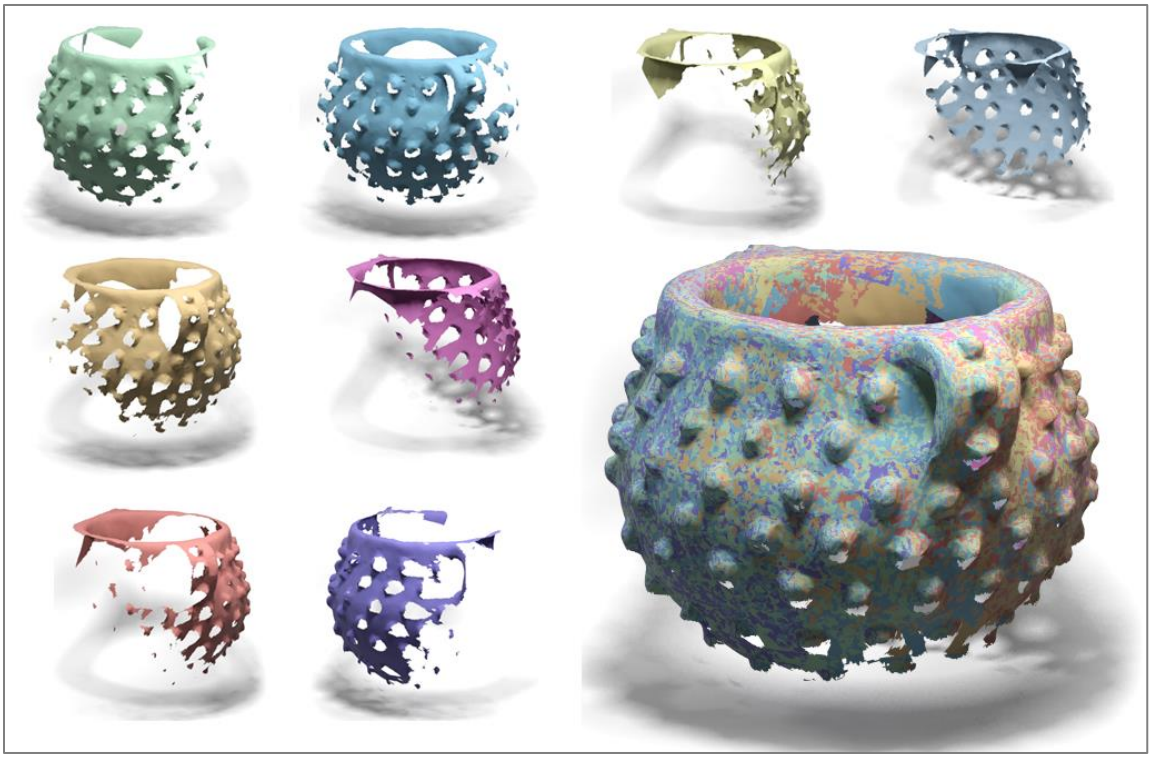

Figure 20: Reconstruction of an object from partially overlapping scans. The insets show the input partial scans in their final aligned position. The initial position of the scans does not influence the registration results.

A final approach, based on the previous one, for the digital reconstruction of cultural heritage is a generic user-guided method which operates directly on generic 3D objects (Papaioannou, & Mavridis, 2015). The methodology followed for geometric registration automatically solves cases, where fragments share good contact area and provides useful tools for the hard cases, where contact area is unusable, small or absent.

The first step is to extract facets from scanned fragments with the use of a segmentation algorithm. The reassembly problem is solved with a three-tier geometric registration approach:

I. An automatic process finds all matching fragment pairs sharing a significant contact surface, given the complete list of fractured facets per fragment, using the coarse-to-fine search strategy of the previous algorithm that is both efficient and robust.
II. A semi-automatic process guided by the user that targets the registration between fragments with significant erosion or large missing parts, i.e. pairs sharing minimal contact surface, where contact surface-based registration approaches fail. Given the matches and respective matching errors generated in the pairwise alignment stages, in this step of the reassembly, a set of fragment

clusters is computed as well as corresponding global transformations of the fragment meshes.

III. The method essentially locates the best candidate planes of symmetry on the object and the user can fill the missing geometry. So in this step, the missing geometry of an object is generated and then is used to match and align any disconnected fragments.

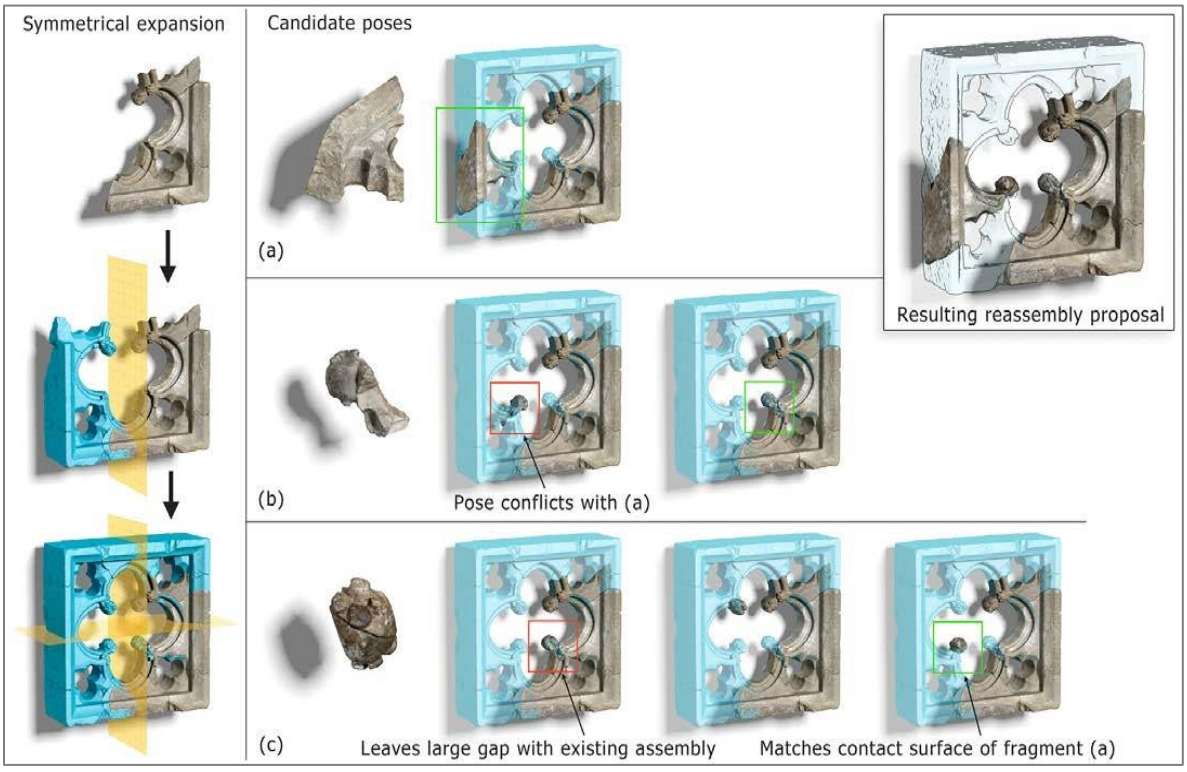

Figure 21: Third tier registration: Symmetry-based fragment registration. Left: using the partial reassembly, we extract a symmetrical expansion of the object. Middle and right: Potential candidate poses for the disjoint parts (a), (b) and (c) are generated and filtered to result in the final reassembly of the object.

In this interactive method, the user determines every stage of the reassembly and can evaluate the results, when there is no sufficient information for an automated procedure. This manual intervention occurs only at large iteration cycles of the method and does not require constant feedback.

Chapter 4 : Strasbourg’s Project: Description of data

4.1 Introduction

The effective documentation and display of ancient artifacts and antiquities is an essential task in the field of cultural heritage conservation.

Before the recording of an object, it is important to study the environment in which it is located and the very nature of the object (building materials, architecture, form, etc.). When the subject of the documentation is a monument, it is necessary that a cognitive background of history exists, but mainly of its architecture, so to better assess the specificities of the object and therefore the most appropriate and suitable methods to be selected. Moreover, Documentation and Conservation of Cultural Heritage is a concept that includes the collection and presentation of all those elements - historical, architectural, bibliographic, and geometric - that describe a monument.

The introduction, recently, of modern information technology and survey instruments, has given a boost to the reconstructions of archaeological sites, above all thanks to the possibility of obtaining more and more accurate measurements, of organizing information in a better way, through the use of digital information systems and structured database and of reconstructing the monument as it was according to its original state in a virtual 3D environment that can be edited and upgraded at any time. In this case, the subject of study is the recording of remnants of an ancient sanctuary of the Pont-Saint Maxence in order to enable the virtual reconstruction of the exterior façade of the sanctuary. This required the implementation of measurements on the field using photogrammetry for the large blocks and a terrestrial laser scanner for the smaller ones. The main purpose was to collect dense point clouds in order to record all the details of the objects. A sample of nearly 100 blocks was collected and digitized.

Throughout the measurements with a terrestrial laser scanner, an enormous volume of data (points) is gathered, which, in order to be usable, should be subject to special treatment. The purpose of this process is to create a three - dimensional model of the object, which will describe clearly and correctly the surface and can then be used in further applications. The processing of such data is quite time consuming and requires special attention at all stages so that the result is satisfying at a certain time and with the software available.

4.2 Pont-Saint-Maxence Project

4.2.1 General Information

Pont-Sainte-Maxence is a commune in the Oise department in northern France, 30 km North of Paris. The city belongs historically to the region of Valois and its existence dates from the time of the Gauls, who were Celtic people inhabiting Gaul - what became present-day France - in the Iron Age and the Roman period (from the 5th century BC to the 5th century AD).

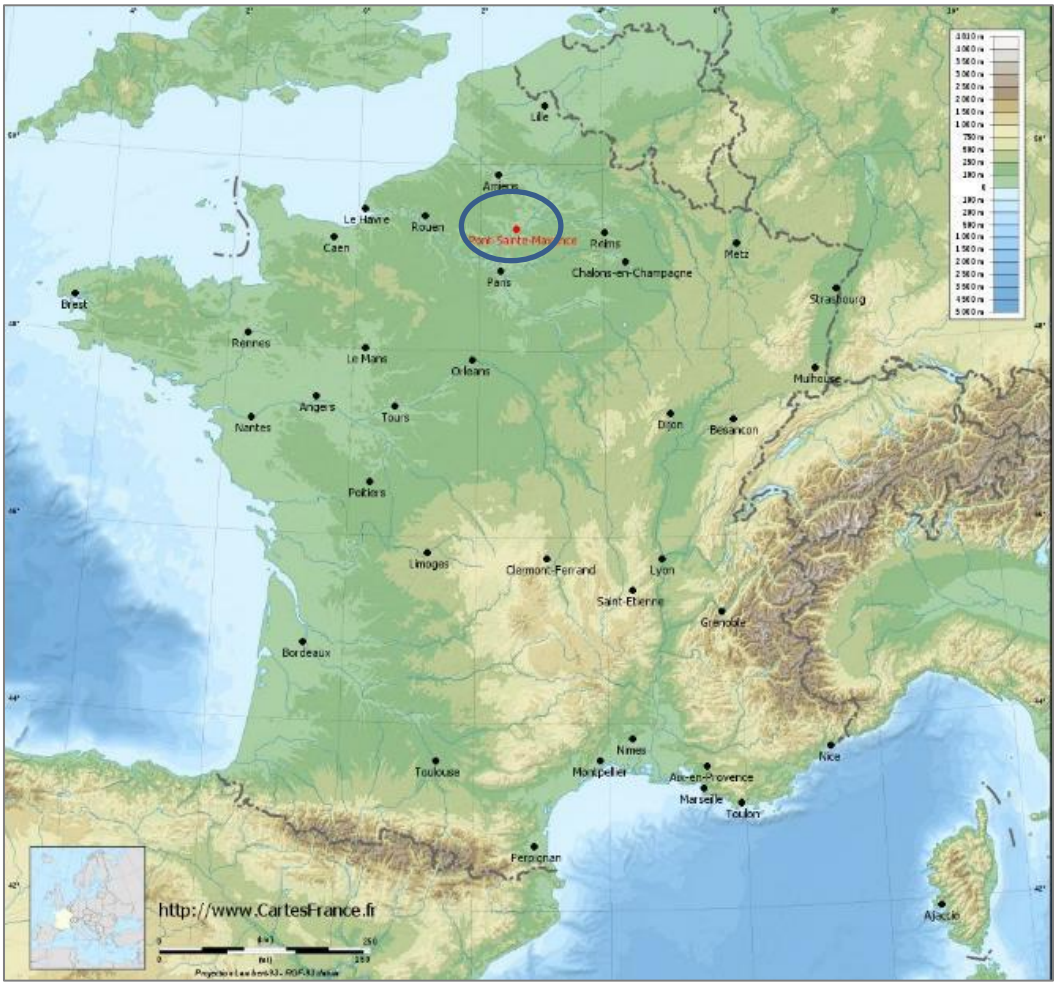

Figure 4-1 : Map of France - Location of Pont Saint Maxence

4.2.2 Sanctuary

In spring 2014, a team of archeologists of INRAP (French National Institute for Preventive Archaeological Research) discovered the remnants of a Gallo-Roman sanctuary, dating from the mid-2nd century A.D, when archeological excavations were conducted on a former football field in order to build a shopping center. The site of

Roman times is located along a Roman road, north of an ancient agglomeration which was probably at the same location of the current town of Pont Saint Maxence. The enormous sanctuary dates from the mid-2nd century A.D. During the excavations, nearly 500 blocks and 6000 fragments were recuperated and their arrangement in architectural sequence quickly made it clear that it was a facade that had brutally collapsed.

According to the elements provided by the responsible of the operation, the presumed entry of the sanctuary was made by a monumental facade of 68 x 105 m long and 9.50m high, exceptional dimensions in Roman Gaul. This sanctuary possessed two small pavilions at the rear of which only the foundations have been preserved. In the center, the “cella”, a substantial masonry platform, was accessible by steps in the front façade. The façade was pierced by an arcade with between 13 and 17 openings, topped by an entablature and an attic frieze that evokes the architectural style of triumphal arches. The frieze bore a dedication in bronze letters. This building had two states of decoration; a first stone, then a colored marble coating was affixed. The blocks and fragments of stone and marble revealed a sculpted decoration of high quality. Numerous fragments represented divine attributes or faces of the gods (Vulcan or Ulysses) which all had dramatic expressions evoking the unique pathos of Hellenistic statuary.

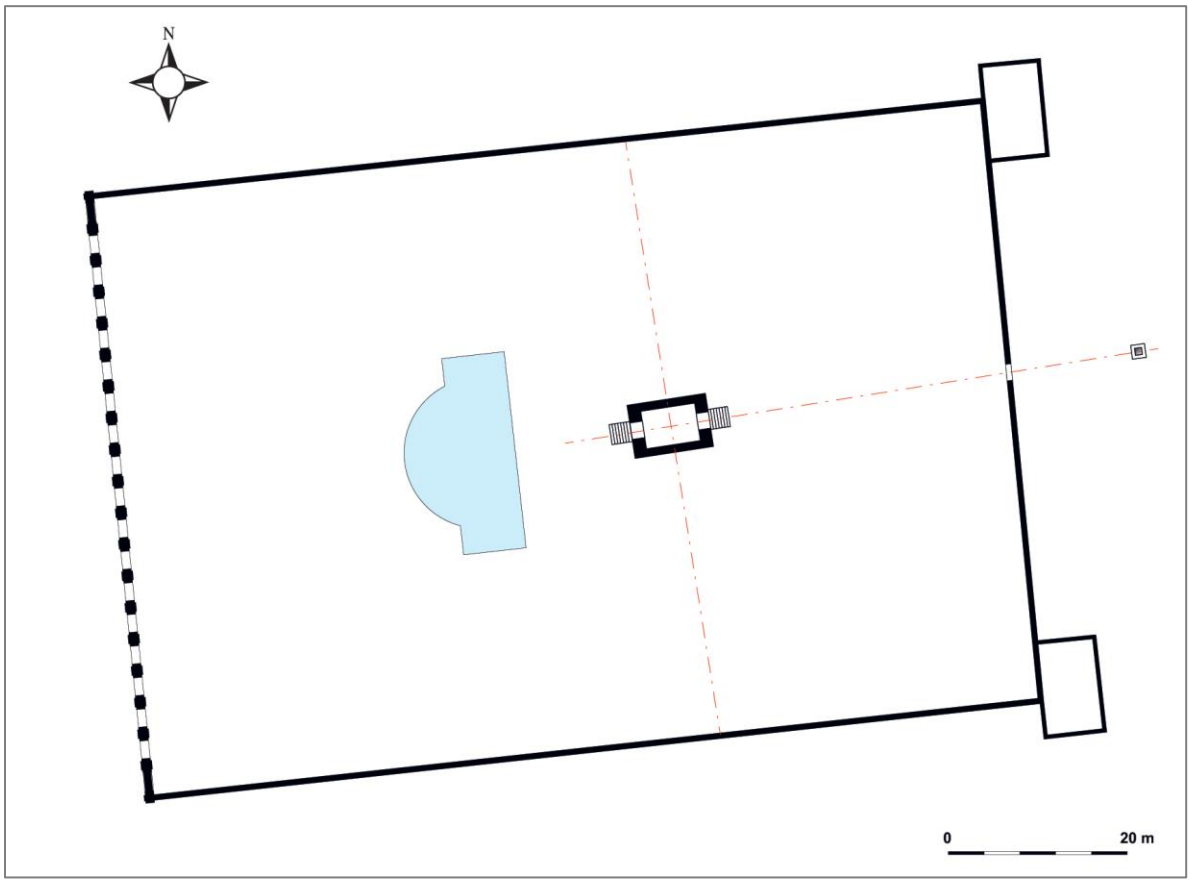

Figure 4-4-2: Map of the monumental state of the site

4.2.3 Hypothesis of Restoration

A few decades after its erection, the facade collapsed, practically in one piece – perhaps as a result of a fault in the foundations linked to the type and slope of the soil beneath – producing a chaotic mass of blocks and fragments. The 500 stone blocks and 6000 fragments discovered represent about 10% of the Roman façade according to the archeologists and among them a sample of 96 blocks was digitized. The methodical study of these fragments makes it possible to propose a reconstruction of the original state of the monument. Their location often corresponds to their position of fall, which orients and facilitates the reassembly. Therefore, a convention has been made that foresees the 3D reconstruction of the elements stated below that will give a complete aspect of the original facade as well as the 3D rendering of the facade in order to depict its fall.

- The entablature composed of 3 architectural elements; architrave, frieze and cornice
- An arcade
- The attic
- The summit heads and griffins

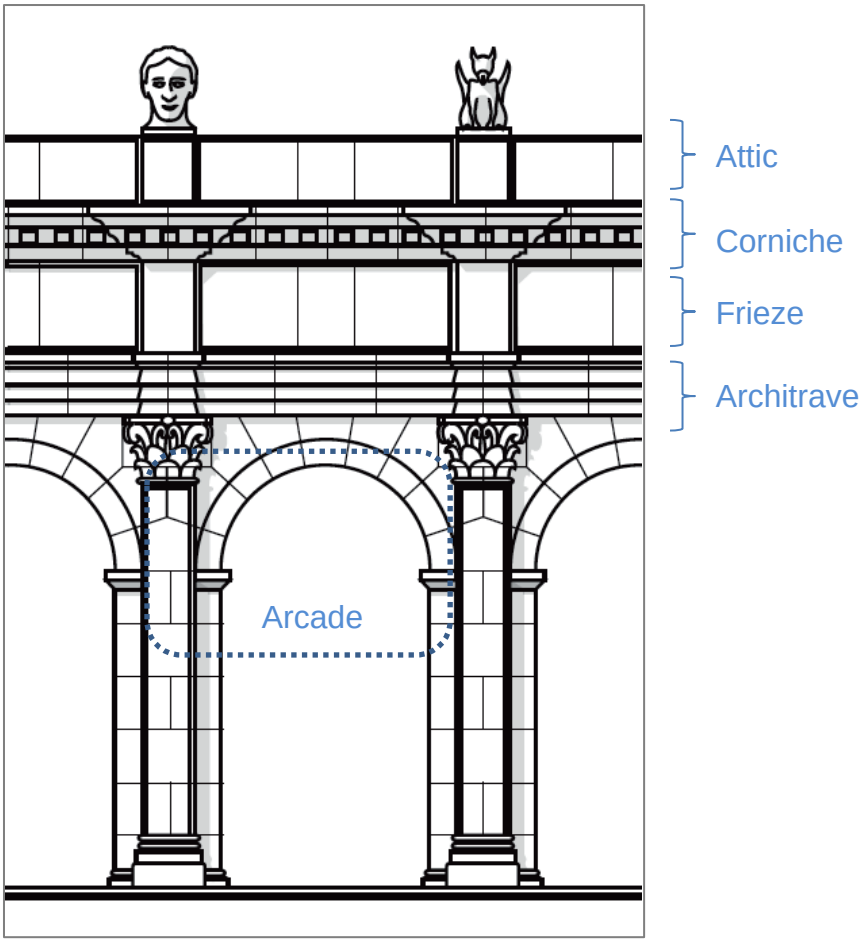

Figure 4-3: Detail of the elevation to be restored

Before analyzing the architectural blocks that would enable the restoration of the facade, the place of maximum extension of collapse had to be found. After examining the area, it was observed that the calculation could be performed in the southern area, where enough blocks features enabled reasoning. The sequence between arches XII and XIII was the most complete to restore the majority of the architectural parts of the facade.

The hypothesis of restitution of 15 arches is shown in figure 4 and the provisional anastylosis of the facade in figure 5.

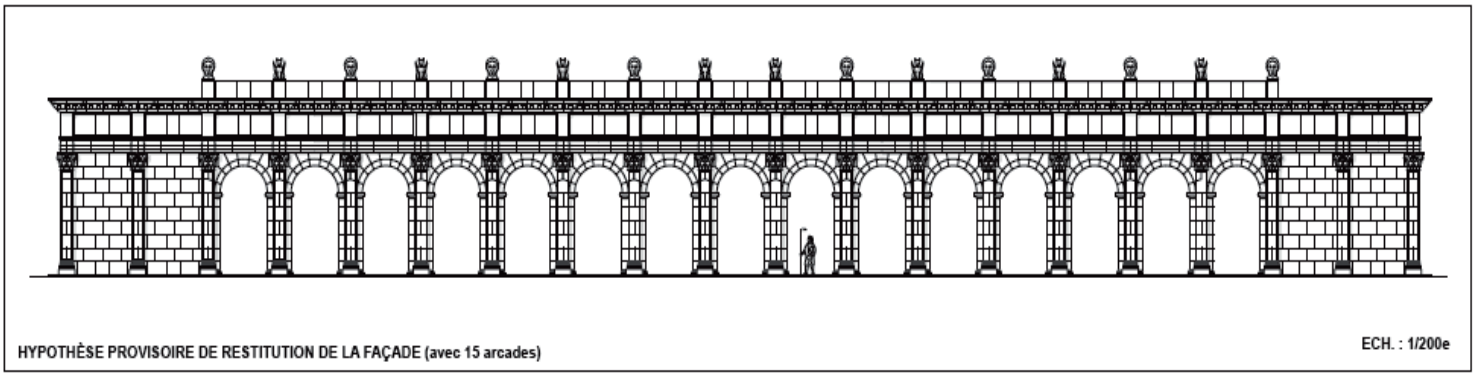

Figure 4-4: Provisional hypothesis of the facade of restitution (INRAP)

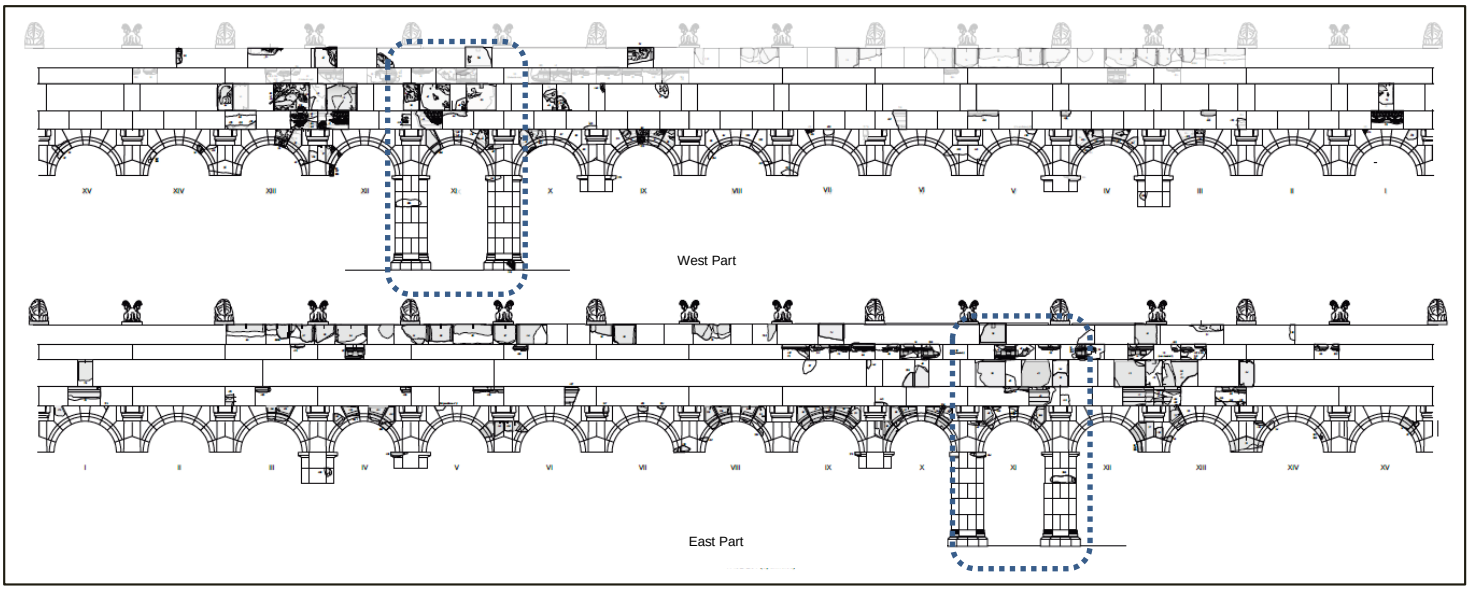

Figure 4-5: Temporary anastylosis of the facade (INRAP); West and East Part

4.2.4 Architectural parts of the sanctuary

At this point, it's worth mentioning some details about the architectural elements of the ancient Gallo-Roman sanctuary that need to be reconstructed. There is little explicit ancient evidence for this sanctuary and the period of its construction is not clear to specify the architecture order with precision. As stated before, the entry of the sanctuary is made by a monumental facade of 68x105m long and 9.50m high which are exceptional dimensions. An arcade of 15 openings with triumphal arches goes through the façade, on top of which lies the entablature and the attic. The arcade is supported by emblematic piers (upright support for an arch), whose capitals are probably composed of a mixed order, combining the volutes of the Ionic order capital with the acanthus leaves of the Corinthian order. The west face, as the exterior, of the facade, whose arches are separated by pilasters with the capital of Composite order, is entirely decorated with sculptures enhanced with paintings, while the inner face is left almost intact.

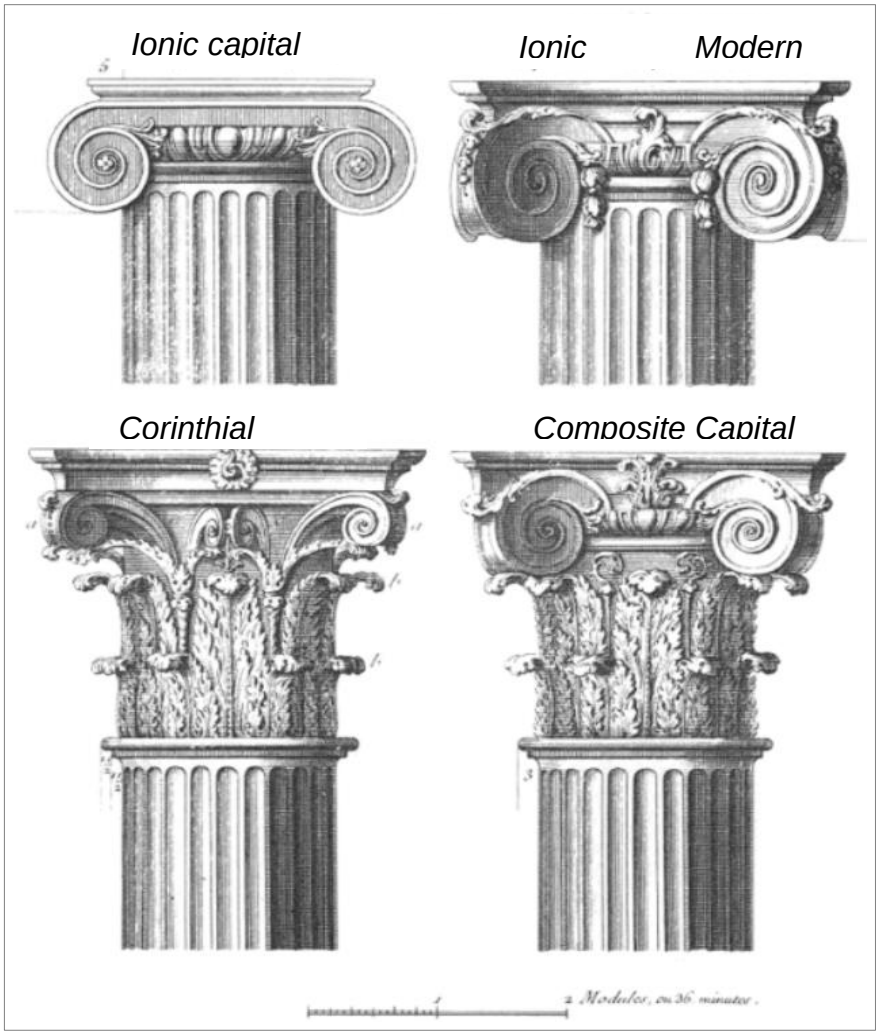

Figure 4-4-6: Ionic and Composite capitals

The lower part of the structure (pedestals, pilasters, capitals)

- The pedestals (base) of each pier are represented by few elements. The rectangular base of the pedestal is 0.25 m high and is decorated on the long side with a plant motif.
- For the pilaster, there are 3 fragments identified as most of its fragments were looted. As an architectural element, the pilaster gives the appearance of a supporting column and to articulate an extent of wall, with only an ornamental function.
- For the composite capitals, 5 potential fragments can be identified which compose a graphic restitution of its shape.
- Two types of blocks quite similar form the transom, which is in architecture a transverse horizontal structural beam, and the base of this facade can be used to reconstruct in 3D the bases and the coronations.

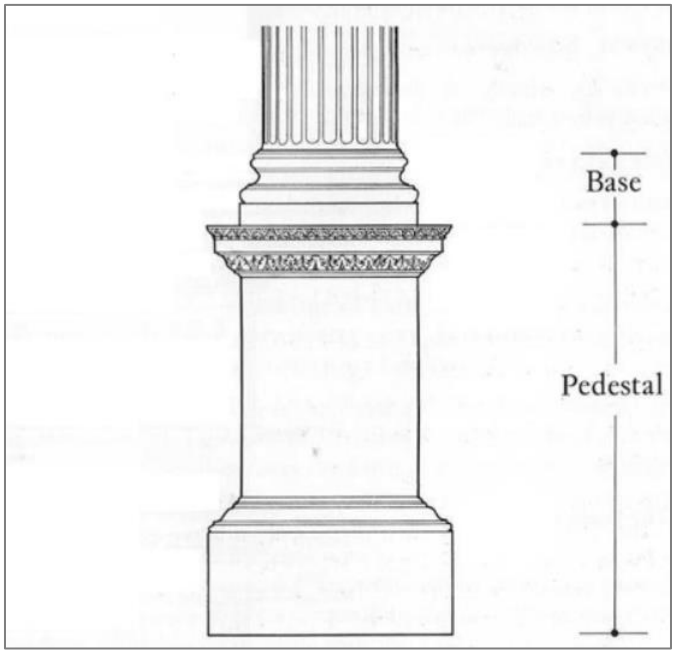

Figure 4-7: Lower part of structure

Arcade

The arcade has retained some painted decorations. The construction consists of a succession of calved arches, with radiating section beds, extrados (outer curves of the arch) with a flat top and similar staircase. Some complete blocks retain traces of paint, especially the red backgrounds in order to point out the figurations. For instance, in the inner curve of the surface of the arch VI, a plant decoration is clearly visible on the red background.

Figure 4-8: Intrados of keystone of the arch VI (© V. Brunet-Gaston, Inrap).

The sequence of 5 blocs, which form the arch IX, could give the bigger picture of the arcade while in total 17 main blocks and 4 fragments were identified.

Entablature and attic

The sequence between arches V, VI, XII and XIII is the most complete for the restoration of the entablature and the attic.

The entablature is composed of the following three architectural elements and some descriptions based on the findings are also stated:

- Architrave: The Ionic architrave, of 0.73 m high, is composed of three lengths of blocks, a central block and two blocks. The architrave is attested by several complete blocks which enable its restoration.
- Frieze: The enormous ionic frieze, of 1.03 m high, bears various scenes from a Hellenistic repertoire. Various fragments were detected and contributed to the formation of the frieze.
- Cornice: The Corinthian cornice, 0.60 m high, is decorated with foliage with anthemion and some of its parts were found on the fields.

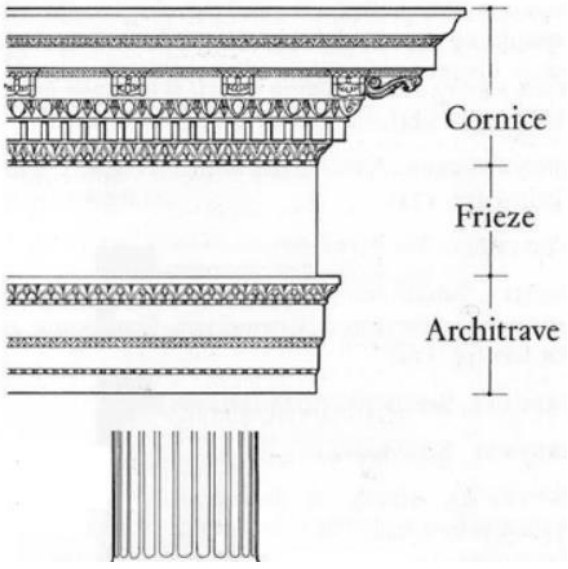

Figure 4-9: Entableture and attic

An attic of 0.79 m high lies on this entablature, adorned with sea creatures. The height of the attic, which approaches the height of the architrave, does not follow the proportions of the whole and it was considered that its implementation was not as rigorous as the inferior parts of the structure. One of the most complete blocks shows a Triton (mythological Greek god, the messenger of the sea) carrying an oar over his head.

Figure 4-10: Attic: Triton carrying an oar (© V. Brunet-Gaston, Inrap).

The summit heads and griffins

On the top of the attic ten massive statues of griffins (animals with eagle's head and lion's body belonging to the procession of Apollo) are lined. The griffins and the marine creatures are attested in the architectural ornamentation, decorating burial monuments of the Gauls as well as temples. There are no complete faces among the fragments found in the excavations, complicating the identification of the godhood but still assumptions can be made.

Figure 4-11: Divine heads (© V. Brunet-Gaston, Inrap).

Various other smaller heads were also found on the site and were collected in order to find their possible position on the façade.

This facade thus offers alongside the classical architectural repertoire of the Roman Gaul times (geometric decoration, rhythmic scrolls, etc.), a typically Greek iconographic and statuary repository with precise mythological themes and cultural references.

All these blocks and fragments were graphically represented by the archeologists so that their possible position on the façade is specified. The next step is the creation of a theoretical model of the entire façade in 3D with assumptions provided by the operation manager. This project was integrated by the laboratory of photogrammetry of INSA in Strasbourg, where 96 fragments were digitized using photogrammetry for the large blocks and a terrestrial laser scanner for the smaller ones. Among the blocks, about 45 are large blocks (having a size of the order of one meter, for a volume of 0.1 to 1.1 m^3). The other blocks (in particular the capitals, transom and base blocks) have smaller dimensions (of the order of 0.01 m^3).

A graphical restitution of the fragments and broken parts of the arches V and VI is below depicted, showing the potential positions of the various fragments.

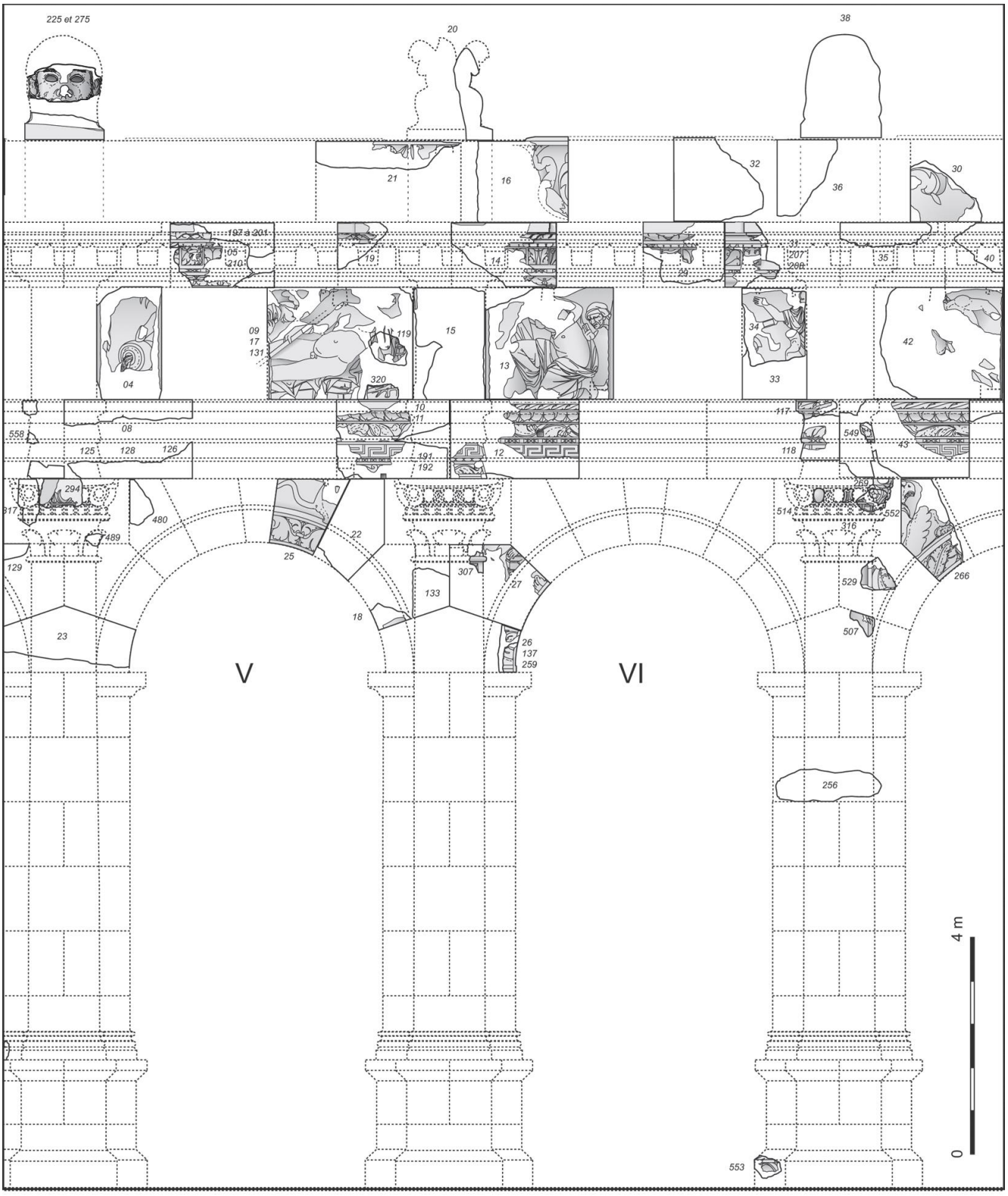

Figure 4-12: Anastylosis of arcade blocks V and VI ((© C. Gaston, Inrap)

4.3 3D Digitization of fragments

The recording of remnants of an ancient sanctuary of the Pont-Saint Maxence is implemented with the use of photogrammetric and lasergrammetric techniques. As previously mentioned, 96 fragments were digitized in total using photogrammetry for the large blocks and a terrestrial laser scanner for the smaller ones. The main purpose was the collection of dense cloud points to capture all the details of the complex fragments.

4.3.1 Small blocks of fragments

The acquisition of the point cloud was carried out by means of a handheld laser scanner "Faro Laser Scanner", which belongs to the laboratory of Photogrammetry "ICUBE" of INSA in Strasbourg, with the accuracy of ±25 μm. This scanner uses the phase-shift principle comparing the phase of the laser source with the same when the radiation comes back again to the scanner after its reflection on object's surface. It is a contact/non-contact measurement system and the *ScanArm's hard probe* and the *Laser Line Probe* can digitize interchangeably without having to remove either component. First, there is a probe at the end of the FaroArm that takes measurement points on command. These probes can be exchanged with other probes depending on the surface or material being measured. A user simply clicks a button on the end of the FaroArm to record a point and special encoders compute the exact position of the probe within a three-dimensional space. This point is recorded in the software and the user moves on to take another measurement. Intricate components can be captured in fine detail as a result of the 2,000 actual points per scanline the new blue laser featuring noise reduction technology. ("Edge and ScanArm HD," n.d.)

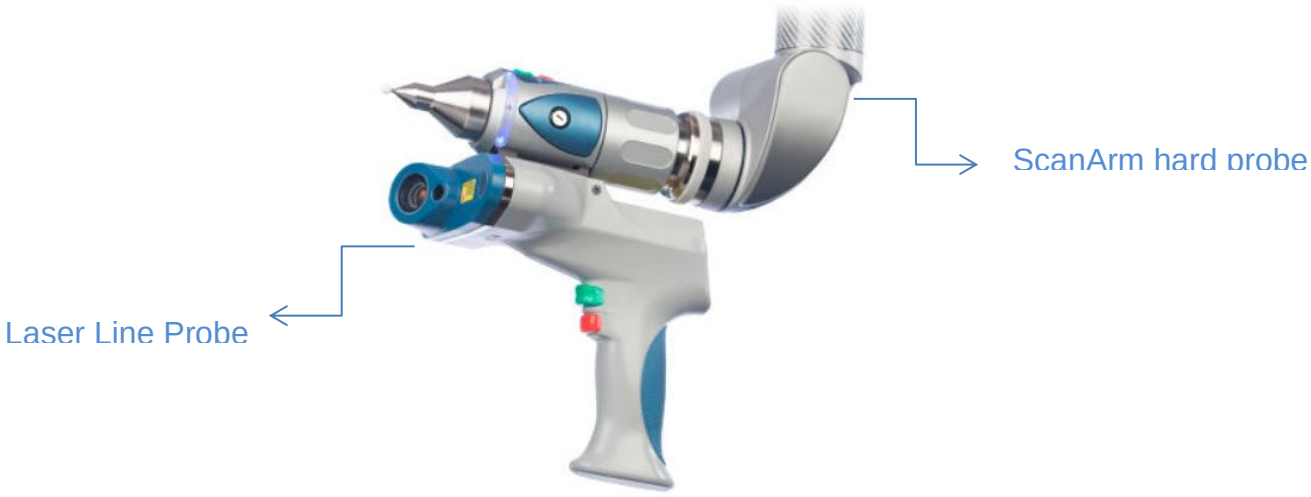

Figure 4-13: FARO SCANARM

The scanner achieved a detailed description of the surfaces of the small fragments. However, a scan taken from a single point of observation was not sufficient to acquire the whole surface of an object, thus the multiplication of viewpoints made it possible, by moving the object or the scanner, to digitize the whole object. This led to the necessity of repositioning each of the scans with respect to each other, so that the set of points are found in the same reference frame. For each block 2 to 3 acquisitions were necessary.

This information occupies a significant volume in the collected data. The file that is produced by the scanner is a raw file and cannot be processed unless it is exported in asci file, pts etc.

4.3.2 Big blocks of fragments

The acquisition of the point cloud was carried out by means of a camera by members of the laboratory as well as the data processing in Agisoft PhotoScan, computer software that performs photogrammetric processing of digital images and generates 3D spatial data. The main advantage in this technique is the oriented texture as the camera can capture high quality textures which provide an important source of information about the three-dimensional structure of the object. A photogrammetric method for creating three-dimensional models of an object from multi-view image sets in order to reconstruct the photographed scene is 'Structure from motion' (SFM). SFM and other computer vision algorithms enable PhotoScan to generate very dense point clouds and accurate three-dimensional meshes of various archeological objects captured in two-dimensional imagery.

The images were taken by the camera Canon EOS 5DS R and for each object of about 0.6 – 1 m, 60 to 100 photos were required. The camera lens attached to the camera had a focal length 28mm.

The table bellows states the camera's characteristics.

Camera Model	Resolution	Focal Length	Pixel Size	Precalibrated
Canon EOS 5DS R (28 mm)	8688*5792	28 mm	4.24* 4.24μm	No

4.4 Point Cloud Registration

Throughout the scanning procedure, the coordinates of points are determined in the scanner's reference system based on their direction and distance from the scanner. These coordinates are calculated in the scanner's reference system at that position. An object is completely scanned when the whole surface is digitized and that requires

usually more than one scans from different, perimeter locations but keeping a common side each time in order to achieve a sufficient overlap. Therefore, the primary data collected by the scanner (point clouds in .imp format) are in different reference systems. A common reference system is therefore required in order to use these data.

All point clouds were imported to the software "Cloud Compare" in a modified extension (ascii files, pts) where all the processes took place. Cloud Compare is a 3D point cloud processing software that can also handle triangular meshes. In this software the point clouds were adjusted to the desired scale, according to the instructions given, and the unnecessary points were deleted, as much more points were collected than needed with the scanner creating noise. These points were manually removed and the point cloud was somehow simplified.

Alignment

Following this, the *cloud registration* or *alignment* process takes place. The registration is basically a rigid body transformation between the independent clouds of points achieved by at least 3 homologous points between clouds. The number of three necessary points results from the fact that the variables in each union are 3 rotations and 3 translations in space. Therefore, the coordinates of a point (X, Y, Z) are essential for the determination of the transitions and 3 elevation points for the rotations in space. However, for the application of laser scanner there is no need of elevation points, as all of the points are 3D scanned. Thus it is ultimately necessary the use of at least 3 homologous points of each cloud in order to be registered and adjusted together. As homologous signs, highly reflective targets are usually used, providing accurate results because they are easily detected.

Two scans of a small fragment were compared and aligned each time. In this case, targets could not be placed on the object as there was a risk of damage and in addition to that, the surface of the fragments was really complex making it hard to find homologous points. However, efforts were made in order to find characteristic points on the surface of the compared scans in order to achieve a satisfying RMS of the order of 0.001m.

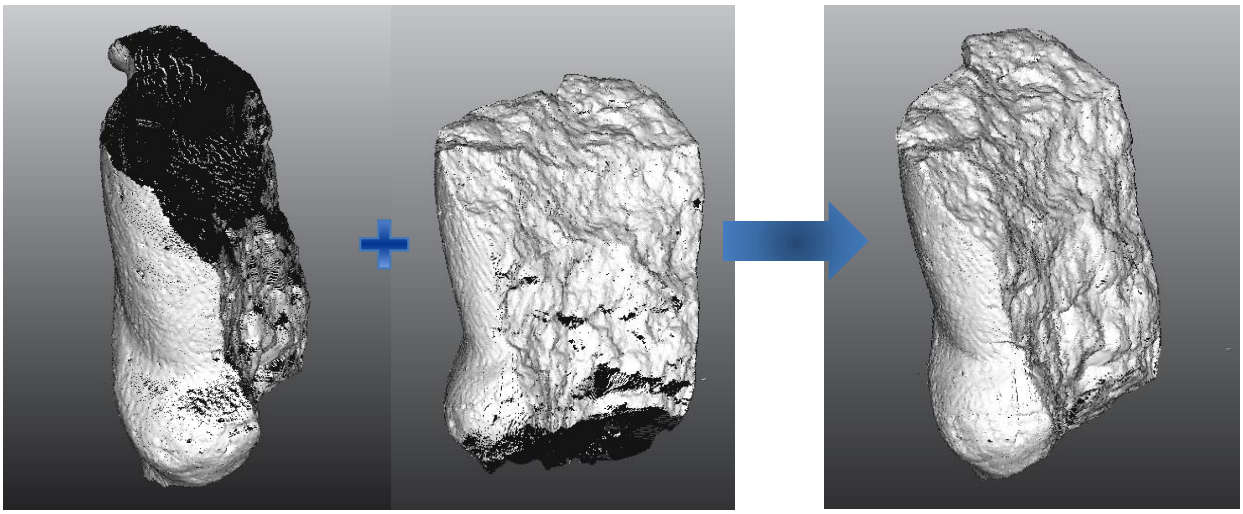

Figure 4-14: Alignment procedure of two fragments

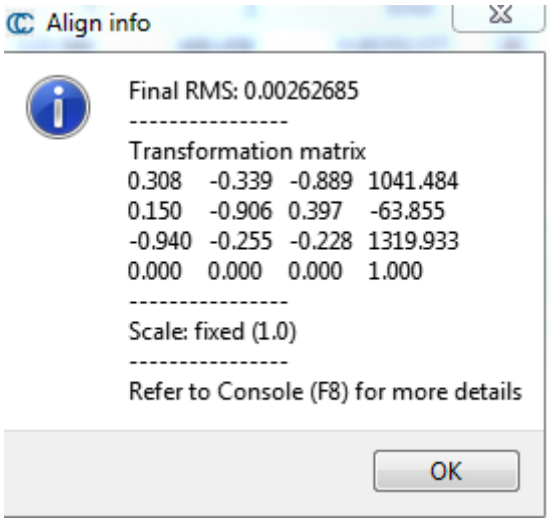

Figure 4-15: RMS of first registration

The registration may be relative, when the clouds are aligned together in the common system of the scanner or absolute in a geodetic reference system (usually a local) if at least three points are measured geodetically.

Fine registration with ICP

The software gives the possibility, after the first registration with the homologous points selected by the user, for a fine registration of all the points with their counterparts using the ICP (Iterative Closest Point) algorithm [Besl,1992]. The iterative closest point (ICP) algorithm is a widely used method for registering the outputs of 3D scanners, which

typically only scan an object from one position at a time. ICP starts with two meshes and an initial estimation for their relative rigid-body transform, and iteratively refines the transformation by repeatedly generating pairs of corresponding points on the meshes and minimizing an error metric. The quality of alignment obtained by this algorithm depends heavily on choosing good pairs of corresponding points in the two datasets as initial approximations. If too many points are chosen from featureless regions of the data, the algorithm converges slowly, finds the wrong pose, or even diverges, especially in the presence of noise or miscalibration in the input data. (Gelfand, et al., 2003)

In any case, a scan will always be considered as the referent with respect to the other which will be mobile. By comparing the common parts of the common surfaces, the distance between the clouds is minimized and they are better adapted to each other. During this process, the random sampling limit was set to approximately 100000 points and gradually the registration error decreased. In addition, the final overlap was specified at the actual portion of the registered cloud that would actually overlap the model/reference cloud if both clouds were registered. The entities were registered with only a partial overlap and the RMS was optimized as it was reduced to 0.1mm.

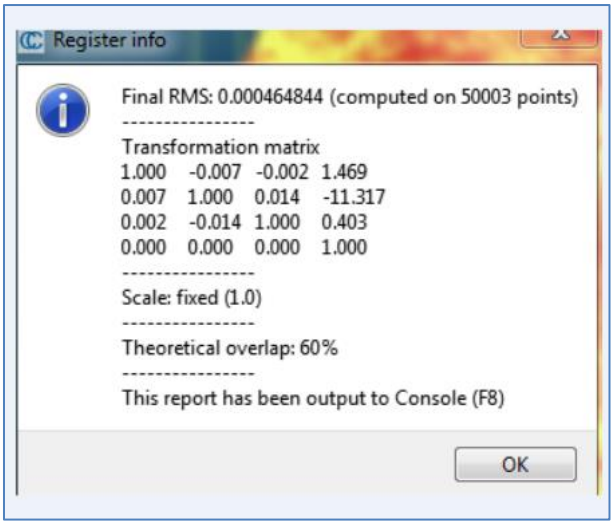

Figure 4-16: RMS of fine registration

Following this, a test was carried out in order to check whether the two point clouds were registered properly and how well one surface overlaps the other to not exceed the RMS. CloudCompare will first compute approximate distances and then the compared cloud is colored with those approximate distances. The Compared cloud is the one on which distances are computed. The Reference cloud is the cloud that is used as reference, i.e. the distances are computed relatively to its points. The distances between two point clouds are computed with the use of the 'nearest neighbor distance' method: for each point of the compared cloud, CloudCompare searches the nearest point in the reference cloud and computes their (Euclidean) distance.

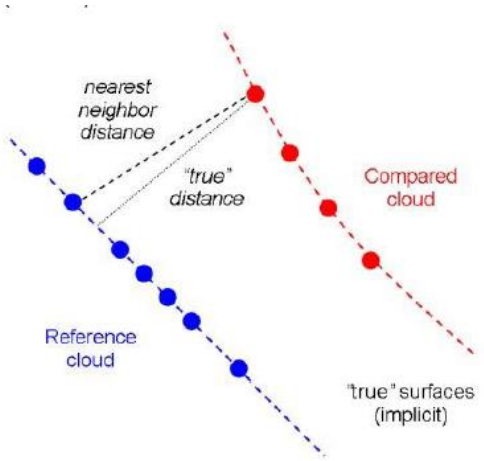

Figure 4-17: Cloud to Cloud distance

The diagram below shows the compared point cloud's distances from the reference cloud while the latter does not appear on the screen. The scale on the right shows the distribution of the points given their distance with the reference cloud. According to the diagram, the volume of the points is inside of a limit that is chosen by the user. The majority of points lie in the green scale which means that these points are below the average of max distance and the cloud is well registered. The points with red color have the longest distance from the reference cloud and show the areas of the greatest deviation.

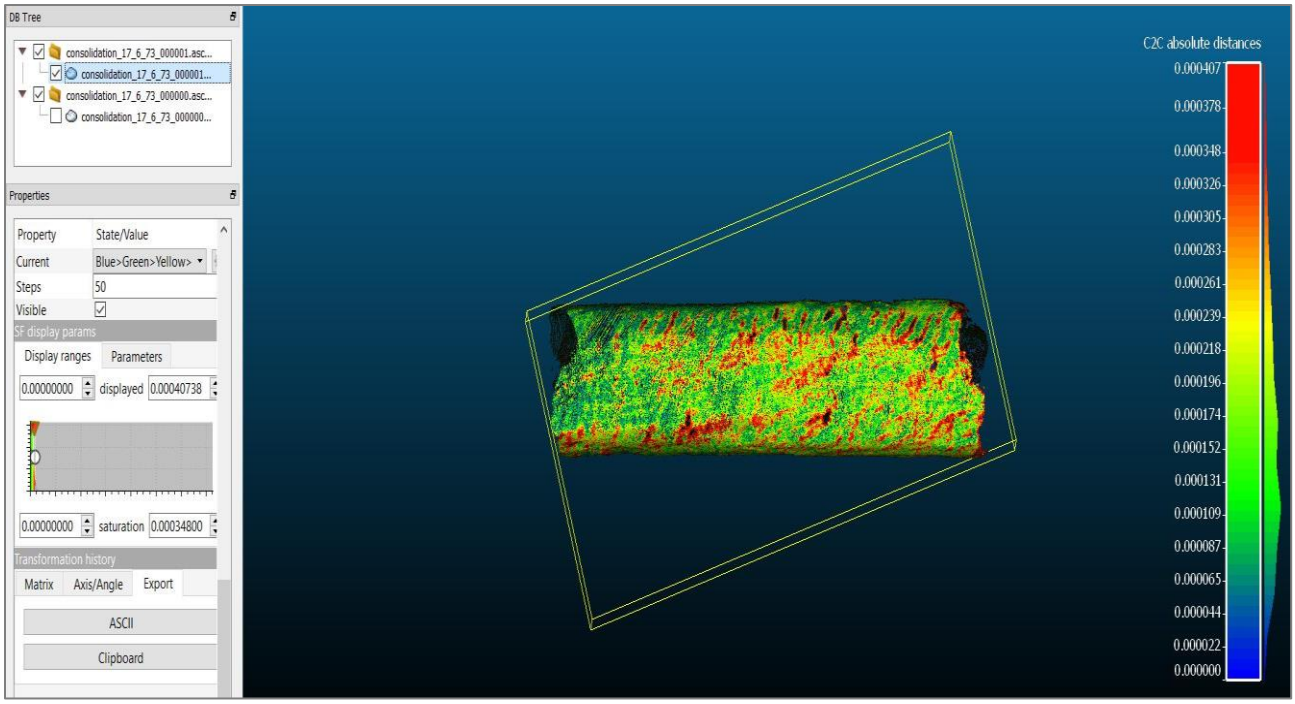

Figure 4-18: Example of Computation of Cloud to Cloud distance

After finishing the registration process, the point clouds were merged into one.

Subsampling

The files produced are relatively large and not easily manipulative. By subsampling a point cloud, the number of points is decreased. Cloud Compare uses three methods: random, spatial and octree based, while maintaining the maximum accuracy and object geometry. In this case, the random mode was used and a number of points were picked in a random manner. The process of subsampling took place, while some segmented parts of the point clouds should be tested in the algorithm of Fragmatch^{+}, which is analyzed in the next chapter.

A dense cloud can adequately represent a surface, but it is difficult to replicate complex areas of detail and edges in a way that there will be immediately perceived by any average user. Subsequently, the fine registration is followed by the modelling of the surface of the fragments with the method of triangulation of Delaunay. This method is analyzed in the chapter 5 while this process takes place in the Matlab software.

Editing operations on the measured points are very important before generating a triangular surface. The pre-processing operations usually are:

- data sampling based on the curvature of the points or uniformly apply.
- noise reduction and outliers' rejection: statistical methods are applied taking into consideration the surface curvature and trying to preserve the measured features.
- holes filling: gaps in the point clouds are closed adding (manually or automatically) new points and using the curvature and density of the surrounding points. (Remondino, 2003)

The point cloud registration process was efficiently performed for 25 fragments in total. Assumptions have been made for their possible position on the façade to virtual reconstruct its initial structure. Given the fact that most of the fragments were significantly deteriorated and had suffered from corrosion, it was difficult to determine conjugate surfaces that could fit plane to plane, which is a prerequisite in order to be tested in Fragmatch+ for their potential union, since the algorithm accepts only plane scanned surfaces. A pair of fragments with higher probability of matching among the others was selected and constituted the practical implementation of the algorithm.

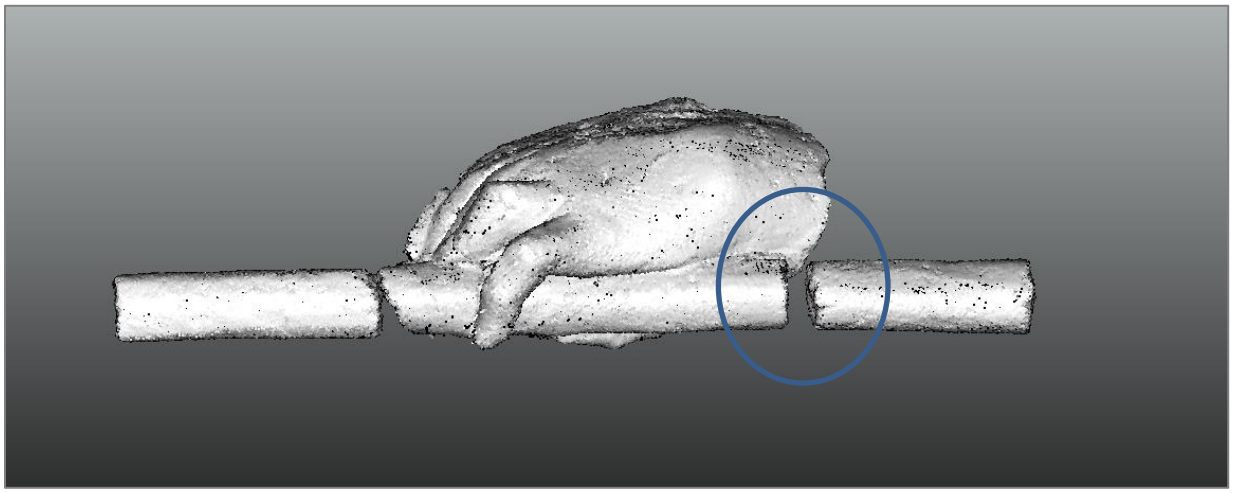

Figure 4-19: Potential conjugate fragments. Tests were carried out for the right pair.

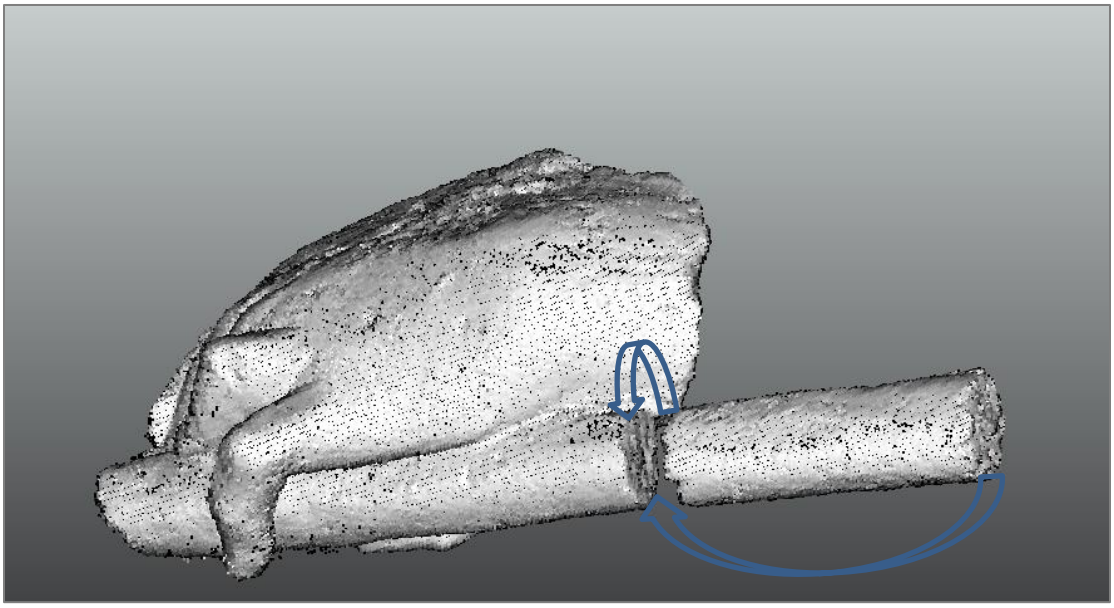

Figure 4-20: Both sides of the right fragment should be tested in order to find the potential fit to the left fragment

The segmentation as well as the subsampling of the surfaces precedes the input of data in the algorithm. By selecting each fragment separately, an effort was made to segment the broken surface respectively to the rest of the fragment. These segmented surfaces were saved and pairwise tested in the algorithm.

An extensive analysis of the Algorithm "Fragmatch+" follows in the next chapter.

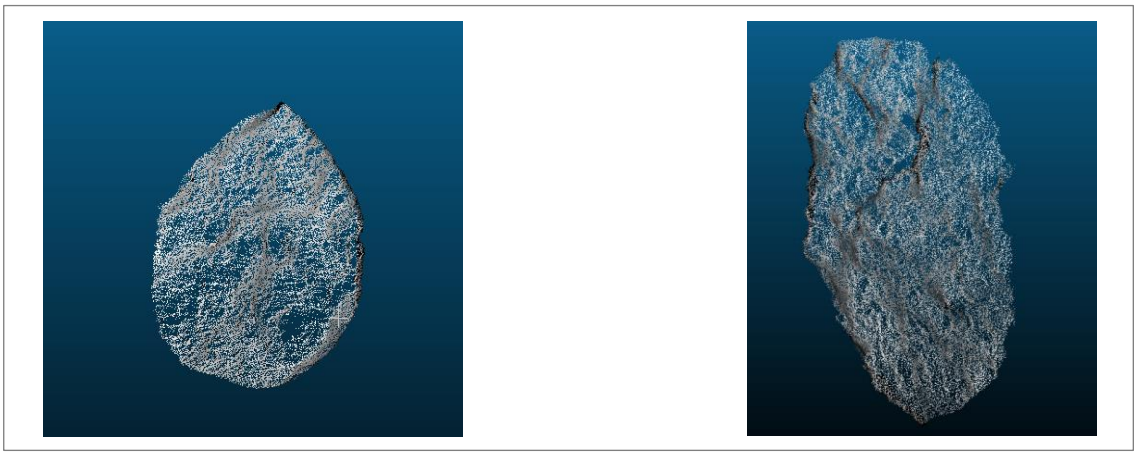

Figure 4-21: Examples of segmented surfaces

Chapter 5 **: Analysis of Algorithm Fragmatch+**

5.1 Introduction

In this chapter the development of an algorithm that joins two surfaces from conjugate fragments is described. The underlying concept of the present algorithm is based on a similar work conducted within the framework of a Diploma Thesis (Filippas, 2013) for detecting conjugate archaeological fragments based mainly on their geometry. That method, called Fragmatch, was based on the comparison of vectors and surface areas. In addition to that, the project integrated in France("Projet Pont-Sainte-Maxence", 2015) gave incentive to the creation of a computer tool, in order to reconstruct broken objects found on the excavation fields.

The idea of the present algorithm came from the fact that although Fragmatch identifies correspondences between conjugate fragments, it does not unite the broken pieces. As an updated version of the aforementioned numerical tool, Fragmatch+ has achieved the unification of conjugate surfaces by applying a rigid body transformation (rotation and translation).

The development of the algorithm consists of two parts. In the first part, the pairwise comparison of the similarity of surfaces takes place in Fragmatch, while in the second part the rigid body transformation of the conjugate surfaces is implemented

The process of matching and merging conjugate fragments occurs in the following sequence:

- Data Input in Fragmatch
- Comparison of data with ICP
- Delaunay Triangulation/ Surface Creation
- Pairwise Matching with Fragmatch –Results
- Export of surfaces and input in the main program
- Conjugated fragments → Rigid body transformation
- Test Cases

5.2 Fragmatch+ : General Information

The initiating idea of the present algorithmic process (Fragmatch+) is that a transformation should accomplish the union of two planar faced objects since the pairwise matching between two broken objects is not enough to reassemble the complete 3D object. The adopted process is based mainly on the 3D geometry of the fragments and proposes a linear and computationally efficient way to reconstruct conjugate fragments.

By conducting a rigid body transformation i.e. synthesis of rotation and translation of the point cloud is expected to coincide with the reference point cloud. The process that leads to the determination of the suitable transformation depicted in eq.1, is extensively analyzed in the following paragraph.

$$(X2)_{transform} = \boldsymbol{R} * X2 + \boldsymbol{\delta r} = X1 \quad (1)$$

where, the transformed point cloud $(X_2)_{transform}$ will coincide with the corresponding points of the reference point cloud X_1.

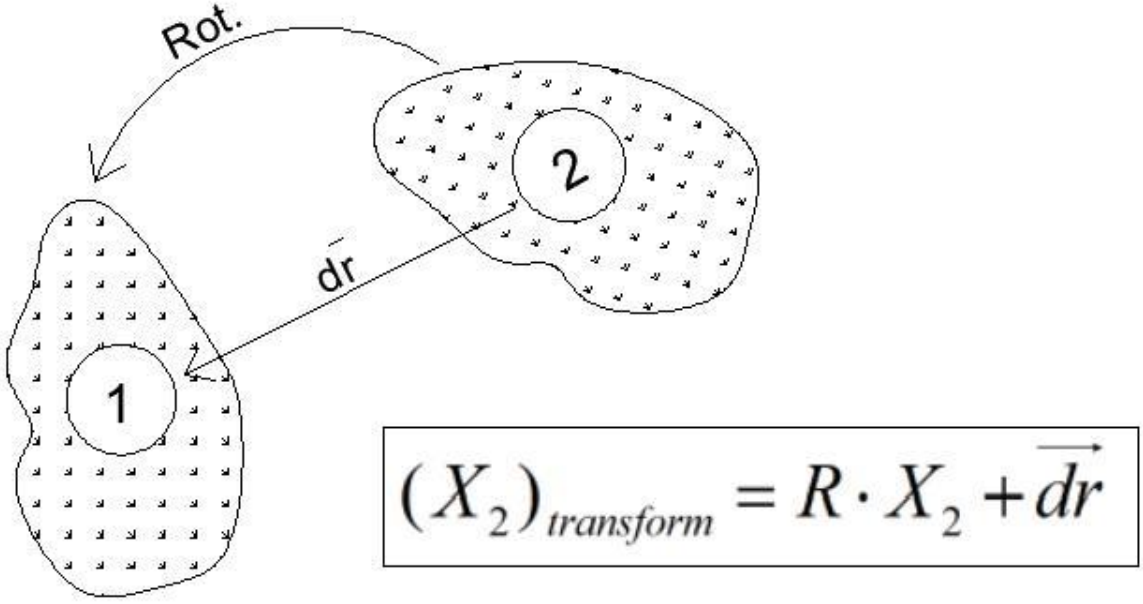

Figure 5-1: Rigid Body Transformation

5.3 Part1: Fragmatch

Before attempting to unify the conjugate fragments, the matching stage has to be performed. The detection of the conjugate fragments takes place with the Fragmatch algorithm, where the broken surfaces are compared for their similarity (Filippas & Georgopoulos, 2013). The ICP algorithm is used as a method to assess the similarity between the various scanned surfaces, whose matching will be examined afterwards. Following this, surfaces and vectors are created for each investigated part in order to continue with the implementation of global or partial matching of the surfaces.

5.3.1 Data Input

The input data are 3D digital models of flat archaeological fragments obtained by 3D laser scanning. At the beginning, point clouds are segmented using an interactive segmentation tool in Cloud Compare, in order to separate the fractured faces from the entire scanned piece.

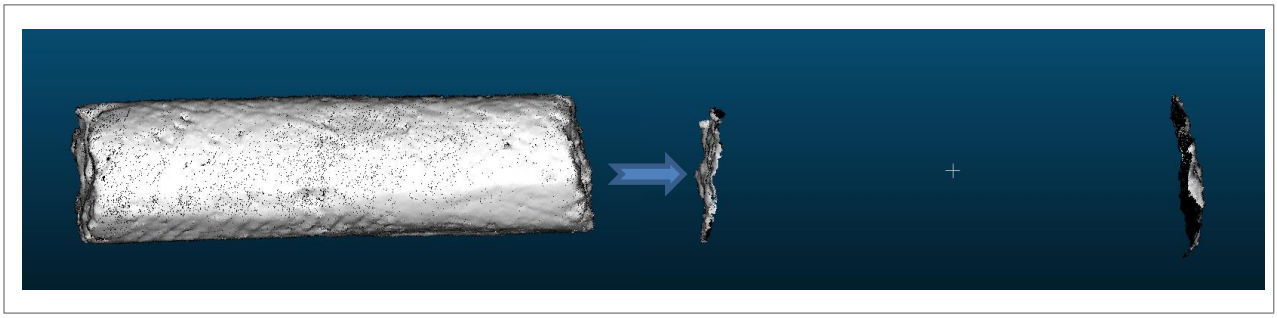

Figure 5-2: Segmentation part

Fragmatch uses point clouds as input data. It requires the X, Y, and Z coordinates for each point of the broken surfaces and not of the whole fragments. It is assumed that during scanning, the broken surface should be located in front of the scanner, so that the Z axis is perpendicular to the main broken face, thus defining the depth of the broken surface.

The software requires that the user manually enters i) The number of fragments, i.e. surfaces, scanned ii) the number of broken surfaces for each fragment and iii) the name of the file for each broken surface, which corresponds to the point cloud which is the main data.

5.3.2 Initialization with ICP algorithm implementation

Before the implementation of the main Fragmatch algorithm, ICP is employed in order to accelerate the execution. The most common use of the ICP is to match two groups of data points into a common coordinate system. However in Fragmatch algorithm it is used as a method to compare the similarity between the various broken surfaces to be matched.

During the application of ICP, two tables (A and B) are created. The results from the pair comparisons of all scanned surfaces are placed in table A. The first two columns of

table A contain the compared surfaces; the third column takes either the value 0 or 1 depending on the success of the ICP matching. The fourth column contains the value of the error, which results from the implementation of ICP algorithm. Table B contains those surfaces which have been compared and the error lies between acceptable values.

5.3.2.1 ICP Algorithm

Since the ICP algorithm is part of the Fragmatch, it was considered appropriate to briefly analyze the way it operates.

The ICP algorithm was developed by Besl and McKay in 1992. It is commonly used to achieve the matching of two point group data in a common coordinate system. The algorithm performs matching of the two clouds through successive iterations. In each iterative step, the algorithm selects the nearest points as corresponding and calculates the necessary transformation E - a rotation R and a translation t (R, t) - that minimizes the sum of the squared error in the equation

$$E(R,t) = \sum_{i=1}^{N_m} \sum_{j=1}^{N_d} w(i,j) |m_i - (Rd_j + t)|^2 \qquad (1)$$

where N_m and N_d, are the number of points in the M set and the data set D respectively, and $w_{j,i}$ is the weight for the harmonization of each point. The weights are assigned as follows: if m_i is the closest point to d_j then $w_{j,i}$=1, otherwise $w_{j,i}$= 0.

The equation (1) can be reduced as follows:

$$E(R,t) = \frac{1}{N} \sum_{i=1}^{N} \left| m_i - (Rd_j + t) \right|^2 \qquad (2)$$

with

$$N = \sum_{i=1}^{N_m} \sum_{j=1}^{N_d} w(i,j) \qquad (3)$$

while the matrix can be represented by a vector containing the pairs of points:

$$v = ((d_1, m_{f(d_1)})), ((d_2, m_{f(d_2)}))\ d_2, \ldots, ((d_{Nd}, m_{f(d_{Nd})})) \qquad (4)$$

with $f(x)$ the search function returning the closest point. The assumption is that at the last iteration stage a point's pair and consequently the vector of the point pairs is correct. The end of repetition is achieved when the mean square error becomes less than a predetermined limit, depending on the desired accuracy: $d_k - d_{k+1} < r$.

The stages of the Algorithm are briefly stated below:

1. Selection of some set of points in one or both meshes.
2. Matching these points to samples in the other mesh.
3. Weighting the corresponding pairs appropriately.
4. Rejecting certain pairs based on looking at each pair individually or considering the entire set of pairs.
5. Assigning an error metric based on the point pairs.
6. Minimizing the error metric.

The point selection strategy and the choice of error metric to be minimized play a dominant role in the rate of convergence and the accuracy of the resulting pose. The major problem is to determine the correct data associations. If the correct correspondences are known, the correct relative rotation/translation will be calculated consequently, otherwise, it is generally impossible to determine the optimal relative rotation/translation in one step. Given the correct data associations, the rigid body transformation, that minimizes the error, can be efficiently computed using solution methods based on Singular value decomposition (SVD) [Arun 87], quaternions [Horn 87], orthonormal matrices [Horn 88] and dual quaternions [Walker 91].

Figure 5-3: ICP converges when the starting positions are "close enough"

Many efficient variants have been introduced on the basic ICP and can be classified to each step accordingly. These variants are able to accelerate the speed of convergence, the alignment procedure and give solution in intricate geometry as well (Levoy,2001).

5.3.3 Creating surfaces and vectors

The point clouds are then converted to surfaces with the help of the standard Delaunay triangulation, which is the only non-linear procedure in the algorithm and is described in the next paragraph. The triangles formed for each separate broken surface are sorted according to their size, while triangles with sides exceeding a limit set manually by the user are excluded. This limit defines each time the maximum triangle side (triangles not larger than the specified limit are formed) which is considered to form the surface most appropriately.

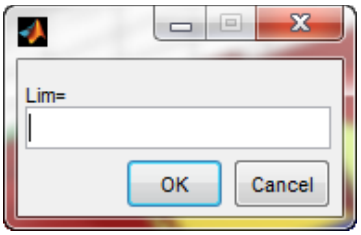

Figure 5-4: Input of limit of side manually

Following this, the normal vectors of all triangles of each surface are determined. The application point for each normal is the center of each triangular surface and its magnitude is equal to the area of the relevant triangle. This process ensures the uniqueness of triangles and vectors.

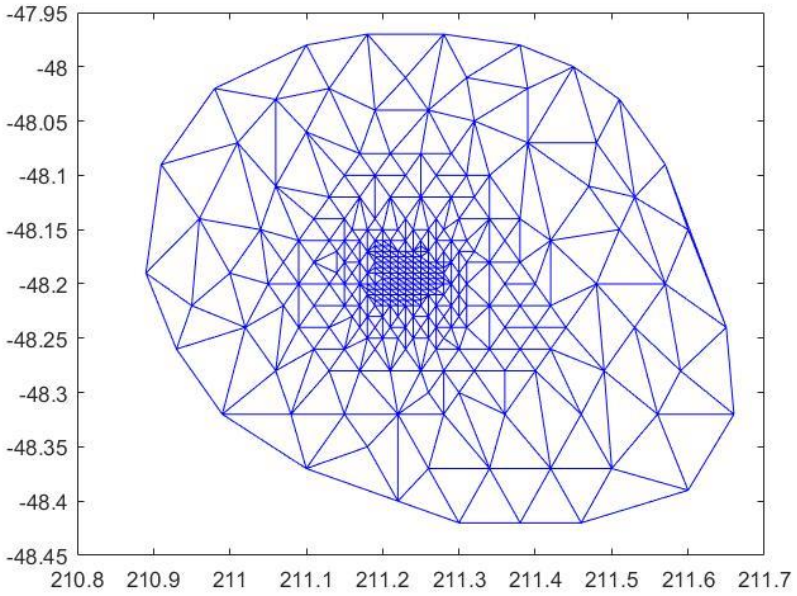

Figure 5-5: Delaunay Triangulation - Display of triangles in the x, y plane in Matlab

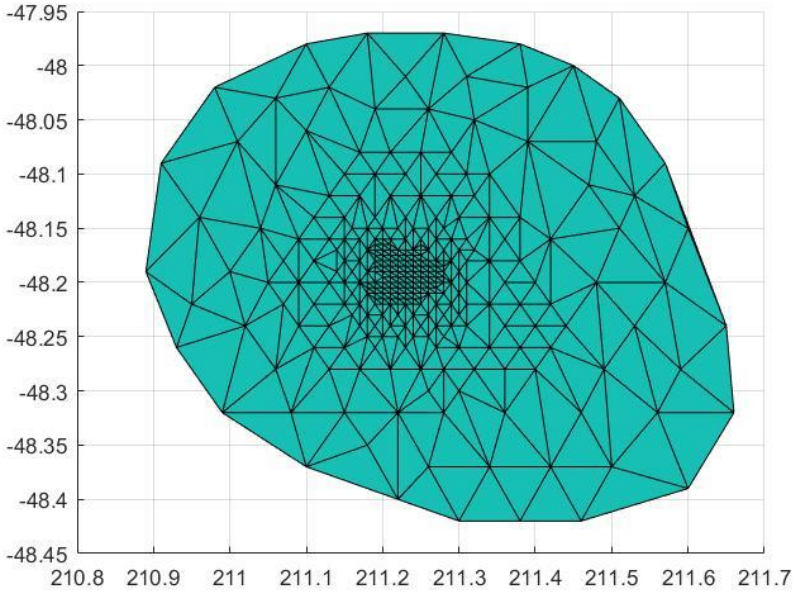

Figure 5-6: Delaunay Triangulation - Display of 2-D surface in Matlab

5.3.3.1 Delaunay Triangulation

As a definition of the term “modelling” someone might say that *it is the (mathematical) construction and computer implementation of an object, by defining points in a 3 dimensional array*. This array is expressed on the X, Y and Z axes of geometric space. Then, different sets of these points are mathematically ’joined’ to create polygons and the polygons joined to create objects. The simplest result is usually displayed as a wireframe model (Remondino, 2003). Namely, it is a process that converts "irregular" point clouds into easily manipulated polygons (usually triangles).

The process of converting a usually unstructured point cloud into a consistent polygonal model is called "triangulation" and is described as a collection of triangular (or quadrilateral) contiguous, non-overlapping faces joined together along their edges. A mesh, also called TIN, Triangulated Irregular Network, therefore contains vertices, edges and faces and its easiest representation is a single face.

The triangulation can take place in the two-dimensional or three-dimensional space (2D, 2.5D, 3D triangulation), depending on the geometry of the object. For this process Delaunay triangulation is commonly implemented.

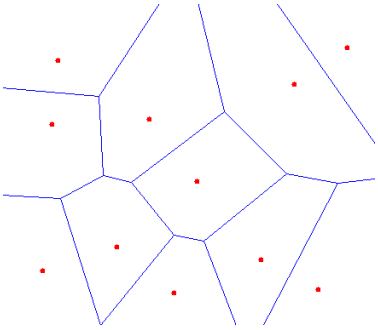

Figure 5-7: Voronoi diagram.

In Voronoi, each region consists of the part of the plane nearest to that node. Connecting the nodes of the Voronoi cells that have common boundaries, the Delaunay triangles are formed

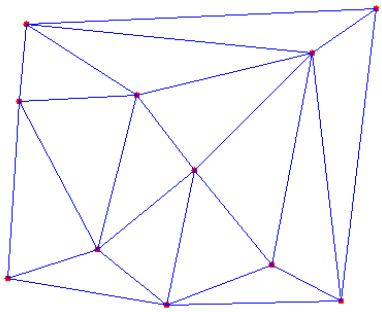

Figure 5-8: Delaunay triangulation

The triangulation in 3D is called *tetrahedralization* or *tetrahedrization*. “A tetrahedralization is a partition of the input domain into a collection of tetrahedra that meet only at shared faces (vertices, edges or triangles). Tetrahedralization results are much more complicated than a 2D triangulation.’’ (Remondino, 2003)

With the help of the standard Delaunay triangulation (a non-linear procedure), the point clouds were converted to surfaces. Delaunay criterion ensures that no vertex lies within the interior of any of the circumcircles of the triangles in the network.

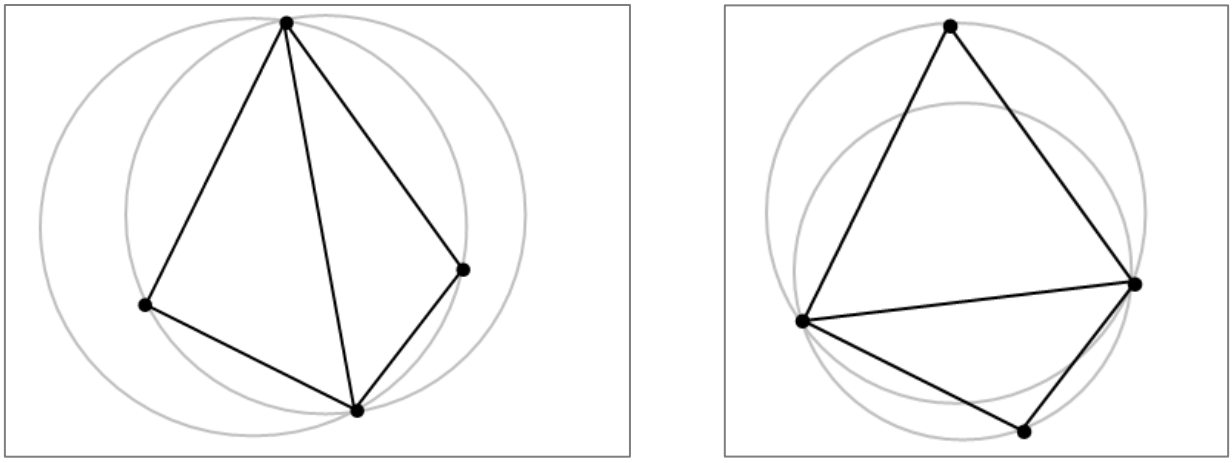

Figure 5-9: 1. The pair of triangles on the left does not meet the Delaunay Condition (the circumcircle contains more than three points). 2. However, the pair on the right meets the Delaunay Condition. Flipping the common edge produces a valid Delaunay Triangulation for the four points.

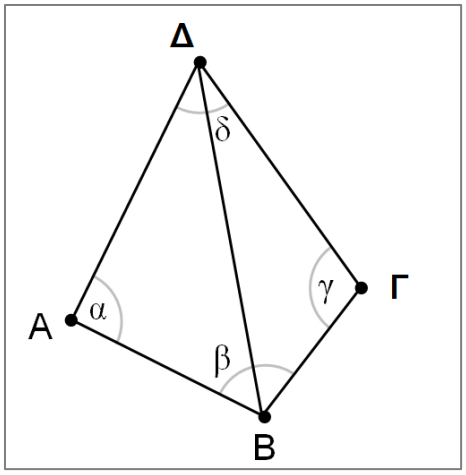

Figure 5-10: A different criterion is the sum of α and γ being smaller than 180°. In this case, this triangulation does not meet this Delaunay condition

5.3.4 Pairwise Matching

Following the creation of surfaces, the pairwise matching takes place. Fragmatch algorithm is developed for that purpose in order to perform global and partial matching of the surfaces. The two surfaces are compared both for the orientation of the sub-surfaces and with respect to the size of the surfaces as well. In cases of fragments that have been further fragmented to smaller pieces, the partial matching is performed following the comparison of the two surfaces that ICP had conducted in the previous step and determined the correspondences between them. The elements, whose difference of areas is less than a predefined threshold, are considered as common and a percentage of their similarity in size as well as their overlap between the two surfaces is determined and displayed by the algorithm. This percentage demonstrates the grade of similarity between the two surfaces. In addition, a percentage of the correlation of the angles determines the matching of the two surfaces.

High possibility of conjugate fragments to be merged is considered when a percentage of 90% in size and angles is attained.

The export of triangulation matrices and surfaces is the next step. Using Fragmatch algorithm it is not necessary to use any other software to create triangles and surfaces. These surfaces that have an acceptable percentage of matching in Fragmatch are imported in the present algorithm in order to attempt assemblage.

5.4 Part 2: Fragmatch^{+}

5.4.1 Development of Fragmatch^{+}

Main Description

The main concept is the determination of a rigid body transformation i.e. the synthesis of rotation and translation of the one point cloud to coincide with the reference point cloud. The requested transformation τ will be:

$$(X2)_{transform} = \boldsymbol{R} * X2 + \boldsymbol{\delta r} = X1 \quad (1)$$

where X_1 is the reference point cloud, X_2 the second point cloud and $(X_2)_{transform}$ the transformed point cloud. The transformed point cloud will coincide with the corresponding points of the reference point cloud X_1.

Input data: Fragmatch+ accepts as input data the broken surfaces of 3D digital models of archaeological fragments obtained by 3D laser scanning as well as the connectivity matrix of triangles which contains the vertex describing each triangle of Delaunay Triangulation. Both clouds of nodal points have been converted into 3D surfaces (Delaunay triangulation) in the previous step and are loaded in the main program.

The transformation τ is determined with the use of a rotation matrix $\boldsymbol{R}$ and a parallel translation $\boldsymbol{\delta r}$. The rotation matrix is composed of 9 unknown coefficients and the column-vector $\boldsymbol{\delta r}$ of 3. The system requires 12 equations to be solved.

$$\mathbf{R} = \begin{matrix} a_{11} & a_{12} & a_{13} \\ a_{21} & a_{22} & a_{23} \\ a_{31} & a_{32} & a_{33} \end{matrix} \qquad \boldsymbol{\delta}\mathbf{r} = \begin{matrix} \beta_{11} \\ \beta_{21} \\ \beta_{31} \end{matrix}$$

The solution of the system requires 4 conjugate points on the surfaces on which the total matching of the two surfaces is expected.

The quest of those points is based entirely on the Delaunay Triangulation of the two point clouds. Assuming that equal triangles of the cloud $X2$ will correspond to equal triangles of the reference point cloud, 4 conjugate points need to be determined and thus 2 triangles need to be identified as identical.

The term “perfect conjugate” is given in order to denote points on the two surfaces that have emerged from the same point (position) when the original body broke.

Assumption

Research process:

1) Determination of equal triangles between the two constructed meshes → The perfect conjugate points are expected to belong to equal triangles on the surfaces → The algorithm runs a process to determine the equal triangles on both sides in two stages:

   i. Stage 1: Stage 1: searching for the equal-area triangles between the two meshes.

A new table is created where it has n rows equal to the quantity of the triangles and two columns. Equal triangles between the first and the second cloud of points are passed into the columns of the table.

Before that, the area of each triangle is calculated. Then these triangles are compared and are saved by column-vector form. In the 1st column the triangles of the first cloud are saved and in the 2nd column the equal-sized triangles of the second cloud.

	Table (eq)	
No	**E1**	**E2**
1	2	891
2	29	230
3	34	2691
4	168	170
5	208	4065
6	524	995
7	652	2640
8	688	776
9	722	2981

E.g. eq(6,1) = 524, eq(6,2)=995: That means that the 6^{th} row shows the equality of the area of the 524^{th} triangle of the reference cloud with the 995^{th} triangle of the second cloud.

The area is calculated as follows by using the cross product of the two triangles:

The cross product or vector product is a binary operation on two vectors in three-dimensional space and is denoted by the symbol $\times$. Given two linearly independent vectors **a** and **b**, the cross product, $\mathbf{a} \times \mathbf{b}$, is a vector that is perpendicular to both **a** and **b** and thus normal to the plane containing them.

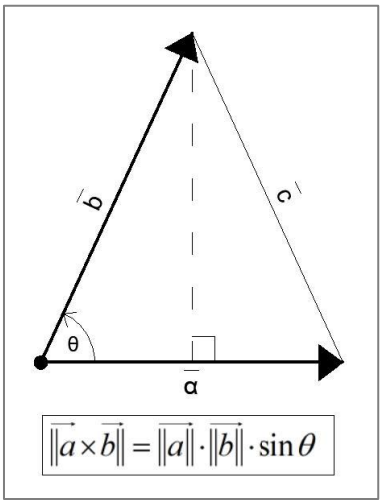

Figure 5-11: Calculation of area of triangles using cross product

The area of the triangle can also be calculated with the norm $||\mathbf{a} \times \mathbf{c}||$ and $||\mathbf{b} \times \mathbf{c}||$.

In programming environment totally equal number do not exist and equal areas are considered those which do not differ more than a small number called epsilon: $\frac{||E1_{(i)} - E1_{(j)}||}{E1_{(i)}} < eps$

This tolerance is defined by the user (semi-automatic method) accordingly.

ii. Stage 2: From the equal-area triangles, the equilateral triangles have to be found. In order to find the equilateral triangles a built-in function is used (function: vertex correspond). This function defines the correspondences of vertices of triangles (at the edge of the equal sides) and simultaneously the equality of the sides of the equal-area triangles is tested.

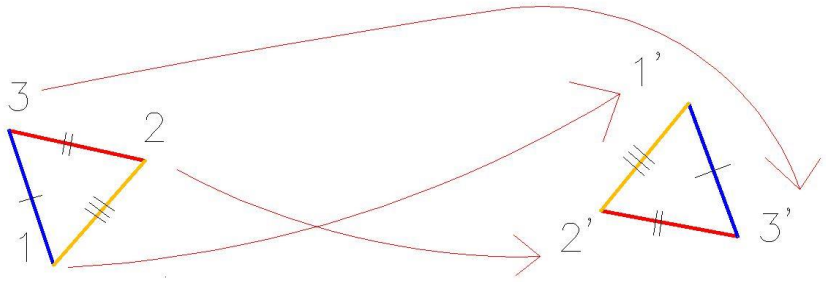

Figure 5-12: This function allows the correspondence of the conjugate triangles vertices.

$$\mathbf{1} \rightarrow \mathbf{1}', \mathbf{2} \rightarrow \mathbf{2}', \mathbf{3} \rightarrow \mathbf{3}'$$

A repetitive process is initiated afterwards where pairs of triangular equalities are investigated, where the 1st equality gives the 3 possible matching points and the 2nd equality of triangles gives the 4th required point in order to calculate the possible rotation matrix. For faster calculations, the algorithm chooses randomly the pairs of the equal triangles

2) Rigid Body Transformation

A "solid body" is geometrically defined as a three-dimensional system XYZ set of points, which when transformed, does not change in shape and size (Καρράς, 1998). In that sense, in a Cartesian orthogonal system the solid-body transformation involves, in general, 6 degrees of freedom expressed by the following 6 parameters:

• 3 components ΔXo, ΔYo, ΔZo of translation $\boldsymbol{\delta r}$ along the 3 axes

• 3 rotations, i.e. along the angles Ω, Φ, K around the axes X, Y, Z, respectively, which define the rotation matrix R.

If x is the position vector of one random point at the three-dimensional system XYZ and x' the position vector of the same point at the three-dimensional system X'Y'Z' which varies by rotation and translation from the first point, then the transformation of the solid body is described as:

$$\mathrm{x}' = \mathrm{R} * \mathrm{x} + \boldsymbol{\delta}\mathbf{r}' \quad \text{or } \mathrm{x}' = \mathrm{R} * (\mathrm{x} + \boldsymbol{\delta}\mathbf{r})$$

In the first case, it is considered that the rotation precedes the translation and thereby the translation takes place after in the system X'Y'Z', while in the second case the

rotation takes place afterwards so the translation is referred to the original system XYZ. It is clear that $\delta r'(= R * \delta r) \neq \delta r$, i.e. the 3 components of the translation depend on the equation form while the rotation matrix remains the same.

In the present algorithm the transformation consisted first of a rotation and then of a translation: $x' = R * x + \boldsymbol{\delta r'}$

Furthermore, the rotation matrix R(3×3) depends on the sequence of the rotations Ω−Φ−K along the axes :

$$\mathbf{R} = \mathbf{R_K R_\varphi R_\Omega}$$

In general, the minimum requirement for the transformation of the solid object with respect to a reference object can be performed by knowing 3 corresponding points at each body. However, the resulting equations are not linear and the system is solved by use of approximate values.

The innovation in this case is the creation of possible rotation matrices, which are produced by the equalities of triangles. Subsequently, the possible rotation matrices are tested according to the criterion of the rotation matrix.

Assuming that a point $\mathbf{X_1} = \begin{matrix} \mathrm{X}_1 \\ \Upsilon_1 \\ \mathrm{Z}_1 \end{matrix}$ in the reference cloud and its similar $\mathbf{X_1'} = \begin{matrix} \mathrm{X}_1' \\ \Upsilon_1' \\ \mathrm{Z}_1' \end{matrix}$ in the second cloud, the rotation matrix is:

$$\mathbf{X_1} = \begin{bmatrix} \mathrm{a}_{11} & \mathrm{a}_{12} & \mathrm{a}_{13} \\ \mathrm{a}_{21} & \mathrm{a}_{22} & \mathrm{a}_{23} \\ \mathrm{a}_{31} & \mathrm{a}_{32} & \mathrm{a}_{33} \end{bmatrix} * \mathbf{X_1'} + \begin{matrix} \delta\mathrm{x} \\ (\delta\mathrm{y}) \\ \delta\mathrm{z} \end{matrix} \quad (2)$$

As mentioned before, each point provides 3 equations. In total, 4 points are required in order to solve linearly the system of 12 equations. The 9 dependent elements of the rotation matrix R, form a nonlinear system of equations which are stated below.

Therefore, two pairs of triangles provide 4 points for the linear calculation of the possible rotation matrix and consequently of the corresponding translation **δr**.

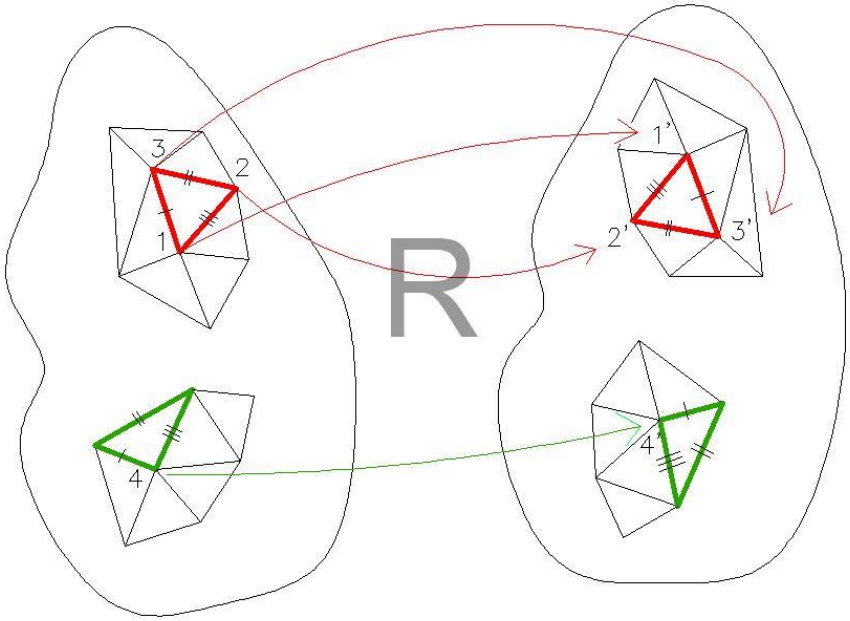

Figure 5-13: 4 points are used for the applied transformation

Firstly, all the rotation matrices are calculated and then their correctness is tested according to the following criteria:

The two requirements are stated below:

I. An investigation is performed using orthogonality equations. Those matrices which do not satisfy the conditions are not taken into account.

The orthogonality conditions $\alpha_{ij}\alpha_{ik} = \delta_{jk}$ require:

1) For j=k=1 that $a_{11}a_{11} + a_{21}a_{21} + a_{31}a_{31} = 1$ which is seen to be the sum of squares of elements in the first column
2) For j=2, k=3 that $a_{12}a_{13} + a_{22}a_{23} + a_{32}a_{33} = 0$ which is seen to be the sum of products of corresponding elements of the second and the third columns
3) Any two columns “multiplied together element by element and summed” to be zero. The sum of squares of elements of any column to be unity (Mase, 1982).

The 6 equations of the orthogonality conditions of the rotation matrix are:

$$a_{11}{}^2 + a_{21}{}^2 + a_{31}{}^2 = 1 \qquad a_{11}a_{12} + a_{21}a_{22} + a_{31}a_{32} = 0$$

$$a_{12}{}^2 + a_{22}{}^2 + a_{32}{}^2 = 1 \qquad a_{11}a_{13} + a_{21}a_{23} + a_{31}a_{33} = 0$$

$$a_{13}{}^2 + a_{23}{}^2 + a_{33}{}^2 = 1 \qquad a_{12}a_{13} + a_{22}a_{23} + a_{32}a_{33} = 0$$

For this function, a tolerance is set in order to ensure the robustness of the equations. The user can manually define the threshold of this tolerance accordingly.

II. The second criterion implies that the correct rotation matrix appears more frequently than the others. Those matrices with the highest rate of appearance have equal norm and this ascertains that the aforementioned conditions of the rotation matrix are satisfied.

Calculation of Rotation Matrix

Assuming that (X_1, X'_1), (X_2, X'_2), (X_3, X'_3), (X_4, X'_4), are pairs of possible conjugate points on the identical triangles of the reference point cloud and the compared point cloud respectively, the transformation is calculated as follows:

$$\boldsymbol{X_1} = \begin{pmatrix} x_1 \\ y_1 \\ z_1 \end{pmatrix} \boldsymbol{X'_1} = \begin{pmatrix} x'_1 \\ y'_1 \\ z'_1 \end{pmatrix} \qquad \boldsymbol{X_2} = \begin{pmatrix} x_2 \\ y_2 \\ z_2 \end{pmatrix} \boldsymbol{X'_2} = \begin{pmatrix} x'_2 \\ y'_2 \\ z'_2 \end{pmatrix}$$

$$\boldsymbol{X_3} = \begin{pmatrix} x_3 \\ y_3 \\ z_3 \end{pmatrix} \boldsymbol{X'_3} = \begin{pmatrix} x'_3 \\ y'_3 \\ z'_3 \end{pmatrix} \qquad \boldsymbol{X_4} = \begin{pmatrix} x_4 \\ y_4 \\ z_4 \end{pmatrix} \boldsymbol{X'_4} = \begin{pmatrix} x'_4 \\ y'_4 \\ z'_4 \end{pmatrix} \Longrightarrow$$

$$\begin{aligned} \boldsymbol{X_1} &= \mathbf{R} * \mathbf{X'_1} + \boldsymbol{\delta r} \\ \boldsymbol{X_2} &= \mathbf{R} * \mathbf{X'_2} + \boldsymbol{\delta r} \\ \boldsymbol{X_3} &= \mathbf{R} * \mathbf{X'_3} + \boldsymbol{\delta r} \\ \boldsymbol{X_4} &= \mathbf{R} * \mathbf{X'_4} + \boldsymbol{\delta r} \end{aligned} \quad \Big\} \text{ Subtraction}$$

$$\left.\begin{aligned}(\boldsymbol{X_2}-\boldsymbol{X_1}) &= \mathbf{R}*(\mathbf{X'_2}-\boldsymbol{X'_1})\\ (\boldsymbol{X_3}-\boldsymbol{X_1}) &= \mathbf{R}*(\mathbf{X'_3}-\boldsymbol{X'_1})\\ (\boldsymbol{X_4}-\boldsymbol{X_1}) &= \mathbf{R}*(\mathbf{X'_4}-\boldsymbol{X'_1})\end{aligned}\right\}$$

$$[(\boldsymbol{X_2}-\boldsymbol{X_1})(\boldsymbol{X_3}-\boldsymbol{X_1})(\boldsymbol{X_4}-\boldsymbol{X_1})] = \mathbf{R}*[(\mathbf{X'_2}-\boldsymbol{X'_1})(\mathbf{X'_3}-\boldsymbol{X'_1})(\mathbf{X'_3}-\boldsymbol{X'_1})] \Rightarrow$$

$$\boldsymbol{R} = [(\boldsymbol{X_2}-\boldsymbol{X_1})(\boldsymbol{X_3}-\boldsymbol{X_1})(\boldsymbol{X_4}-\boldsymbol{X_1})] * inv\,[(\mathbf{X'_2}-\boldsymbol{X'_1})(\mathbf{X'_3}-\boldsymbol{X'_1})(\mathbf{X'_3}-\boldsymbol{X'_1})]$$

or

$$\boldsymbol{R} = \begin{matrix}(x_2-x_1) & (x_3-x_1) & (x_4-x_1)\\ (y_2-y_1) & (y_3-x_1) & (y_4-y_1)\\ (z_2-z_1) & (z_3-z_1) & (z_4-z_1)\end{matrix} * inv \begin{matrix}(x'_2-x'_1) & (x'_3-x'_1) & (x'_4-x'_1)\\ (y'_2-y'_1) & (y'_3-x'_1) & (y'_4-y'_1)\\ (z'_2-z'_1) & (z'_3-z'_1) & (z'_4-z'_1)\end{matrix}$$

Replacing **R** in the equation $\boldsymbol{\delta r}$ is calculated accordingly:

$$\boldsymbol{\delta r} = \mathbf{X_1} - \mathbf{R}*\mathbf{X'_1}$$

or

$$\boldsymbol{\delta r} = \boldsymbol{X_2} - \boldsymbol{R}*\boldsymbol{X'_2}$$

or

$$\boldsymbol{\delta r} = \mathbf{X_3} - \mathbf{R}*\mathbf{X'_3}$$

or

$$\boldsymbol{\delta r} = \mathbf{X_4} - \mathbf{R}*\mathbf{X'_4}$$

5.5 Test Cases

5.5.1 Sphere

The idea of transformation was first applied on a quadrant, which was rotated and translated and then returned to its initial position.

With the use of the sphere equation: $x^2 + y^2 + z^2 = 1$ a quadrant with center (0,0) is formed and the radius is set to 1.

i. Simulation with a rotation around z-axis:

A second quadrant is created from the first with a rotation of 30 degrees in the z axis and a translation of 1. The rotation matrix and the translation matrix are:

$$\mathbf{R} = \begin{pmatrix} \cos 30° & -\sin 30° & 0 \\ \sin 30° & \cos 30° & 0 \\ 0 & 0 & 1 \end{pmatrix} \qquad \boldsymbol{\delta r} = \begin{pmatrix} 1 \\ 1 \\ 1 \end{pmatrix}$$

By applying this transformation, the transformed quadrant is depicted below having its center (1,1) , radius 1 and a projection to the z axis in 2. It is obvious that the transformed quadrant has maintained the same angles as well as the distances between the points.

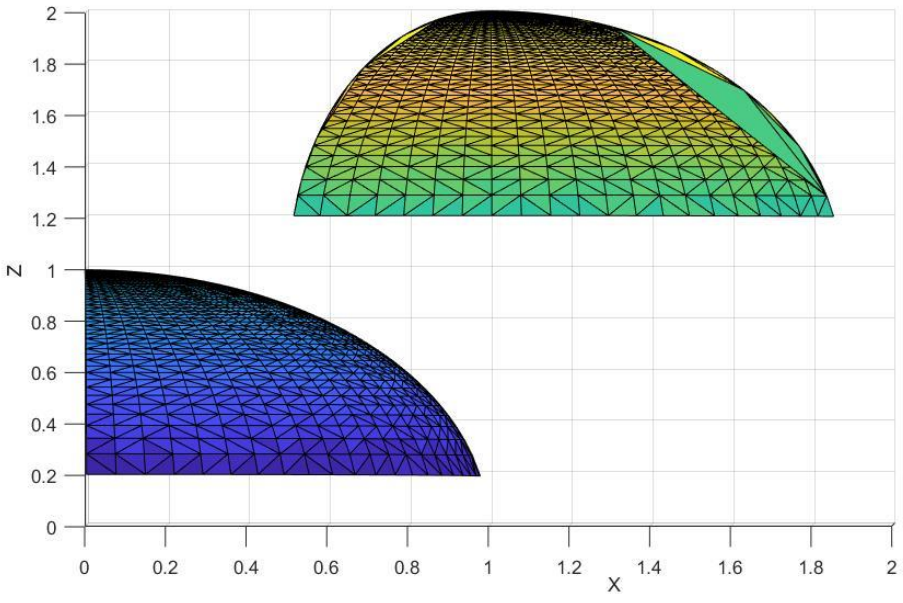

Figure 5-14: x-z planes of the spheres

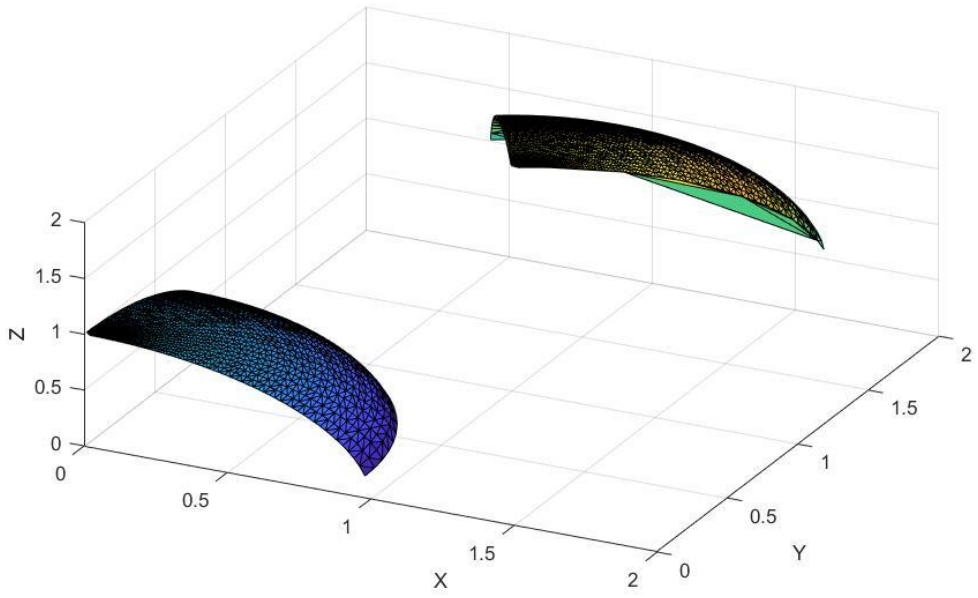

Figure 5-15 : Simulation of quadrants

Consequently a reverse procedure begins as the algorithm considers the two quadrants as two different conjugate objects and attempts to unite them by finding the desired transformation. The first stage is the creation of surfaces with the Delaunay Triangulation and then the algorithm tries to find equal triangles along the surfaces. Given that the second quadrant was created in Matlab, the tolerance limit is set to 10^{-8} and the algorithm estimates strictly the equalities between the triangles. The result of the assemblage shows the two quadrants placed into one and the coefficients α_{ij} are correctly determined.

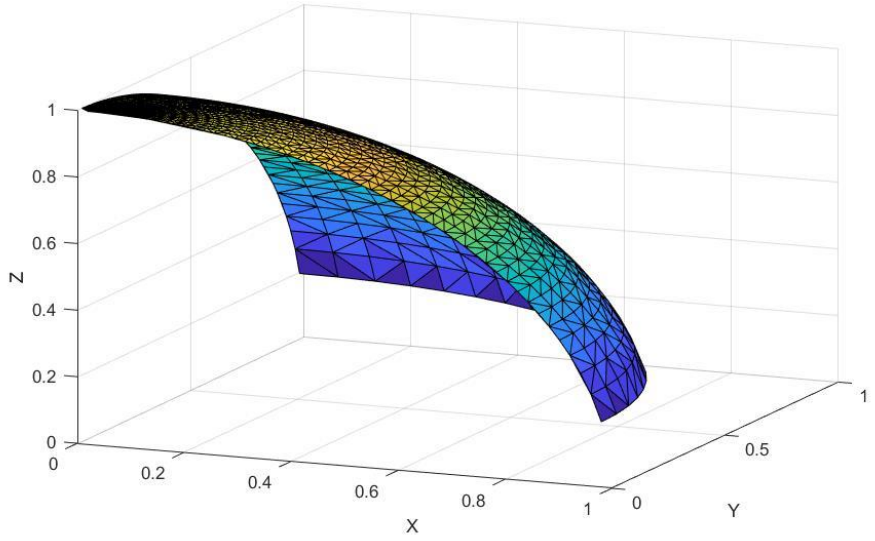

Figure 5-16: The two quadrants joined into one

ii. <u>Simulation with rotation around the 3 axes</u>

In this case, the second quadrant is created as a copy of the first one but a rotation about all X, Y, Z axes was applied instead. A translation of 25 meters was applied as well. The rotation matrix and the translation matrix in this case are:

$$\mathbf{R} = \begin{pmatrix} \cos 30° & -\sin 30° & 0 \\ \sin 30° & \cos 30° & 0 \\ 0 & 0 & 1 \end{pmatrix} \begin{pmatrix} \cos 30° & 0 & \sin 30° \\ 0 & 1 & 0 \\ -\sin 30° & 0 & \cos 30° \end{pmatrix} \begin{pmatrix} 1 & 0 & 0 \\ 0 & \cos 30° & -\sin 30° \\ 0 & \sin 30° & \cos 30° \end{pmatrix}$$

and

$$\boldsymbol{\delta}\mathbf{r} = \begin{pmatrix} 25 \\ 25 \\ 25 \end{pmatrix}$$

This transformation results in the desired union of the two quadrants.

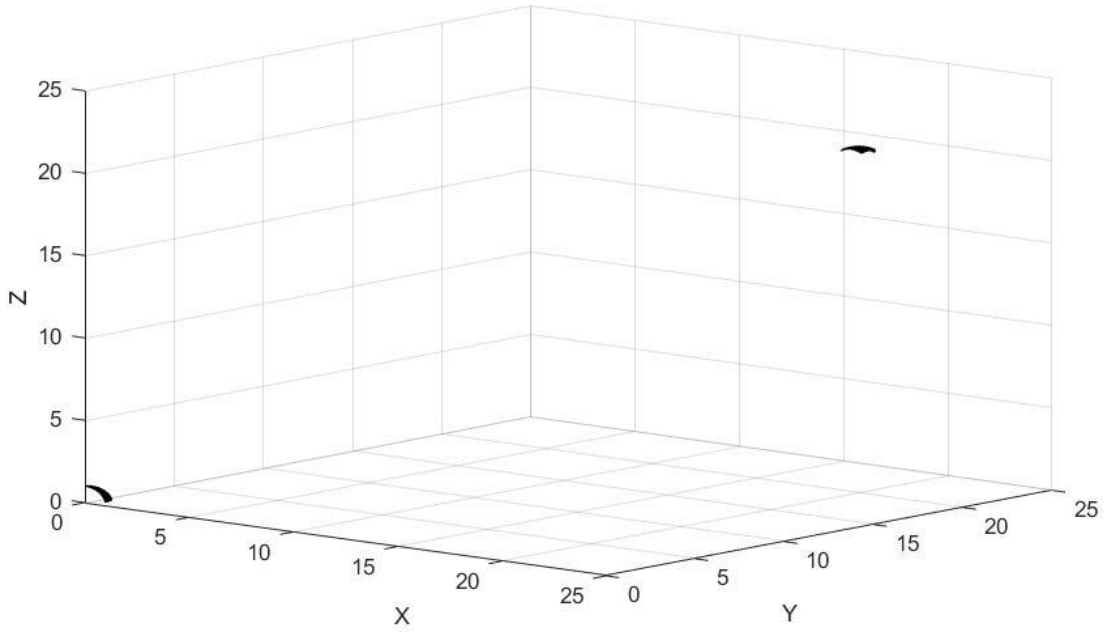

Figure 5-17: 3D view of the quadrants

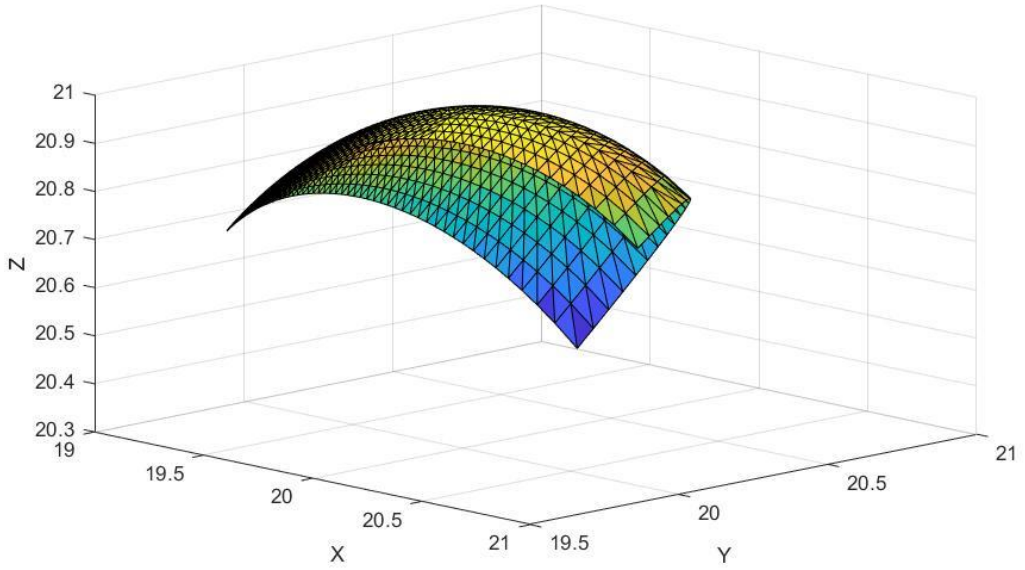

Figure 5-18: Rotated quadrant along the three axes

By applying this transformation, the algorithm calculates efficiently the rotation matrix and adjusts the conjugate quadrants. In this point, it is important to mention that small rotations around x and y axis are acceptable as long as they don't create a problem during Delaunay Triangulation. As the Delaunay triangles are formed through the projection of the object in the x-y plane, a big rotation about these axes would not represent the surface of the object appropriately, resulting in a deficient depiction of the surface.

The applied transformation has merged the conjugate quadrants with high accuracy as can be seen in Fig. 19.

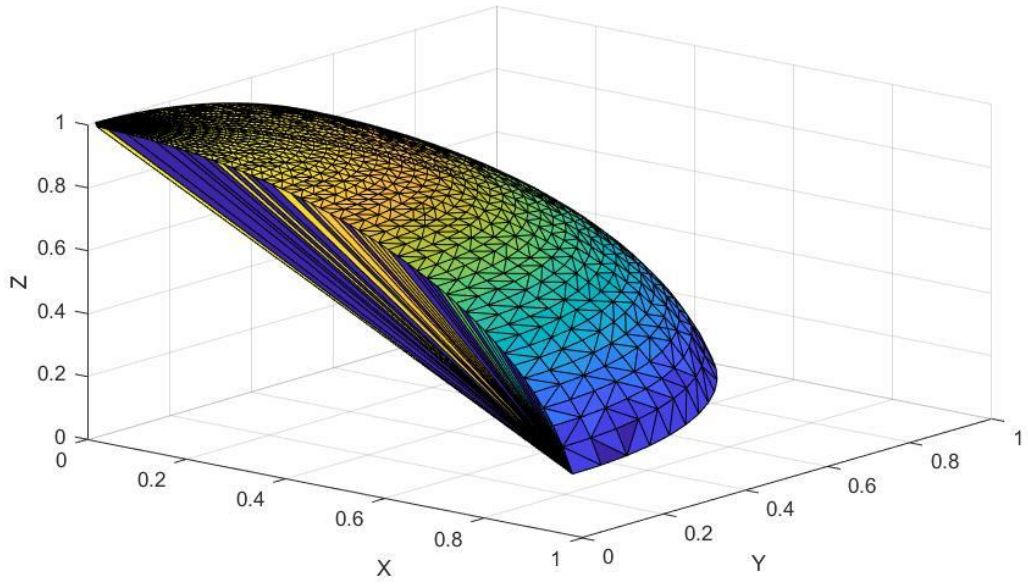

Figure 5-19: Union of conjugate quadrants

The examples described above, were the basis of the development for the present algorithm in order to unify intricate surfaces of planar faced fragments. In those examples, the surfaces were created using the Delaunay Triangulation in Matlab and the criteria of the rotation matrix were not implemented as the matching of equal triangles resulted always in the correct transformation.

5.5.2 Examples of real fragments

In this section, results of a practical implementation of the algorithm are presented. The fragments, used for these tests, were presented in chapter 4 and were segmented in Cloud Compare in order to separate the broken surfaces. These fractured, eroded and shattered surfaces were tested by the developed algorithm. A shattered object generates completely irregular surfaces which can be difficult to distinguish. Scans were performed with the laser scanner FaroArm and provided dense point clouds of each object.

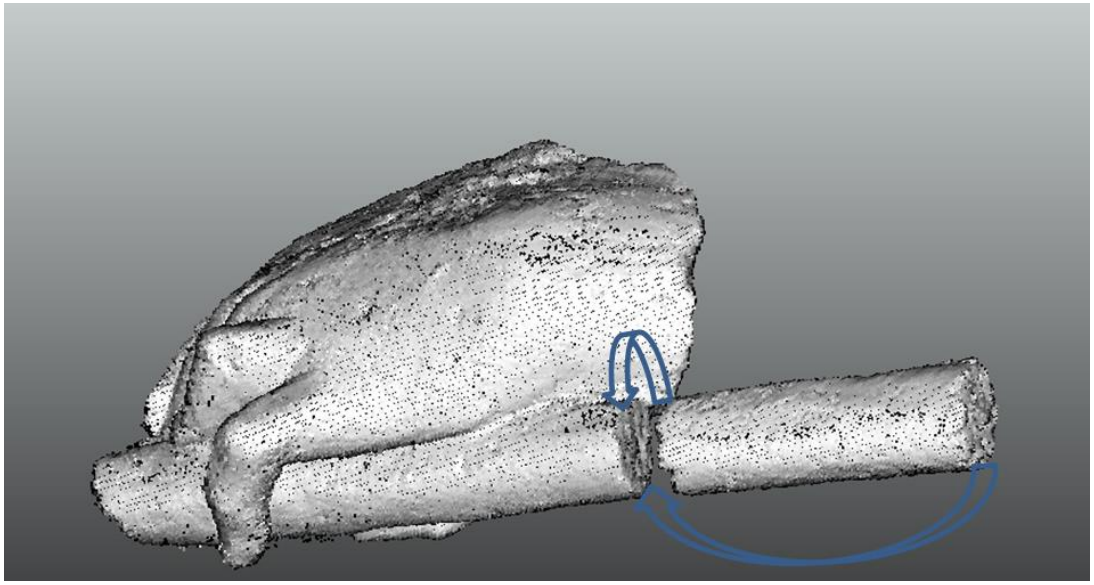

Figure 5-20: cylindrical conjugate fragments and potential fits of surfaces

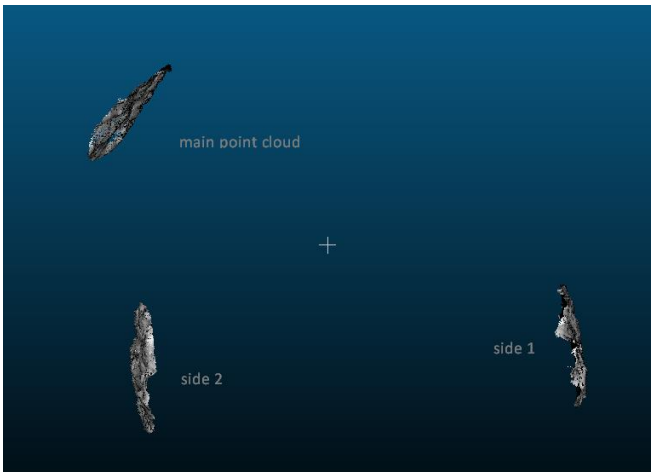

Figure 5-21: The main point cloud belongs to the reference fragment (hand holding a cylindrical object). Each side of its hypothetical conjugate fragment is named after side 1 & side 2

For each point cloud, a conjugate piece was created in Matlab. The main point cloud consisted of approximately 50000 points, while side 1 and side 2 consisted of 1200000 points approximately with an average area of 1.3mm^2. At the beginning, those point clouds were subsampled to 25000 points and then to 6000 points. Since those clouds of points generate a random and irregular surface, various simulations were conducted using each surface with its created conjugate pair in order to test the robustness of the algorithm. The steps of the algorithm are analyzed in each case. Each time, the algorithm accepts two fragments as input data applies the transformation in order to unify them.

i. Number of points in the point cloud

The first simulation aims to determine the algorithm's ability to unify two conjugate surfaces with the same number of points and created triangles in order to identify the limits of the algorithm. The algorithm was applied twice to test a pair of fragments of 25000 points and a pair of 6000 points.

As described in the previous paragraph, Delaunay triangles are exported from Fragmatch and used as input data in Fragmatch+ along with the point cloud. The average size of a triangle's side was approximately 6mm. The matching percentage is 100% both in size and angles, something that could be easily anticipated as each pair consists of two identical conjugate surfaces.

The equal triangles of each point cloud are calculated from the equal area triangles of each surface, 4 conjugate points (in 2 triangles) are in the quest which would satisfy the conditions of the rotation matrix in order the transformation to be applied. The equal

triangles of each point cloud are calculated and from the equal area triangles of each surface, 4 conjugate points (in 2 triangles) are in the quest which would satisfy the conditions of the rotation matrix in order the transformation to be applied.

Pair of 6000 points: A rotation along X, Y, and Z axes of 30 degrees is applied to the conjugate fragment before the initiation of the iterative process. The selected accuracy of equal triangles was set to 10^{-6} and among the 11930 equalities found, the algorithm tried to determine the suitable transformation. In total, the rotation matrix was found 225 times which proves that not all equal triangles are conjugate and satisfy the requirements that were set. The reference cloud, the conjugate fragment as well as the unification of the surfaces are depicted in the pictures below.

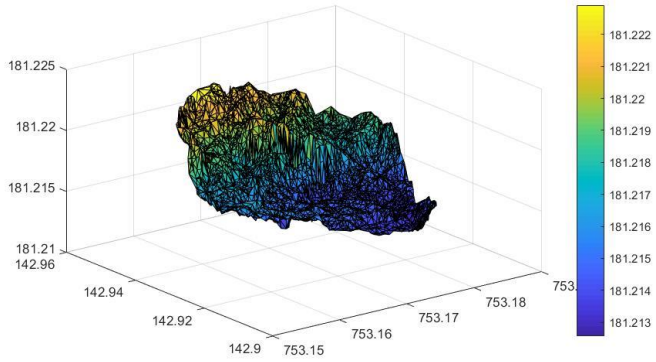

Figure 5-22: reference cloud

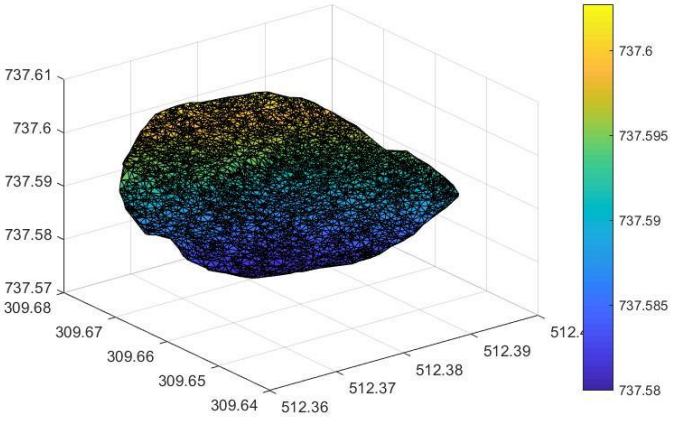

Figure 5-23: cloud2 rotated around the 3 axes

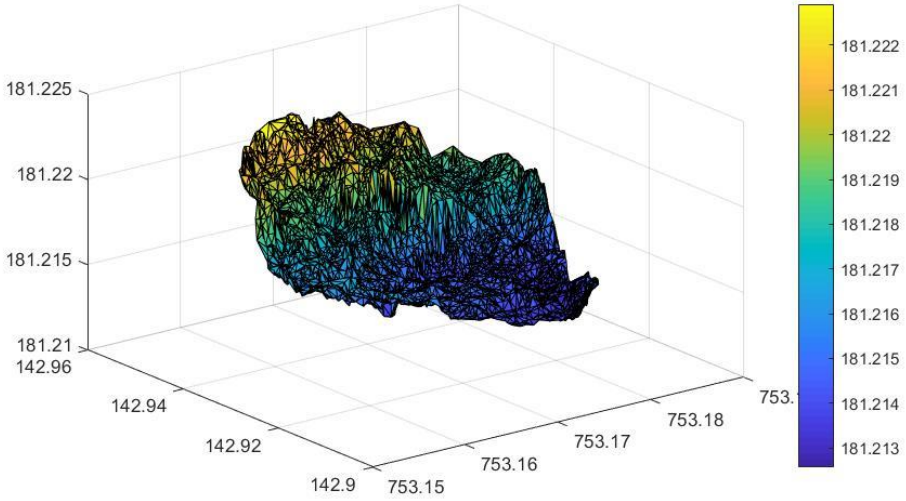

Figure 5-24: Unification of fragments

Pair of fragments of 25000 points

A rotation of 30 degrees about the Z axis is applied this time to the conjugate fragment before the initiation of the iterative process. This pair of surfaces consists of an enormous number of triangles, which makes the finding of equal triangles a demanding process. The process can be accelerated by comparing a smaller number of equal triangles, chosen randomly, in order to execute the transformation. In this case, a risk of omitting equal triangles that could be used for the transformation exists. However, since these surfaces are identical, this does not arise any problem in the present case. The limit is set to 10^{-6} and the equalities tested this time are 5540 and, among them, 245 equal rotation matrices were found. The reference cloud, the conjugate fragment as well as the unification of the surfaces are depicted in the pictures below.

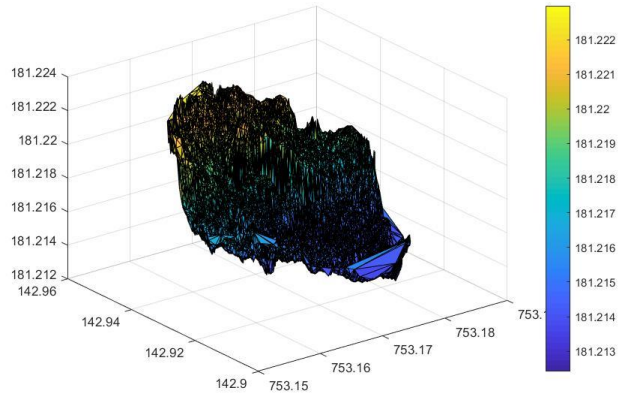

Figure 5-25: Reference point cloud

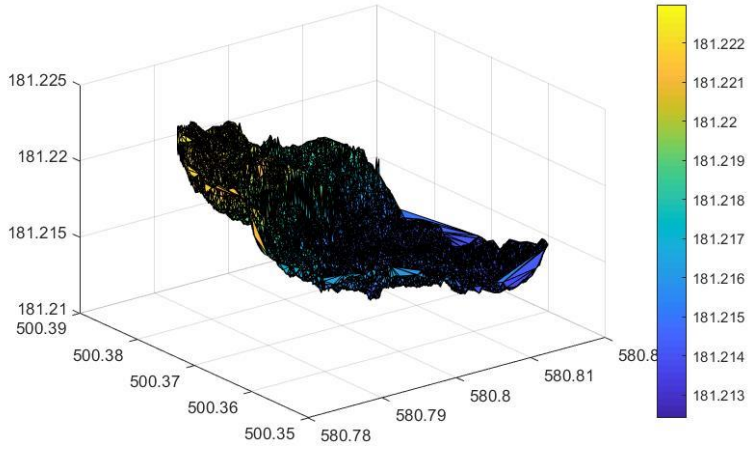

Figure 5-26: Rotated of second cloud around z axis

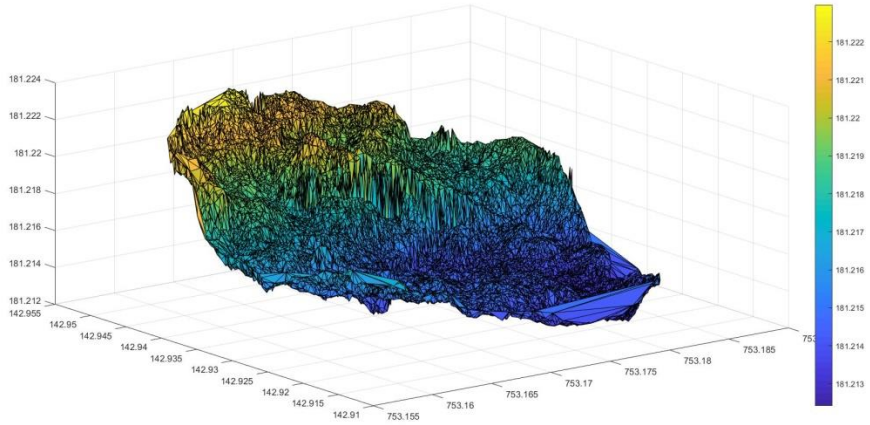

Figure 5-27: Successful Union of fragments

ii. Wear of surfaces

One of the most common phenomena in the archaeological findings is the deterioration of their surfaces. Most findings, due to their contact with the soil, their exposure to the environment and time as well as human impact, their surfaces have been corroded and deformed. The algorithm is applied to test two pair of fragments. In both cases the reference point cloud contains 25000 points and is compared with two other point clouds from which arbitrary points have been eliminated but the initial geometry and shape of the surface were preserved.

First simulation: the reference point cloud of 25000 points is tested with its conjugate point cloud of 12000 distributed uniformly points on the surface for the preservation of the geometry. For the Delaunay triangulation the average side of triangles was set to 7mm. The matching percentage calculated in Fragmatch is 86% which is considered acceptable. A rotation of the conjugate fragment about X, Y and Z axes is applied before the initiation of the iterative process. The accuracy for defining equal triangles was set to 10^{-6} and among the 4100 equalities of triangles found; the algorithm determined the suitable transformation. In total, the rotation matrix was found only 4 times which proves that not all equal area triangles are conjugate and satisfy the requirements that were set. The reference cloud, the conjugate fragment as well as the unification of the surfaces are depicted in the pictures below.

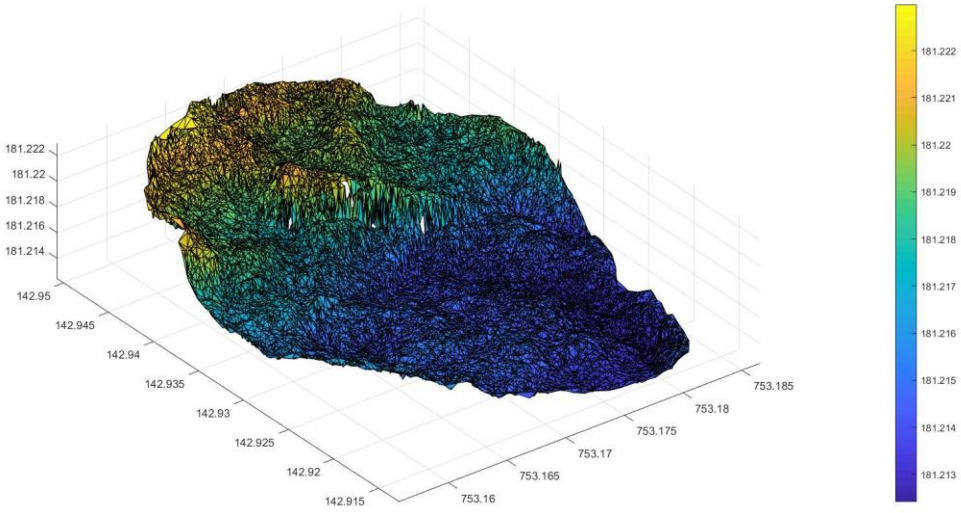

Figure 5-28: Reference point cloud

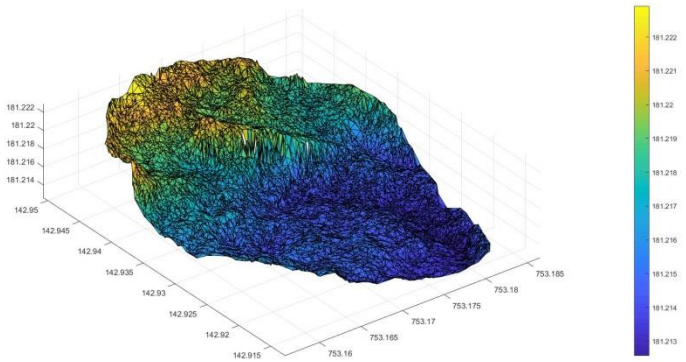

Figure 5-29: Second point cloud after Delaunay Triangulation before rotation and translation

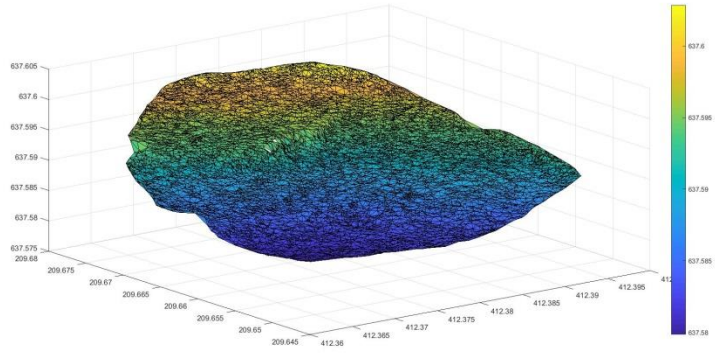

Figure 5-30: Rotation of second cloud along the 3 axes and translation

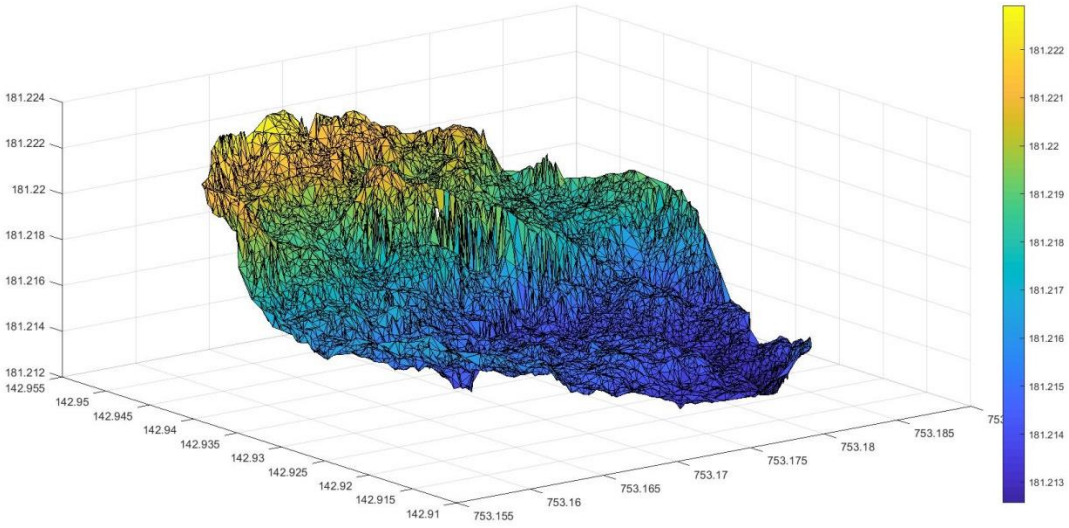

Figure 5-31: Successful Union of fragments

Second Simulation: the reference point cloud of 25000 points is tested with its conjugate point cloud of 6000 distributed uniformly points on the surface. For the Delaunay triangulation, the average side of triangle was set to 6mm. The matching percentage calculated in Fragmatch is 75% which is considered acceptable as the total overlap of the two surfaces accounts for nearly 60%. A rotation along X, Y, Z axes of 30 degrees is applied to the conjugate fragment and the process begins. The threshold of equal triangles was set to 10^{-3} and among the 23500 equalities of triangles found, the algorithm searches to determine the suitable transformation. In total, the rotation matrix was found 320 times and the two clouds were properly unified. The reference cloud, the conjugate fragment as well as the unification of the surfaces are depicted in the pictures below.

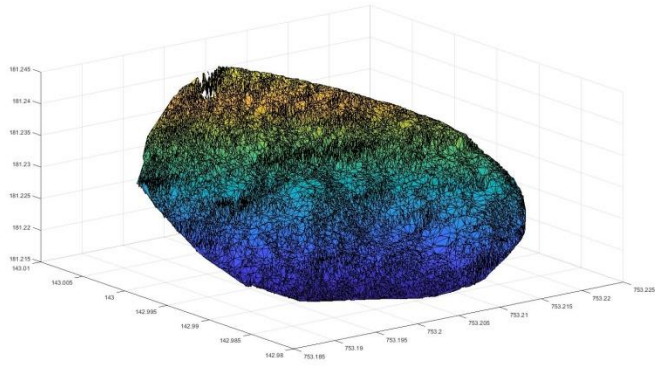

Figure 5-32: Reference point cloud

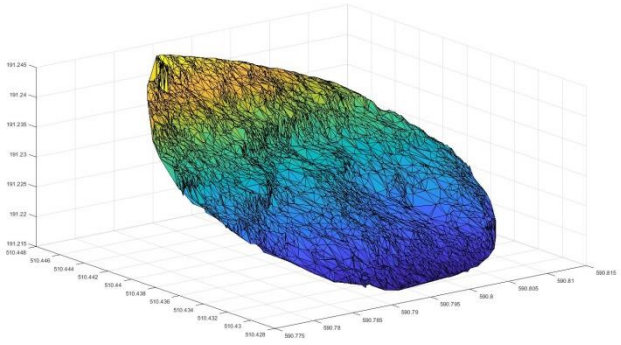

Figure 5-33: cloud 2 with rotation of 30 degrees along the three axis

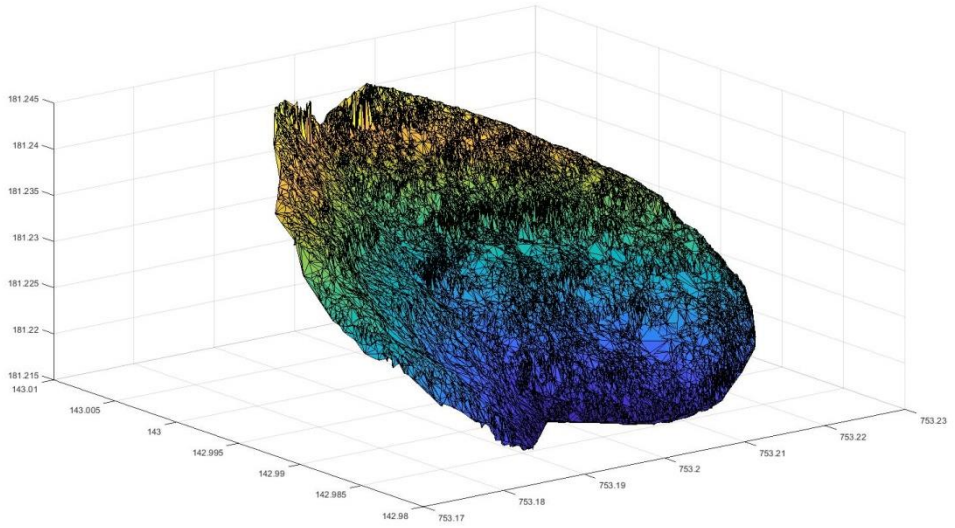

Figure 5-34: Successful Union of fragments

iii. Next a simulation between two different sized fragments was implemented.

A shattered object generates completely irregular surfaces and a partial union can be implemented between different size fragments. A conjugate shattered point cloud was created in Cloud Compare using the segmentation tool which consisted of approximately 5900 points and was followingly tested with its conjugate total point cloud of 25000 points. A rotation about the Z axis of 30 degrees is applied to the fractured fragment before the initiation of the iterative process. The accuracy used to define the equal triangles was set to 10^{-6} and among the 32170 equalities of triangles found; the algorithm determined the suitable transformation. In total, the rotation matrix was found 702 times and the two clouds were properly merged. The reference cloud, the conjugate fragment as well as the unification of the surfaces are depicted in the pictures below.

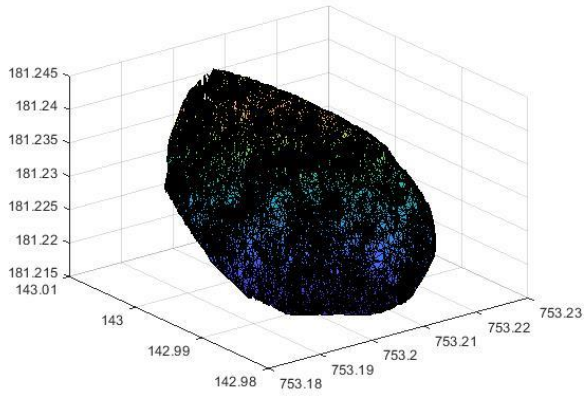

Figure 5-35: Reference point cloud

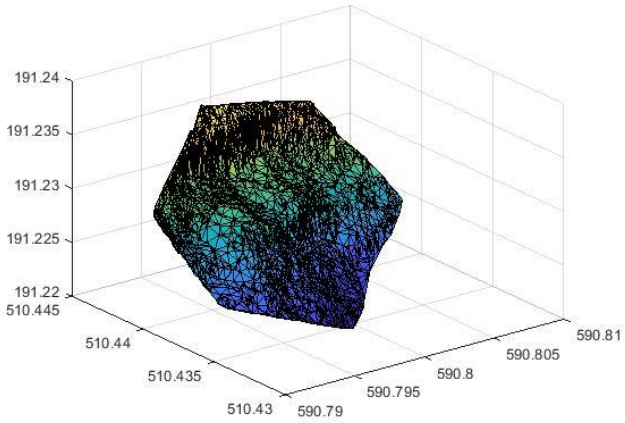

Figure 5-36: Shattered conjugate surface

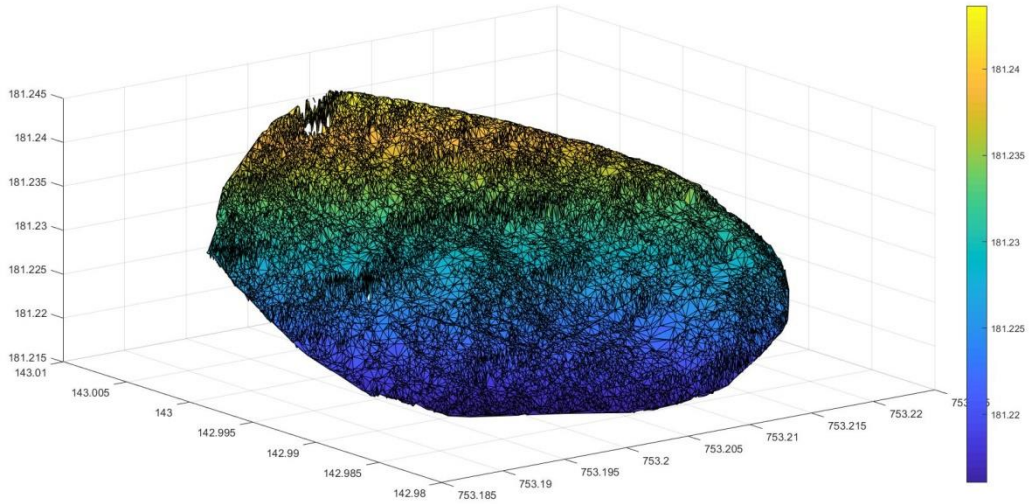

Figure 5-37: Successful Union of fragments

iv. Limits of noise

The current simulation aims to determine the limits of tolerable noise in the data. In this case variations in depth (dz) up to 5mm have been randomly distributed at some points of the second point cloud. A conjugate surface of the reference object was created with randomly distributed noise across the surface. It was noticed that the percentage of resemblance is reduced when the wear of the second surface increases. A rotation about Z axis of 30 degrees was applied to the fractured fragment before the initiation of the iterative process and the following three examples are presented:

Wear (1mm): The accuracy of defining equal triangles was set to 10^{-6} and among the 6200 equalities of triangles found; the algorithm determined the suitable transformation. In total, the rotation matrix was found 540 times and the two clouds were properly merged. The reference cloud is depicted in figure 38, the conjugate fragment in figure 39 and their union in figure 40.

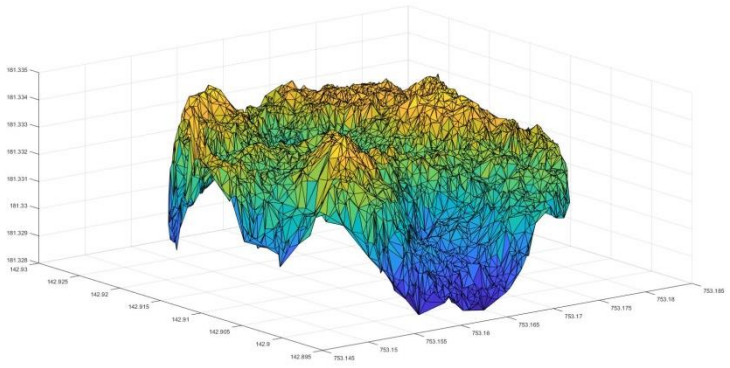

Figure 5-38: Reference point cloud

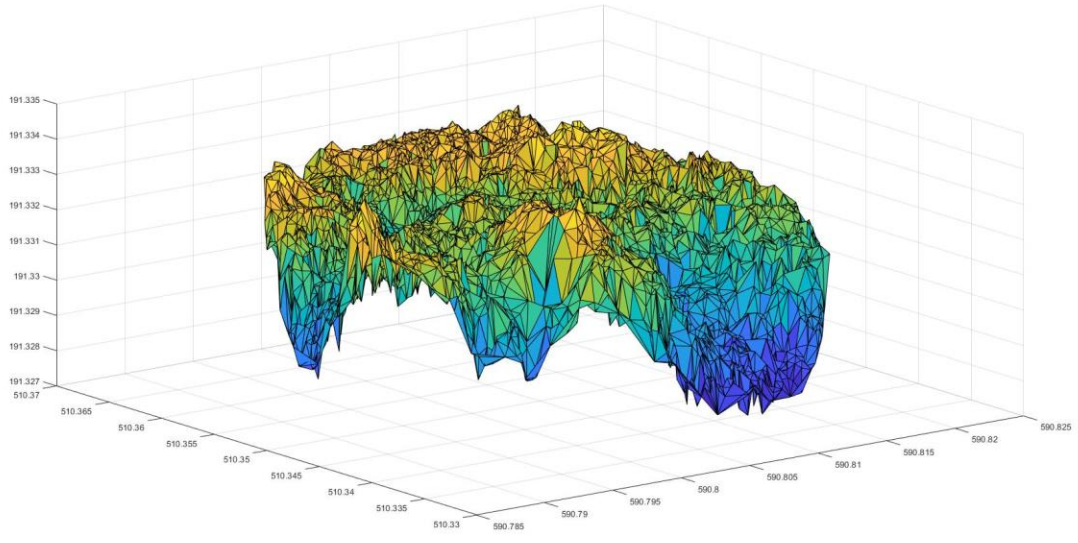

Figure 5-39: surface with wear of 0.01mm randomly distributed

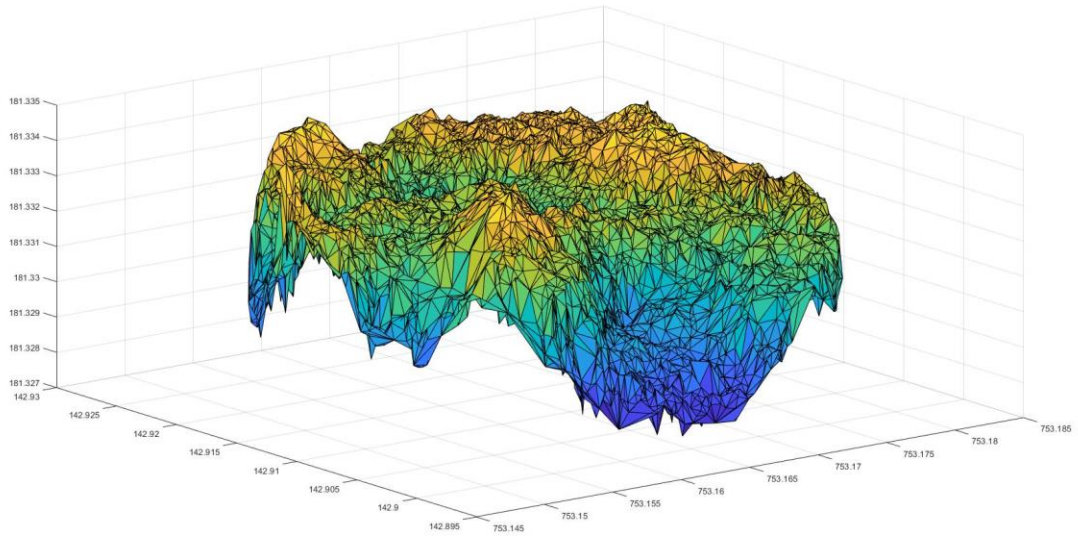

Figure 5-40: Successful Union of fragments

Wear (2mm): The accuracy of defining equal triangles was set to 10^{-6} and among the 5500 equalities of triangles found; the algorithm determined the suitable transformation. In total, the rotation matrix was found 470 times and the two clouds were properly

merged. The reference cloud is depicted in figure 41, the conjugate fragment in figure 42 and their union in figure 43.

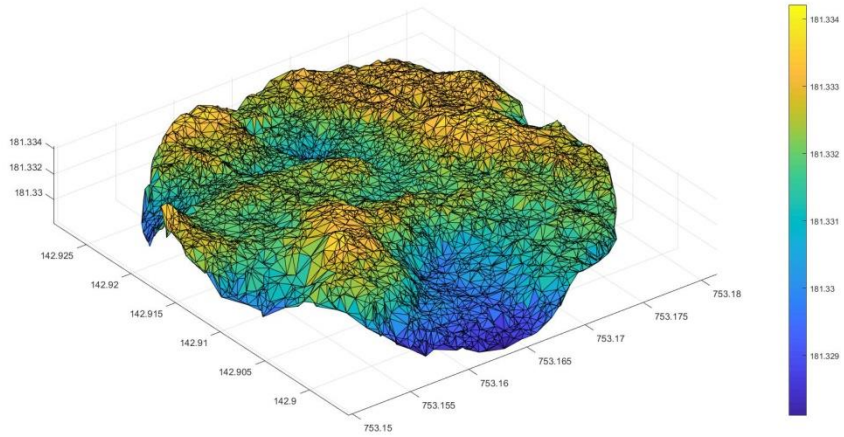

Figure 5-41: reference surface

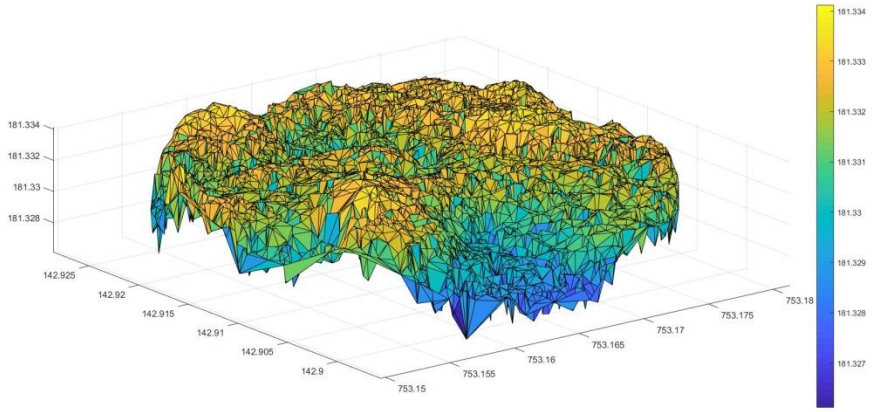

Figure 5-42: surface with wear of 0.02mm randomly distributed

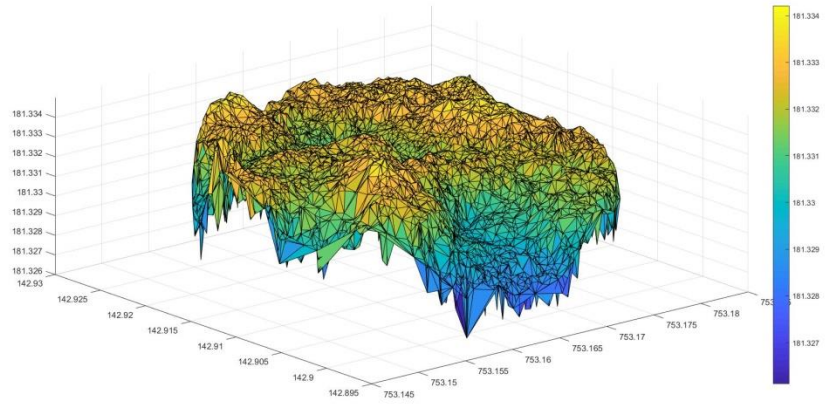

Figure 5-43: Successful Union of fragments

Wear (5mm): The accuracy of defining equal triangles was set to 10^{-6} and among the 1500 equalities of triangles found; the algorithm determined the suitable transformation. In total, the rotation matrix was found 120 times and the two clouds were properly merged. The reference cloud is depicted in figure 44, the conjugate fragment in figure 45 and their union in figure 46.

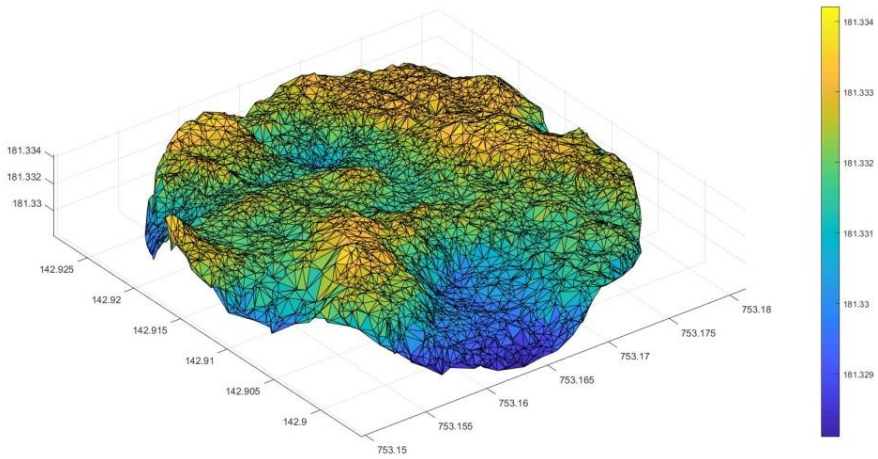

Figure 5-44: Reference surface

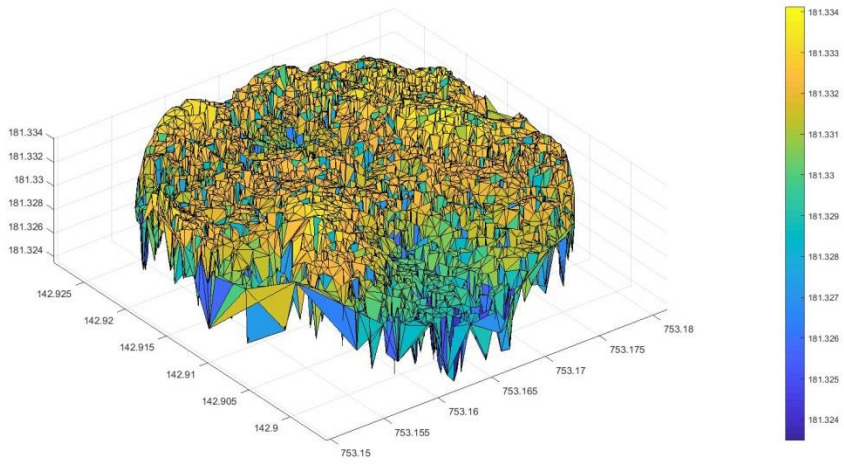

Figure 5-45: surface with wear of 0.05mm randomly distributed

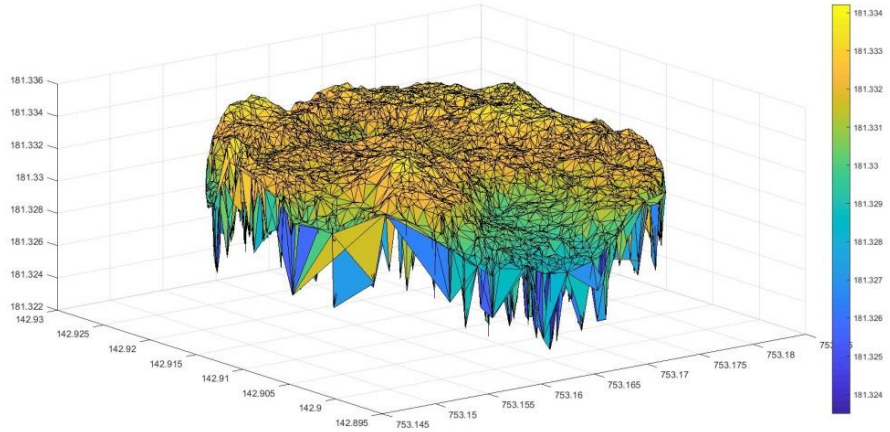

Figure 5-46: Successful Union of fragments

It is observed that as the wear is being increased, the calculated equal triangles are being decreased and even few equal triangles result in the desired matrix.

Attempt of unification of real conjugate fragments

The last example presents an effort to assemble the two real hypothetical conjugate fragments the main broken fragment with the side 2 or side 1 of the other fragment (figure 5-20). Both pairs were firstly tested in Fragmatch for their matching percentage. The ICP matching as well as the percentage of surface similarity (99%) based on the

area of the surface, which results from the global matching were successful in both cases. However the angle's tolerance percentage was found at 50%. These results show that these surfaces are possibly conjugate and due to decimation of the area, better results could not be achieved. Despite this decimation the areas of interest have maintained essential level of detail but given the fact that substantial small pieces might be missing the union of each pair could not be achieved as the present algorithm could not find an acceptable transformation. The algorithm could not detect conjugate points in both surfaces and thus calculate the rotation matrix.

Another factor that could cause the problem is the scanning process. Given the fact that these broken surfaces belong to two different broken objects and their 3D digitation took place at different time, the scanning direction may vary. In addition, during each scan, the error metric that enters in the measurements cannot be avoided. These two factors result in different scanning point and the Delaunay triangles may differ. Observing the two surfaces both in Cloud Compare and in Matlab, differences on the anaglyph of each surface are undeniable.

Approaching the tolerance of the orthogonality conditions to zero, the algorithm calculates a rotation matrix which is not acceptable and slightly disfigures the shape of the transformed cloud. The result of union presented in figure 48 is not correct.

```
rotation =

  -0.955752128712378  -0.035397716353282   0.035397716353282
   0.035398296800978  -0.028318173495371  -0.971681826504629
  -0.022068832541459  -0.982443531205494  -0.017720322301129
```

Figure 5-47: Rotation Matrix calculated in Matlab which does not satisfy the orthogonality conditions

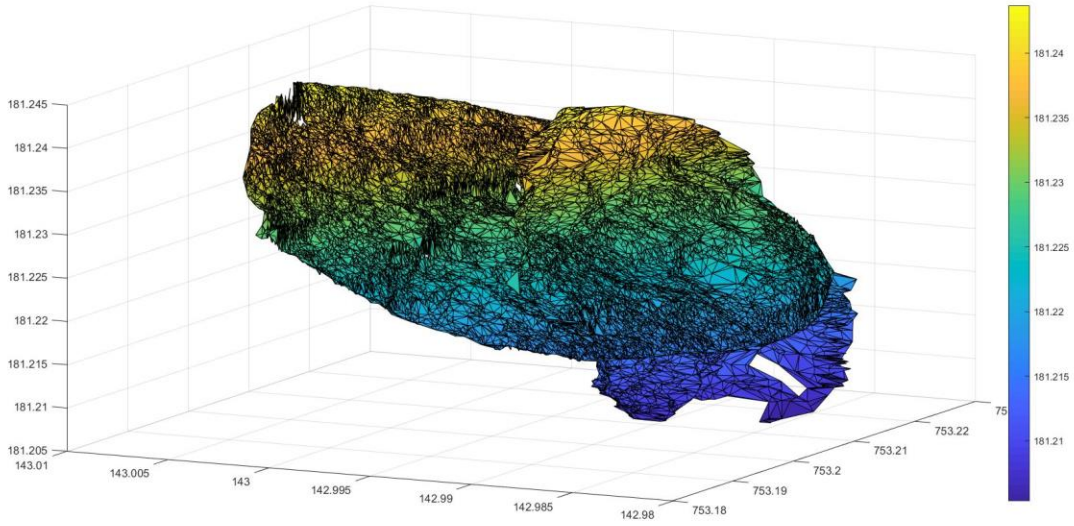

Figure 5-48: Unsuccessful union- the surfaces have merged into each other in an arbitrary way

Chapter 6 **: Conclusions**

6.1: Conclusions

The present work dealt with the problem of uniting conjugate fragments. The main difficulty concerning the numerical realization of the assemblage is that no correspondence among the points of the conjugate surfaces is known in advance.

The 3D digitization of the surfaces requires a suitable scanner which should achieve the optimum combination of the maximum volume of measured points and the workload. The recording of potential conjugate fragments should be carried out by the use of a laser scanner with the same specifications (resolution, density of points etc.). This plays an important role on the creation of surfaces of the fragments which are then tested on Fragmatch+.

The adopted solution presented in the current thesis and validated through several test cases considers a Rigid Body Transformation of the form:

$$\begin{pmatrix} X_1 \\ Y_1 \\ Z_1 \end{pmatrix} = R * \begin{pmatrix} X_1' \\ Y_1' \\ Z_1' \end{pmatrix} + \begin{pmatrix} \Delta x \\ \Delta y \\ \Delta z \end{pmatrix} \quad (1)$$

where, R is a rotation matrix of the form $R = \begin{bmatrix} a_{11} & a_{12} & a_{13} \\ a_{21} & a_{22} & a_{23} \\ a_{31} & a_{32} & a_{33} \end{bmatrix}$

and δr a translation vector of the form **δr**=$\begin{pmatrix} \Delta x \\ \Delta y \\ \Delta z \end{pmatrix}$

From the aforementioned expressions, it is deduced that (3x3)+3=12 parameters are necessary for determining a Rigid Body Transformation

The following conditions of orthogonality of the rotation matrix R, form a nonlinear system of equations which, in most cases, is difficult and computationally expensive to solve.

$$\begin{aligned} {a_{11}}^2 + {a_{21}}^2 + {a_{31}}^2 &= 1 & a_{11}a_{12} + a_{21}a_{22} + a_{31}a_{32} &= 0 \\ {a_{12}}^2 + {a_{22}}^2 + {a_{32}}^2 &= 1 & a_{11}a_{13} + a_{21}a_{23} + a_{31}a_{33} &= 0 \quad (2) \\ {a_{13}}^2 + {a_{23}}^2 + {a_{33}}^2 &= 1 & a_{12}a_{13} + a_{22}a_{23} + a_{32}a_{33} &= 0 \end{aligned}$$

The adopted method applies the principle that the transformation

$$x' = R * x + \boldsymbol{\delta r}'$$

is evaluated among the equal and corresponding triangles obtained from Delaunay triangulation, by solving a system of linear equations formulated using 4 corresponding points. The correct rotation matrix R was obtained after imposing the satisfaction of the orthogonality conditions a posteriori.

Summarizing all written above, the most important advantages and disadvantages of Fragmatch+ are stated below:

Pros and cons

(+)

- ✓ The present method linearly solves the system of equations in order to identify the rotation matrix.
- ✓ The algorithm uses vector geometry and tables ensuring the computer efficiency of the program.
- ✓ As it can be noticed from the featured case studies, the present method works effectively even in case of surfaces which have small number of equal and corresponding Delaunay triangles.
- ✓ The surfaces of different shape and size can be assembled, since there is acceptable resemblance between them.
- ✓ A smaller fragment which might be separated from the main surface can be also merged since both pieces have similar triangulation.

(-)

- × The present method is quite sensitive on Delaunay triangulation.
- × The projected surfaces of the two conjugate fragments must be similar on the XY plane (if not, an appropriate rotation should be carried out).
- × Only the fragmented surfaces are used as input, ignoring the whole object.
- × Restrictions on the size of tabular points might apply, due to the inability of Matlab to manage excessive volume of data.

6.2 Future Work

The present algorithm created as an update of the method of detecting conjugate fragments as it achieves the unification of plane to plane surfaces. The rationale of the algorithm can be used as the basis for future research:

1. After the unification of the two surfaces, the minimum distances between the points of the two clouds that have not "coincided" could be calculated. The distances less than a minimum threshold could be assumed to be a conjugate point but due to wear they have not coincided. The average of these minimum distances could be calculated and constitute a measure of the success of the unification of the two surfaces.

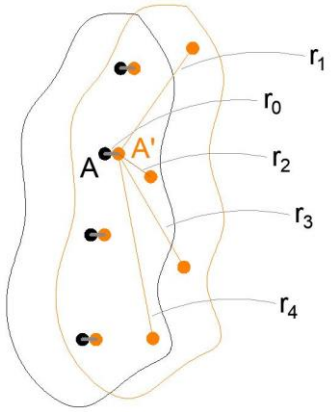

Figure 6-1: Calculation of the minimum threshold r

2. An update of the algorithm could take into account the lateral surfaces which would search the best fit among the surfaces for the reference surface.
3. An additional update would be in the identification of geometrical characteristics of the surfaces or in the detection of color. A classification of the properties of each fragment could facilitate the search of equal characteristics on the two surfaces in order to achieve the matching of the two surfaces.
4. In addition, in cases where a partial unification was achieved, an automatic virtual completion of the missing part could be added and enhance the result.
5. A transcription of the algorithm in another programming language would allow the input of any size of data.
6. A global database containing surfaces of scanned broken fragments could correspond and unify automatically two conjugate fragments as soon as the system detects their similarity based on similar characteristics of their surfaces.

Bibliography

International Bibliography

1. 2D and 3D Computer Vision Analysis of Gaze , Gender and Age. (2016).
2. Abdel-Bary EBRAHIM Professor, M. (2013). 3D Laser Scanners' Techniques Overview. *International Journal of Science and Research Index Copernicus Value Impact Factor*, *14611*(10), 2319–7064.
3. Andreadis, A., Papaioannou, G., & Mavridis, P. (2015). Generalized digital reassembly using geometric registration. *2015 Digital Heritage International Congress, Digital Heritage 2015*, 549–556.
4. Belenguer, C. S., & Vidal, E. V. (2012). Archaeological fragment characterization and 3D reconstruction based on projective GPU depth maps. *Proceedings of the 2012 18th International Conference on Virtual Systems and Multimedia, VSMM 2012: Virtual Systems in the Information Society*, 275–282.
5. Brown, B. J., Toler-Franklin, C., Nehab, D., Burns, M., Dobkin, D., Vlachopoulos, A., … Weyrich, T. (2008). A system for high-volume acquisition and matching of fresco fragments. *ACM Transactions on Graphics*, *27*(3), 1.
6. Brunet-Gaston, V., & Gaston, C. (n.d.). En guise de comparaison, un sanctuaire antique à Pont-Sainte-Maxence (Oise).
7. Fabio, R. (n.d.). FROM POINT CLOUD TO SURFACE: THE MODELING AND VISUALIZATION PROBLEM. *International Archives of the Photogrammetry, Remote Sensing and Spatial Information Sciences*, 5–10. Retrieved from http://www.isprs.org/proceedings/XXXIV/5-W10/papers/remondin.pdf
8. Filippas, D., & Georgopoulos, A. (n.d.). DEVELOPMENT OF AN ALGORITHMIC PROCEDURE FOR THE DETECTION OF CONJUGATE FRAGMENTS.
9. Freeman, H., & Garder, L. (1964). Apictorial Jigsaw Puzzles: The Computer Solution of a Problem in Pattern Recognition. *IEEE Transactions on Electronic Computers*, *EC-13*(2), 118–127.
10. Gelfand, N., Ikemoto, L., Rusinkiewicz, S., & Levoy, M. (2003). Geometrically stable sampling for the ICP algorithm. *Proceedings of International Conference on 3-D Digital Imaging and Modeling, 3DIM*, *2003–Janua*, 260–267.
11. Goldberg, D., Malon, C., & Bern, M. (2004). A global approach to automatic solution of jigsaw puzzles. *Computational Geometry: Theory and Applications*, *28*(2–3 SPEC. ISS.), 165–174.
12. Huang, Q.-X., Flöry, S., Gelfand, N., Hofer, M., & Pottmann, H. (2006). Reassembling fractured objects by geometric matching. *ACM SIGGRAPH 2006 Papers on - SIGGRAPH '06*, 569.
13. Kampel, M., & Sablatnig, R. (2004). On 3D mosaicing of rotationally symmetric ceramic fragments. *Proceedings of the 17th International Conference on Pattern Recognition, 2004. ICPR 2004.*, *00*(C), 265–268 Vol.2.
14. Koller, D., & Levoy, M. (2006). Computer-aided reconstruction and new matches in the forma urbis romae. *Bullettino Della Commissione …*. Retrieved from http://graphics.stanford.edu/papers/forma-bullcom/forma-bullcom-text.pdf
15. MARIANNE DEUBER, S. C. A. S. N. (2014). Dense Image Matching. *GIM International*, (September), 23–25.
16. Mase, G. E. (n.d.). Theory And Problems of Continuum Mechanics Schaum's Outline Series.

17. Matthews, N. a. (2008). Aerial and Close-Range Photogrammetric Technology. *Technical Note 428*, 42.
18. Mavridis, P., Andreadis, A., & Papaioannou, G. (2015). Fractured Object Reassembly via Robust Surface Registration. *Eurographics*. Retrieved from http://www.presious.eu/sites/default/files/EG15_Reassembly_final.pdf
19. Papaioannou, G., Karabassi, E. A., & Theoharis, T. (2002). Reconstruction of three-dimensional objects through matching of their parts. *IEEE Transactions on Pattern Analysis and Machine Intelligence*, *24*(1), 114–124.
20. Maxence, P.-, Inrap, T., & Picardie, D. (2014). The discovery of a Gallo-Roman monumental sanctuary and its statuary at Pont-Saint- Maxence, (May).
21. Papaodysseus, C., Arabadjis, D., Exarhos, M., Rousopoulos, P., Zannos, S., Panagopoulos, M., & Papazoglou-Manioudaki, L. (2012). Efficient solution to the 3D problem of automatic wall paintings reassembly. *Computers and Mathematics with Applications*, *64*(8), 2712–2734.
22. Pavlidis, G., Koutsoudis, A., Fotis, A., Vassilios, T., & Christodoulos, C. (2007). Methods for 3D digitization of Cultural Heritage. Journal of cultural Heritage, 93–98.
23. Projet Pont-Sainte-Maxence : description des interventions souhaitées Restitution 3D et intervention de conservation-restauration de la pierre nécessaire pour la 3D Expertise et conservation-restauration (pigments et mortiers, objets métalliques). (2015).
24. Remondino, F., Spera, M. G., Menna, F., & Foundation, B. K. (2014). STATE OF THE ART IN HIGH DENSITY IMAGE MATCHING. *The Photogrammetric Record*, *29*(146), 144–166.
25. Remondino, F., Spera, M. G., Nocerino, E., Menna, F., & Nex, F. (2013). Dense image matching: comparisons and analyses, 47–54.
26. Sizikova, E., & Funkhouser, T. (2017). Wall Painting Reconstruction Using a Genetic Algorithm. *J. Comput. Cult. Herit.*, *11*(1), 3:1--3:17.
27. Stathopoulou, E., Valanis, A., Lerma, J., & Georgopoulos, A. (2012). *HIGH AND LOW RESOLUTION TEXTURED MODELS OF COMPLEX ARCHITECTURAL SURFACES*. *The International Archives of the Photogrammetry, Remote Sensing and Spatial Information Sciences* (Vol. XXXVIII-5/W16).
28. Szeliski, R. (2010). Computer Vision: Algorithms and Applications. Retrieved from http://szeliski.org/Book/.
29. Véronique BRUNET-GASTON Christophe GASTON, P. (n.d.). Les dieux du stade : une façade monumentale gallo-romaine d'exception Nord-Picardie «Hauts de France», Oise Pont-Sainte-Maxence «Le Champ Lahyre».
30. Willis, A. R., & Cooper, D. B. (2008). Computational reconstruction of ancient artifacts: From ruins to relics. *IEEE Signal Processing Magazine*, *25*(4), 65–83.
31. Zheng, S. Y., Huang, R. Y., Li, J., & Wang, Z. (2014). Reassembling 3D Thin Fragments of Unknown Geometry in Cultural Heritage. *ISPRS Annals of Photogrammetry, Remote Sensing and Spatial Information Sciences*, *II-5*(June), 393–399.

Greek Bibliography

32. Καρράς, Γ. (1998). Τομέας Τοπογραφίας Γραμμικοί Μετασχηματισμοί Συντεταγμένων στην Φωτογραμμετρία.
33. Μπούρας, Χ.Θ., 1999 "Μαθήματα Ιστορίας της Αρχιτεκτονικής" ΠΡΩΤΟΣ ΤΟΜΟΣ

34. Πρόκος, Α.Ι.,2012 *"Δημιουργία Φωτογραμμετρικού Σαρωτή Laser με Χρήση Πρόσθετων Γεωμετρικών Δεσμεύσεων"*
35. Τοπογραφίας, Τ., Φωτογραμμετρίας, Ε., & Εργασία, Δ. (n.d.). Εθνικό Μετσόβιο Πολυτεχνείο Σχολή Αγρονόμων & Τοπογράφων Μηχανικών Ανάπτυξη αλγοριθμικής διαδικασίας για τον εντοπισμό συζυγών θραυσμάτων.

Sites

36. http://www.aeroexpo.online/prod/faro/product-184499-25247.html
37. https://www.britannica.com/
38. https://ch.mathworks.com/
39. https://www.europeana.eu/portal/en
40. https://www.pontsaintemaxence.fr/?page_id=1048

Table of figures

Figure 2-1: The principle behind structured-light 3D scanners, which is based on the distortion of a known light pattern observed from a certain viewpoint. 7
Figure 2-2: Shape from structured light 9
Figure 2-3: Shape from silhouette 9
Figure 3-1: For pieces that fit perfectly, the lengths of the bold parts of horizontal lines should be equal 16
Figure 3-2 : There are 8 eligible pockets at this step. 16
Figure 3-3 : Fragment matching with rotational symmetry. 18
Figure 3-4: Relative pose of the two meshes during the matching process 19
Figure 3-5: The use of z-buffer to calculate the point-to-point distances for the matching. The z-buffers for the two objects are shown at the bottom left and right. 20
Figure 3-6: Fragments 156, 667 and 134 with their boundary incision annotations indicated 21
Figure 4-1 : Map of France - Location of Pont Saint Maxence 34
Figure 4-4-2: Map of the monumental state of the site 35
Figure 4-3: Detail of the elevation to be restored 36
Figure 4-4: Provisional hypothesis of the facade of restitution (INRAP) 37
Figure 4-5: Temporary anastylosis of the facade (INRAP); West and East Part 37
Figure 4-4-6: Ionic and Composite capitals 38
Figure 4-7: Lower part of structure 39
Figure 4-8: Intrados of keystone of the arch VI (© V. Brunet-Gaston, Inrap). 40
Figure 4-9: Entableture and attic 40
Figure 4-10: Attic: Triton carrying an oar (© V. Brunet-Gaston, Inrap). 41
Figure 4-11: Divine heads (© V. Brunet-Gaston, Inrap). 41
Figure 4-12: Anastylosis of arcade blocks V and VI ((© C. Gaston, Inrap) 43

Figure 4-13: FARO SCANARM 44
Figure 4-14: Alignment procedure of two fragments 47
Figure 4-15: RMS of first registration 47
Figure 4-16: RMS of fine registration 48
Figure 4-17: Cloud to Cloud distance 49
Figure 4-18: Example of Computation of Cloud to Cloud distance 50
Figure 4-19: Potential conjugate fragments. Tests were carried out for the right pair. 51
Figure 4-20: Both sides of the right fragment should be tested in order to find the potential fit to the left fragment 52
Figure 4-21: Examples of segmented surfaces 52
Figure 5-1: Rigid Body Transformation 55
Figure 5-2: Segmentation part 56
Figure 5-3: ICP converges when the starting positions are “close enough’’ 58
Figure 5-4: Input of limit of side manually 59
Figure 5-5: Delaunay Triangulation - Display of triangles in the x, y plane in Matlab 60
Figure 5-6: Delaunay Triangulation - Display of 2-D surface in Matlab 60
Figure 5-7: Voronoi diagram. Figure 5-8: Delaunay triangulation 61
Figure 5-9: 1. The pair of triangles on the left does not meet the Delaunay Condition (the circumcircle contains more than three points). 2. However, the pair on the right meets the Delaunay Condition. Flipping the common edge produces a valid Delaunay Triangulation for the four points. 62
Figure 5-10: A different criterion is the sum of α and γ being smaller than 180°. In this case, this triangulation does not meet this Delaunay condition 63
Figure 5-11: Calculation of area of triangles using cross product 66
Figure 5-12: This function allows the correspondence of the conjugate triangles vertices 67
Figure 5-13: 4 points are used for the applied transformation 69
Figure 5-14: x-z planes of the spheres 72
Figure 5-15 : Simulation of quadrants 73
Figure 5-16: The two quadrants joined into one 74
Figure 5-17: 3D view of the quadrants 75
Figure 5-18: Rotated quadrant along the three axes 75
Figure 5-19: Union of conjugate quadrants 76
Figure 5-20: cylindrical conjugate fragments and potential fits of surfaces 77
Figure 5-21: The main point cloud belongs to the reference fragment (hand holding a cylindrical object). Each side of its hypothetical conjugate fragment is named after side 1 & side 2 78
Figure 5-22: reference cloud 79
Figure 5-23: cloud2 rotated around the 3 axes 79
Figure 5-24: Unification of fragments 80
Figure 5-25: Reference point cloud 81
Figure 5-26: Rotated of second cloud around z axis 81
Figure 5-27: Successful Union of fragments 81
Figure 5-28: Reference point cloud 82

Figure 5-29: Second point cloud after Delaunay Triangulation before rotation and translation.....83
Figure 5-30: Rotation of second cloud along the 3 axes and translation 83
Figure 5-31: Successful Union of fragments 83
Figure 5-32: Reference point cloud 84
Figure 5-33: cloud 2 with rotation of 30 degrees along the three axis 84
Figure 5-34: Successful Union of fragments 85
Figure 5-35: Reference point cloud 86
Figure 5-36: Shattered conjugate surface.....86
Figure 5-37: Successful Union of fragments 86
Figure 5-38: Reference point cloud 87
Figure 5-39: surface with wear of 0.01mm randomly distributed 88
Figure 5-40: Successful Union of fragments 88
Figure 5-41: reference surface.....89
Figure 5-42: surface with wear of 0.02mm randomly distributed 89
Figure 5-43: Successful Union of fragments 90
Figure 5-44: Reference surface 90
Figure 5-45: surface with wear of 0.05mm randomly distributed 91
Figure 5-46: Successful Union of fragments 91
Figure 5-47: Rotation Matrix calculated in Matlab which does not satisfy the orthogonality conditions.....92
Figure 5-48: Unsuccessful union- the surfaces have merged into each other in an arbitrary way.....93
Figure 6-1: Calculation of the minimum threshold r 97